

AD 712024

Technical Report No. 31 Project No. NR 014-113

Arpa Order No. 125

An Optical Spectroscopic Investigation  
of Helium and Nitrogen Plasmas

Melvyn Samuel Manalis  
Author

H. P. Broida  
Contractor

Research supported in part by the U.S. Advanced Research Projects Agency through the U.S. Office of Naval Research, Contract No. N00014-69-A-0200-8004, General Motors Corporation, and the Air Force Rocket Propulsion Laboratory.

Distribution of this document is unlimited.

Reproduced by the  
CLEARINGHOUSE  
for Federal Scientific & Technical  
Information Springfield Va. 22151

This document has been approved  
for public release and sale; its  
distribution is unlimited.

**BEST  
AVAILABLE COPY**

UNIVERSITY OF CALIFORNIA  
Santa Barbara

An Optical Spectroscopic Investigation  
of Helium and Nitrogen Plasmas

A Dissertation submitted in partial satisfaction  
of the requirements for the degree of

Doctor of Philosophy

in

Physics

by

Melvyn Samuel Manalis

Committee in charge:

Professor Herbert P. Broida, Chairman

Professor Paul J. Kelly

Professor Stanton Peale

Professor David T. Phillips

Professor Glen Wade

June 1970

The dissertation of Melvyn Samuel Madala is approved:

David F. Phillips

Stanton J. Peale

Paul J. Kelly

Glen Wade

F. P. Brock  
Committee Chairman

-----  
Dean, Graduate Division

June 1970

ii

#### ACKNOWLEDGMENTS

The author wishes to express his gratitude to Professor H. P. Broida for providing an excellent environment for pursuing research. In addition, his suggestions and helpful guidance were of great value. Special acknowledgment is due to Professor Stanton Peale for many useful discussions and his helpful criticism of Chapter III.

Thanks is due to Mrs. Merrie Walker and Mr. Anthony Korda for their aid in putting the manuscript in its final form.

Grateful acknowledgment is made to my parents and wife for their constant support and encouragement throughout my educational career.

Financial support from General Motors Corporation, the Advanced Research Projects Agency, and the Air Force Rocket Propulsion Laboratory is acknowledged.

## VITA

October 16, 1939      Born, Los Angeles, California

1961                  B.A., Mathematics, San Fernando Valley  
State College

1961-1963            Teaching Assistant, Department of Physics,  
University of New Hampshire

1963-1964            Physics Instructor, Colby College,  
Waterville, Maine

1964                  M.S., Physics, University of New Hampshire

1964                  Teaching Assistant, University of  
California, Santa Barbara

1965 (Summer)        Scientist, Jet Propulsion Laboratory,  
California Institute of Technology

1966                  General Motors Research Fellow

1966 (Summer)        Research Scientist II, University  
of Colorado

1967-1969            Research Assistant, University of  
California, Santa Barbara

1967 (Summer)        Physicist, National Bureau of Standards,  
Washington, D.C.

## PUBLICATIONS

The Li(d, $\alpha$ ) Reactions at Deuteron Energies Between 175-300 KeV, Phys. Rev. 136, B1741 (1964).  
M.S. thesis, University of New Hampshire, 1964.

A New Method for Excitation of Neutral Atomic Nitrogen, Bull. Am. Phys. Soc., 12, 1146 (1967).

Vibrational Distributions of the  $H_2(B^3\Pi_g - A^3\Sigma_u^+)$  System Produced in a Helium Afterglow, Bull. Am. Phys. Soc., 13, 1666 (1968).

## ABSTRACT

### An Optical Spectroscopic Investigation of Helium and Nitrogen Plasmas

by

Melvyn Samuel Manalis

Energetic species and their respective energy exchange processes in a cool, high density helium plasma has been reviewed. Light from a flowing helium afterglow was observed from 2500 to 10,500 Å using an Ebert double-pass scanning monochromator coupled to standard dc detecting equipment. Experimental data in the form of relative populations of atomic helium states provided motivation for a theory which may explain the manner in which ionization is maintained in the afterglow region of the helium plasma. A bimodal electron distribution was found to exist in this plasma; the electron temperatures were measured spectroscopically to be in the neighborhood of  $10^3$  and  $10^4$  K.

Molecular nitrogen was used as a probe to detect various energetic species present in the helium afterglow. In addition to the usual systems observed when  $N_2$  is injected into the helium afterglow, light from many levels of atomic nitrogen and three new vibrational population distributions of the first positive system of molecular nitrogen were observed. Two independent mechanisms

for exciting the atomic nitrogen were isolated. One mechanism consisted of a two step collisional process where  $N_2$  was dissociated by metastable molecular helium  $He_2^M$ , and the excited N was produced by collisions with electrons. The temperature associated with the N level population was about  $10^4$  K, confirming the existence of the high energy electrons found in the helium afterglow. The second mechanism for populating N was single electron recombination of nitrogen atomic ions formed in the dissociative charge transfer reaction of ionized helium,  $He^+$ , with molecular nitrogen. Approximately 400 new III lines were observed from an inverted population distribution.

## TABLE OF CONTENTS

	Page
I INTRODUCTION . . . . .	1
II EXPERIMENTAL APPARATUS AND TECHNIQUES . . . . .	4
2.1 Optical Detection System . . . . .	4
2.2 Source of the Helium Plasma . . . . .	4
2.3 Qualitative Observations . . . . .	5
III THE HELIUM PLASMA . . . . .	14
3.1 Statement of the Problem . . . . .	14
3.2 Experimental Results . . . . .	18
3.3 Development of the Two Electron Temperature Model . . . . .	25
3.4 Data Interpretation . . . . .	40
3.5 Application to Stellar Atmospheres . . . . .	45
3.6 Calculation of the Three-Body Recombination Coefficient . . . . .	46
3.7 Electron-Electron Relaxation . . . . .	49
3.8 "Linked" Diffusion of Electrons . . . . .	52
3.9 General Discussion of the Model . . . . .	55
IV ATOMIC NITROGEN . . . . .	67
4.1 Spectra and Data . . . . .	67
4.2 Complete Energy Level Diagrams for NI . . . . .	70
4.3 Two Mechanisms for Production of NI . . . . .	81
4.4 The Problem of Identification of Lines . . . . .	89

	Page
4.5 Interpretation of Results . . . . .	89
V MOLECULAR NITROGEN . . . . .	95
VI CONCLUSION . . . . .	107
REFERENCES . . . . .	110
APPENDIX I	
Wavelengths for HI Spectrum . . . . .	114

LIST OF TABLES

TABLE	Page
3.1 Transition Probabilities for HeI $2s^2S - np^2P^o$ Series . .	19
3.2 Results of Numerically Integrating $F_n(\rho)$ . . . . .	33
3.3 Numerical Values for the Pertinent Quantities of the Two Electron Temperature Model . . . . .	38
3.4 Experimental Parameters . . . . .	41
5.1 Summary of Reactions with $H_2$ and the Helium Afterglow . .	98

## LIST OF FIGURES

FIGURE	Page
2.1 Plasma Source . . . . .	9
2.2 Energy Level Diagram for Helium Species . . . . .	11
2.3 Helium Afterglow and NI Spectrum . . . . .	13
3.1 Partial Energy Level Diagram for HeI . . . . .	22
3.2 Relative Population Density for HeI $2s\ ^3S - np\ ^3P^o$ . . .	24
3.3 The Integral $F_n(s)$ . . . . .	32
3.4 Electron Energy Distributions . . . . .	58
3.5 Relative Population Density for HeI $2p\ ^3P^o - nd\ ^3D$ (Thornton, 1968) . . . . .	64
3.6 Relative Population Density for HeI $2p\ ^3P^o\ nd\ ^3D$ (Hinnov and Hirschberg, 1962) . . . . .	66
4.1 NI Plate . . . . .	72
4.2 NI Energy Level Diagram . . . . .	76
4.3 NI Partial Energy Level Diagram . . . . .	78
4.4 Colored NI Partial Energy Level Diagram . . . . .	80
4.5 Two Mechanisms for NI . . . . .	84
4.6 NI Spectra (4250 A region) . . . . .	86
4.7 NI Spectra (3900 A region) . . . . .	88
4.8 NI Population Distribution . . . . .	94
5.1 $N_2$ First Positive System . . . . .	100
5.2 Relative Vibrational Population of the $N_2\ B\ ^3\Pi$ State ( $v'=10$ ) . . . . .	102

FIGURE	Page
5.3 Partial $N_2$ Energy Level Diagram . . . . .	104
5.4 Relative Vibrational Population of the $N_2$ B $^3\Pi$ State . .	106

## I INTRODUCTION

The energetic particles present in the helium afterglow have been used to excite selectively various atomic and molecular species in the laboratory. Accurate rate constants and densities of excited species can be determined using the data from these experiments. A recent and very comprehensive investigation of this subject has been published by Ferguson, Fehsenfeld and Schmeltekopf (1969). One purpose of the present work is to provide a self-consistent, usable model to describe the fundamental energy exchange mechanism in the helium plasma.

Light from a flowing helium afterglow was observed between 2500 to 10,500 Å using an Ebert double-pass scanning monochromator coupled to standard dc detecting equipment. In an attempt to understand measured relative intensities of atomic helium transitions, a model has been developed to explain the manner in which ionization is maintained in the afterglow region of the plasma. The assumptions included in this model are: (1) a bimodal electron distribution exists in the plasma; (2) the major energy exchange processes which occur in the plasma are three-body recombination and ionization

collisions of ground and excited states of atomic helium; (3) the functional dependence of the ionization cross section is given by the classical theory of J. J. Thomson for ionization of gases. The two temperatures of the electrons were measured spectroscopically to be near  $10^3$  and  $10^4$  K, while the relative density of high temperature to low temperature electrons was measured to be about 0.1.

Molecular nitrogen was used as a probe to detect various energetic species present in the helium afterglow since it has a large interaction probability to produce light when bombarded by these species. In addition to the usual systems observed when  $N_2$  is injected into the helium afterglow (Collins and Robertson, 1964c; Dunn, 1966), several vibrational population distributions of the first positive system were observed. One population distribution was unique in that the tenth vibrational level was considerably more populated than neighboring levels. Approximately one percent of the nitrogen molecules in the  $B^3\Pi_g$  state were in the tenth vibrational level distribution, while the population distribution of the remaining molecules could be described by a temperature of  $4000 \pm 150$  K. This phenomenon may be an example of collisional induced level crossing in homonuclear diatomic molecules.

In addition to the observation of the molecular nitrogen systems, two independent mechanisms for exciting atomic nitrogen were isolated. One mechanism consisted of a two step collisional process where  $N_2$  was dissociated by metastable molecular helium,  $He_2^M$ , and the excited neutral atomic nitrogen,  $NI$ , was produced by collisions with

electrons. The temperature of the NI levels was about  $10^4$  K, confirming the existence of the high energy electrons found in the helium afterglow. The second mechanism for populating NI was single electron recombination of nitrogen atomic ions. The ions are formed in the dissociative charge transfer reaction of ionized helium,  $\text{He}^+$ , with molecular nitrogen. Approximately 400 new NI lines were observed with an inverted population distribution.

To aid in the data analysis, specific computer programs were developed to determine the response characteristics of the detection systems used in the experiments, and to present spectroscopic data in a manner which would facilitate the recognition of a Boltzmann population distribution among the observed energy levels of any atomic or molecular system (Applebaum and Manalis, 1970).

## II EXPERIMENTAL APPARATUS AND TECHNIQUES

### 2.1 Optical Detection System

The optical detection system used in these experiments was conventional dc detection equipment. All sources that were investigated were bright and thus relatively convenient for spectroscopic measurement. An Ebert double pass scanning monochromator was used with various photomultiplier tubes, gratings and optical filters. The choice of particular accessories depended on the spectral region investigated. A calibrated quartz-iodine lamp was used to measure the relative response of the optical detection system. An excellent description of the detection system used in this laboratory is given in a Ph.D. thesis by C. Liu (1969).

### 2.2 Source of the Helium Plasma

The source which was used to excite the helium is illustrated in Fig. 2.1. Excitation of the helium gas was achieved by flowing the gas through a liquid nitrogen cooled charcoal trap and between a hollow cylindrical stainless steel cathode and a grounded ring anode at a speed of  $10^4$  cm/sec. The source was operated at a pressure near

one torr, an electrode current of 500 ma, and a potential near 1 kV. The flow rate of the helium gas was about 275 atm-cc/sec. More details on this source and the effects of impurities on the excited helium can be found in a Ph.D. thesis written by J. Dunn (1966).

The region between the electrodes is referred to as the discharge region and the region beyond the ring anode is referred to as the afterglow region. Target gases such as molecular nitrogen, argon or hydrogen were added through gas inlet #1 or #2. These gas inlets could be rotated to improve the mixing of gases.

Figure 2.2 illustrates the amount of energy which was available from the helium species present in the helium afterglow. There are four energetic species in the plasma: the atomic ion,  $\text{He}^+$ , the molecular ion  $\text{He}_2^+$  and the metastable atom,  $\text{He}^M$ , the metastable molecular,  $\text{He}_2^M$ . However, the presence of another energetic species was needed to explain the many reactions that were observed when molecular nitrogen was added to the afterglow. This species was found to be relatively energetic electrons with a temperature of  $10^4$  K.

### 2.3 Qualitative Observations

Using the eye to observe changes in color, intensity and relative positions of the radiating species while varying the experimental parameters, was an important part of the experimental procedure used in this work. It was these qualitative procedures which led to the first observation of the various vibrational distributions of the  $\text{N}_2$  first positive system (see Chapter V) and to a

relatively clean source of atomic nitrogen. For example, when molecular nitrogen was injected into the helium afterglow, a blue glow occurred in the neighborhood of the gas inlet and further downstream a faint green glow occurred. Spectroscopic measurements indicated that the blue glow consisted of strong emission from the  $N_2^+$  first negative system and weak emission from atomic nitrogen. The green glow consisted mainly of atomic nitrogen lines (see Fig. 2.3, lower spectrum) but with different relative intensities from the NI lines which appear in the blue region. When the molecular nitrogen flow rate is increased by about one order of magnitude, the blue and green glows vanish and a strong red glow appears. The spectrum of this glow consisted of an unusual vibrational distribution of the first positive system of molecular nitrogen. If the flow rate is then doubled, the red vanishes and a turquoise blue glow appears. Preliminary spectra indicated that this glow may contain emission from the  $N_2$  ( $E^3\Sigma$ ) state.

If one directs a rf field near the plasma frequency towards the afterglow, reactions that involve slow electrons and ions will be quenched. When rf power is pumped into the afterglow at the plasma frequency, ambipolar diffusion inhibits electron-ion recombination, causing the quenching effect (see section 3.8). It was found that the green atomic nitrogen glow was completely quenched with this procedure (see chapter IV). Thus, this procedure was a very useful tool to aid in separating the many reactions which occur

simultaneously in the plasma.

Another qualitative observation which proved useful was to add a third gas into inlet #1 and observe the effects on the reactions of a target gas which was injected into the afterglow through inlet #2. In some cases, the third gas will remove an energetic helium species which is a precursor of a reaction with the target gas. This procedure was used to learn one of the mechanisms which produces excited atomic nitrogen. From the work of Dunn (1966), it was verified that argon has a large cross section for removal of metastable helium atoms. The experiment was to inject molecular nitrogen into inlet #2 and observe radiation from atomic nitrogen at inlet #2 while adding argon gas through inlet #1. As a result, the intensity of the nitrogen lines remained unchanged. The conclusion was that metastable helium atoms had little to do with the production of excited NI. Now, under these exact experimental conditions a rf field was directed towards the NI source at inlet #2. Since there was no change in the intensity of NI radiation, neither helium ions, metastable atoms nor slow electrons were instrumental in exciting atomic nitrogen. The only precursors which remained were metastable helium molecules and energetic electrons. Thus, a two step process involving these two energetic species probably caused the excitation of NI (see section 4.3).

Figure 2.1

Low pressure (1 torr) is source of the helium plasma. Excitation of the helium was achieved by flowing the gas through a liquid nitrogen cooled charcoal trap and between a hollow cylindrical (6.5 diameter by 8.0 cm in length) stainless steel cathode and a grounded ring anode (6.5 cm diameter). The operating electrode voltage and current were 1 kV and 500 ma, respectively. The nitrogen plasma was created by adding molecular nitrogen through gas jets 1 and 2.

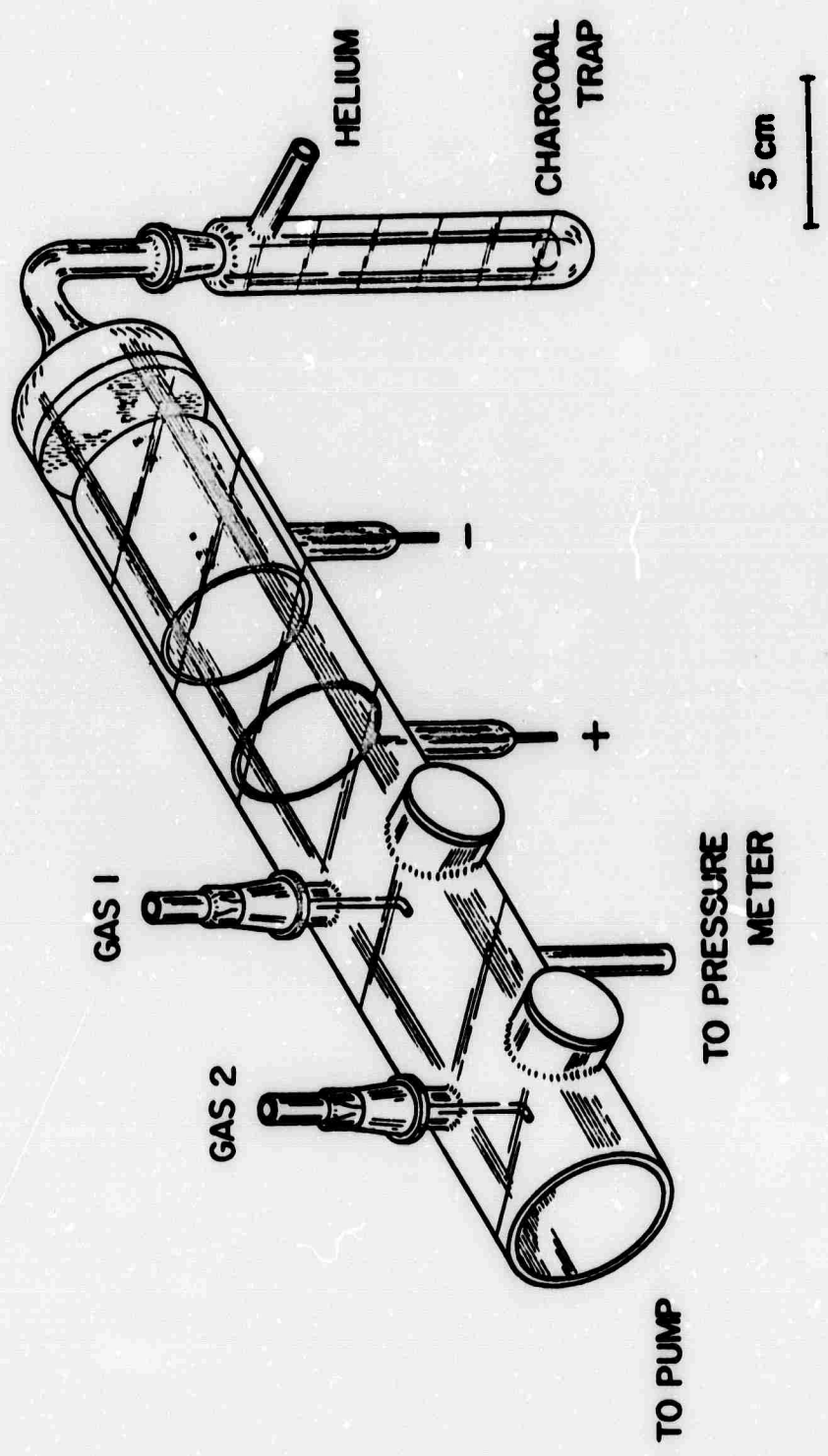


Figure 2.2

The partial energy level diagram indicates the amount of energy which is available from the helium species present in the helium afterglow. The horizontal line on the molecular levels indicates the spread of energy which is available from vibrational energy.

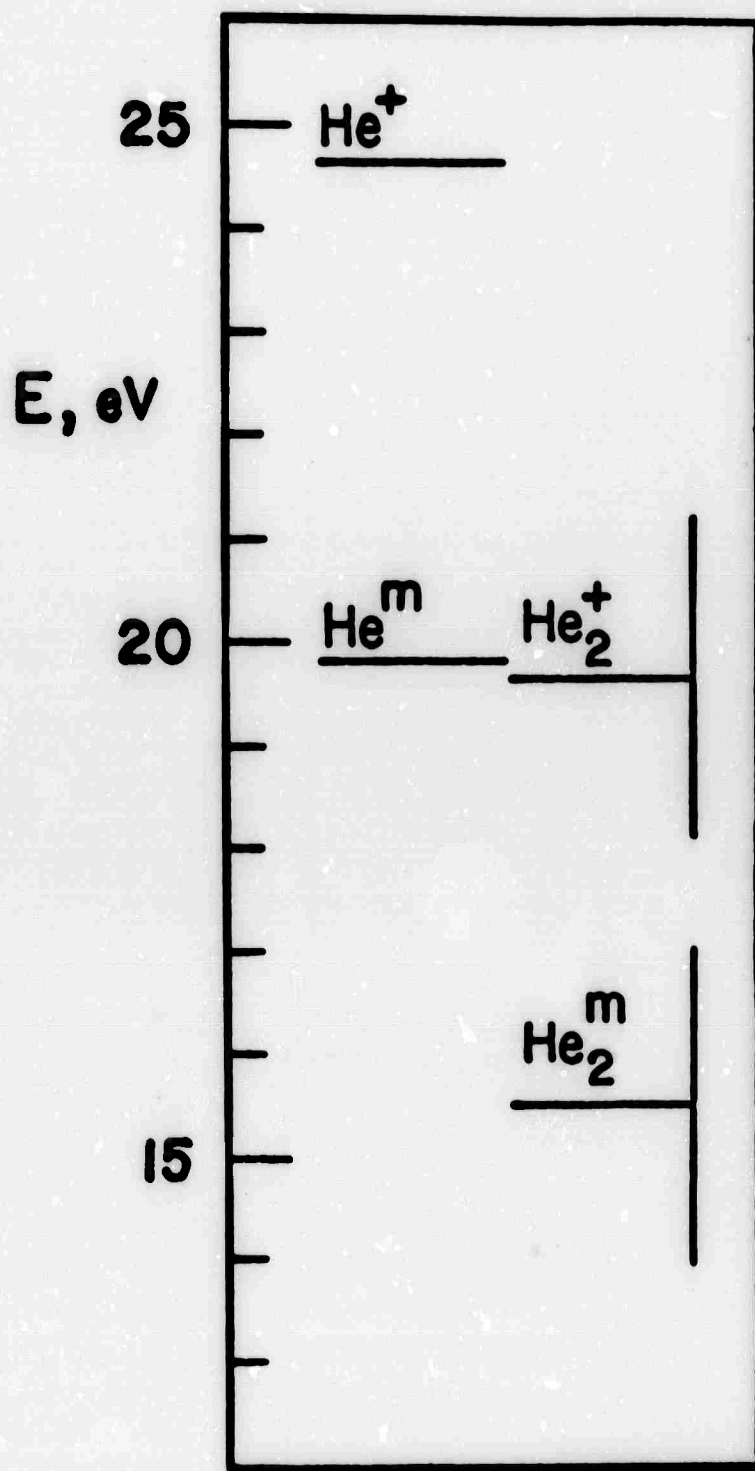
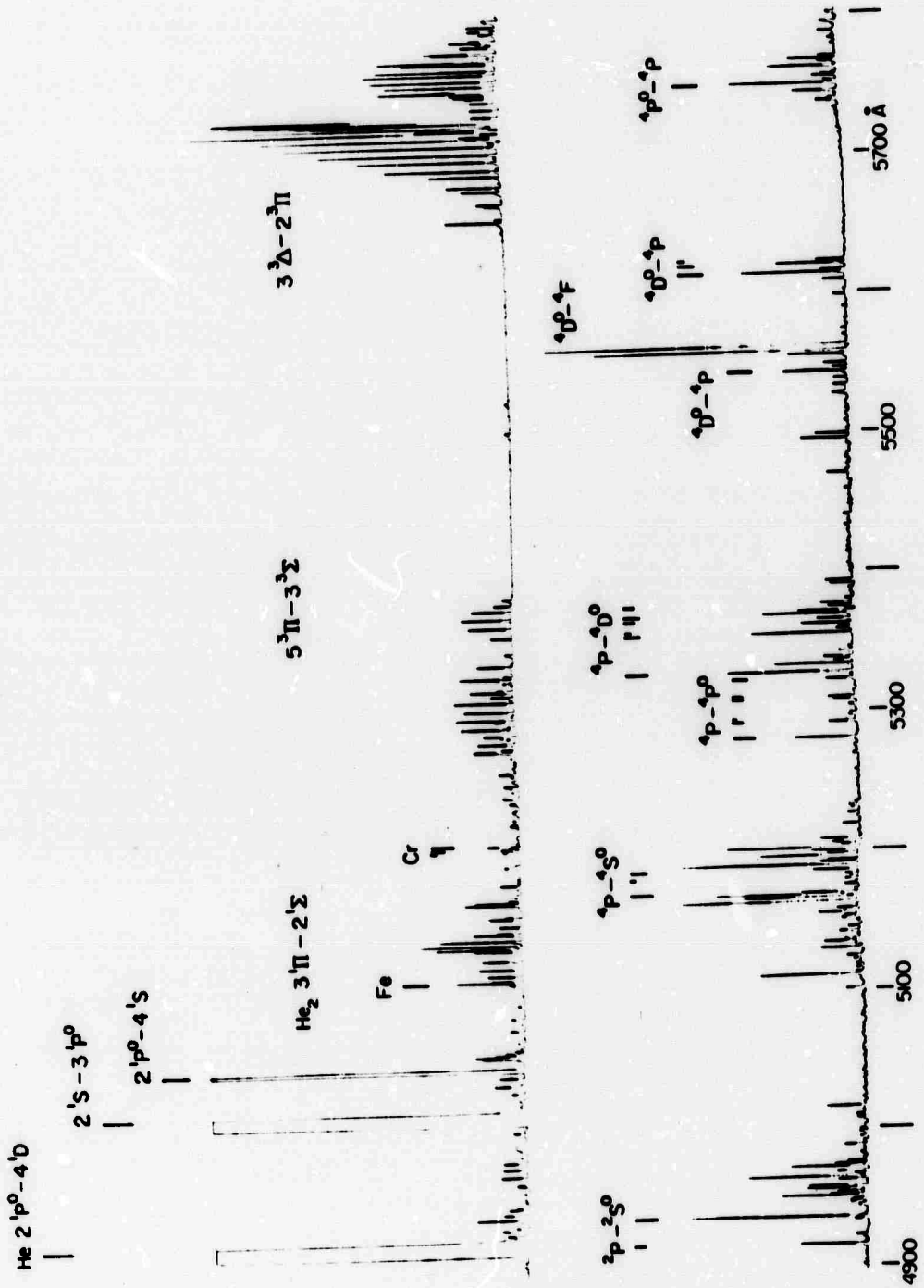


Figure 2.3

A photograph of the actual photoelectric data from the helium afterglow at a pressure of 1 torr is shown on the upper figure. It was observed by an Ebert double-pass scanning monochromator. The atomic emission is two to three orders of magnitude greater than the emission from the helium molecule. Also seen in the spectrum are the brightest lines of iron and chromium which occur because of electrode sputtering. The spectrum shown in the lower figure resulted when molecular nitrogen was added to the afterglow. Analysis of the complete spectrum indicates that it is predominately atomic nitrogen. Many new unclassified III lines are shown in the figure.



### III THE HELIUM PLASMA

#### 3.1 Statement of the Problem

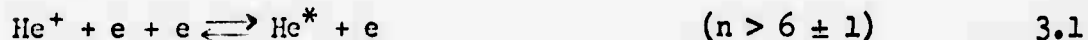
A large percentage of the light which radiates from the helium plasma originates from transitions between the energy levels of atomic helium. If the mechanisms for populating and depopulating these levels can be understood, then the fundamental energy exchange processes in the plasma itself can be better understood. There has not been a satisfactory theoretical explanation for the observed population of these energy levels. This is because the number of energy exchange processes included in previous theories is large, and no single closed expression for the population of energy levels as a function of the principle quantum number has been written.

To illustrate this problem one needs to measure the relative intensities of the light resulting from transitions between energy levels of a Rydberg series in HeI. These intensities are converted to populations using calculated transition probabilities. The logarithm of the population is then plotted as a function of the electron binding energy of the excited states. If the plot is linear, the population of the energy levels may be described by a

Boltzmann temperature. It may turn out that only some of the levels can be described by this temperature. This is the case for the light emitted from a helium plasma with electron densities between  $10^9$  and  $10^{13}$   $\text{cm}^{-3}$  (Collins and Robertson, 1964a and Hinnoy and Hirschberg, 1962).

These researchers have found that for a principle quantum number  $n$  greater than  $6 \pm 1$ , the levels of HeI are in a Boltzmann equilibrium. Furthermore, they conclude that the temperature measured by the above procedure was the plasma electron temperature, proving that the levels are in a Boltzmann-Saha equilibrium. Their measured electron temperature was about 1400 K (0.1eV). For  $n < 6$ , the experimental populations are much less than one would expect from those calculated from the Boltzmann-Saha equilibrium temperature.

Thus, the currently accepted explanation for the emission of atomic light from a helium plasma is divided into two regions, one for  $n > 6$ , and the other for  $n < 6$ . For  $n > 6$ , the mechanism is three-body recombination and its inverse process, ionization from an excited state.



$\text{He}^*$  represents a helium atom in any one of its energy states. The balancing between these two processes gives rise to Boltzmann-Saha equilibrium.

It is necessary to emphasize that the electron density in these helium plasmas ranges from  $10^9$  to  $10^{13}$   $\text{cm}^{-3}$ . For this density range, the limiting form to recombination is three-body or collisional recombination (Bates and Dalgarno, 1962).

For  $n < 6$  the major contribution to the population of the He levels results from transitions between bound states through super-elastic and inelastic collisions with electrons.



One must know the collisional transition probabilities in order to apply this part of the theory to the experimental data. In addition to these two mechanisms, other secondary methods which populate and depopulate levels may be trapped resonant radiation, cascading and radiative decay.

Recently Thornton (1968) has completed an exhaustive experimental and theoretical investigation of the problem. The importance of his experimental observation that he reported a bimodal electron distribution consisting of a low energy group of electrons (0.1eV) and a higher energy group of electrons ( $10 \pm 5\text{eV}$ ) whose density is one to two orders of magnitude less than the lower energy group. The conductivity of the plasma is controlled by the density of the low energy group of electrons while the plasma itself is maintained by the less numerous group of high energy electrons.

Thornton's theoretical fit to the experimental data consisted of solving a many term (about ten) rate equation for the level population as a function of the binding energy of the excited electron. Some of the energy exchange processes included in his theory are ionization and recombination of electrons, superelastic and inelastic collisions with electrons, and radiative decay. The essential difference between this theory and others is the treatment of the electron distribution as bimodal. He fits his data for  $n=3$  to  $n=10$  with two models. Both of these models are complicated and involve many energy exchange processes.

Therefore, the problem is basically theoretical and may be stated as follows: Is it possible to fit the experimental data for the population of energy levels in a helium plasma with a simple closed expression as a function of the principle quantum number? What follows is an attempt to solve this problem. The working model is called the "two electron temperature model" and assumes that the plasma consists of helium atoms and ions, and a non-Maxwellian distribution of electrons approximated by two independent Maxwellian electron distributions. The electron-electron relaxation time between these two groups was calculated and demonstrates that this time is sufficient to allow the high energy electrons to exist long enough to participate in ionizing atoms before losing their energy to the low energy electrons. The only energy exchange processes which are built into the model are ionization and recombination.

### 3.2 Experimental Results

The  $2s\ ^3S - np\ ^3P^o$  series in orthohelium was selected for observation because of the large range of binding energy available to the excited electron in this series, and because the light from most of its levels could be detected in the laboratory (from  $n=2$  to 16). It is striking to note that nowhere in the literature does a complete population study of this series exist. Most researchers have chosen the  $2p\ ^3P^o - nd\ ^3D$  series for their investigation because the wavelengths of the spectral lines emitted in this series are located in a region where accurate measurements can be made with a minimum of difficulty. But, as can be seen from the partial energy level diagram for HeI (Fig. 3.1), the lowest value of the principle quantum number for this series is three, and thus the available binding energy for the electron is reduced by a factor of nine fourths. As will be seen, this extension of the electron binding energy range will provide information that will greatly influence the interpretation of the experimental data.

The measured relative population density of state  $n$  in arbitrary units is proportional to the product of the intensity ( $I_{nn'}$ ) and wavelength ( $\lambda$ ), and inversely proportional to the atomic transition probability ( $A_{nn'}$ ).

TABLE 3.1 HeI  $2s\ ^3S - np\ ^3P^o$  series.

n	Wavelength A	Transition Probability sec <sup>-1</sup>
2	10830.3	$0.109 \times 10^8$
3	3888.65	0.121
4	3187.74	0.059
5	2945.10	0.031
6	2829.08	0.018
7	2723.19	0.012
8	2696.12	0.008
9	2677.14	0.006
10	2663.27	0.004
11	2652.85	0.003

$$N_n \propto \frac{\lambda I_{nn'}}{A_{nn'}}$$

3.2

This relationship is valid only when the radiation density in the plasma is small enough that induced emission is negligible (Condon and Shortley, 1963). Since the wavelength for the transitions in helium are well known (Martin 1960), the error in  $N_n$  is in the measured intensities and calculated transition probabilities.

The transition probabilities were calculated from a prescription described by Goldberg (1939). The results of the calculation agreed favorably with the values published by the National Bureau of Standards (Wiese, 1966). The estimated accuracy of the values obtained from Goldberg's procedure is 10%. The results of the calculation are shown in Table 3.1.

The accuracy to which the relative intensity of the lines could be measured depends upon their wavelengths (see Fig. 3.1). Light from the  $2s \ ^3S - 2p \ ^3P^0$  transition has a wavelength of 10,830 Å and was detected by a RCA 7102 liquid nitrogen cooled photomultiplier tube, coupled to a scanning monochromator with a 7500 Å blaze grating. The estimated accuracy of measuring the intensity of this line relative to the  $2s \ ^3S - 3p \ ^3P^0$  (3889 Å) is 30%. The relative intensity of the lines whose wavelengths range from 2800 to 4000 Å can be measured with an accuracy of 10%. For transitions with wavelengths less than 2800 Å, the experimental error of the measured intensities

Figure 3.1

Partial energy level diagram showing the decay scheme for two Rydberg series in orthohelium;  $2s\ ^3S - np\ ^3P^o$  and  $2p\ ^3P^o - nd\ ^3D$ . The  $2s\ ^3S$  state is metastable.  $E_n$  is the energy above the ground state (not shown on diagram) and  $X_n$  is the binding energy of the excited electron. Since the first ionization potential for He is 24.59eV,  $X_n = 24.59 - E_n$ . Noted on the diagram is the approximate wavelengths of the series limit.

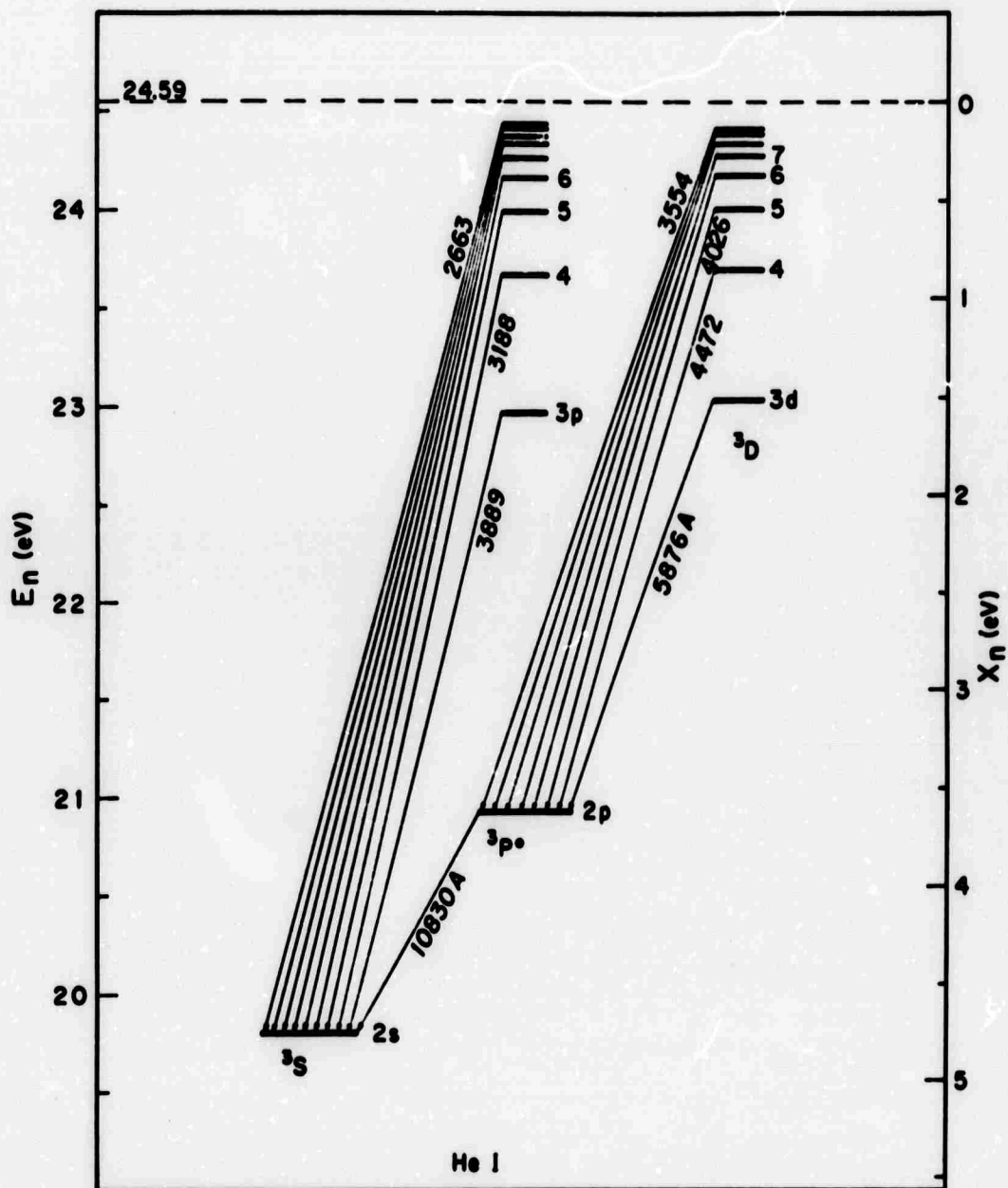
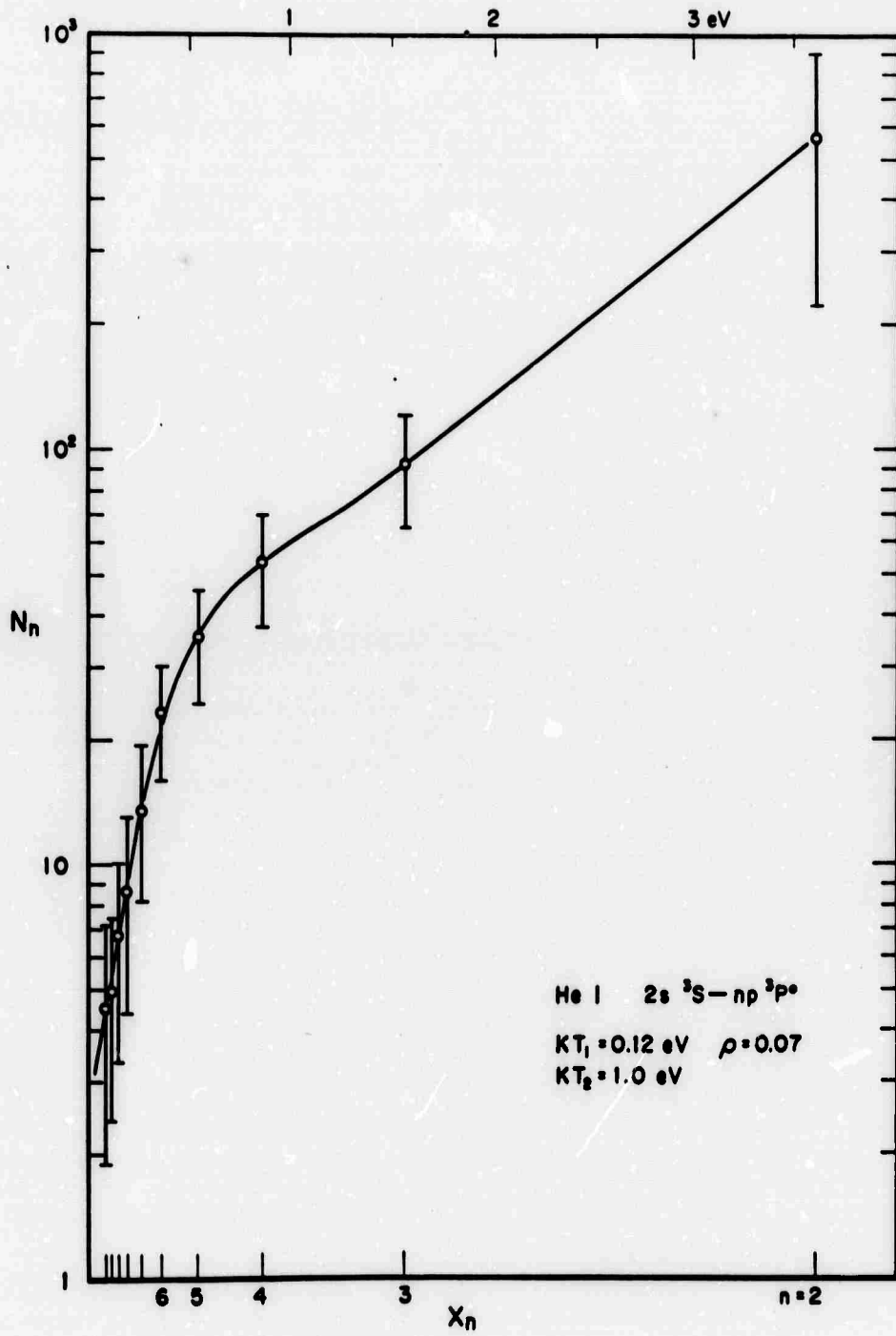


Figure 3.2

The relative population density (arbitrary units) observed at position #1 in the afterglow as a function of the electron binding energies of the  $np \ ^3P^o$  states. The pressure was one torr and the electrode current was 500 ma. The errors of the points shown on the figure for  $n=2$  and near the series limit are larger than those for  $n=3$  to 6 because of the increased uncertainty in the measured relative intensities in the respective spectral regions. The solid line represents the value of the calculated populations based on the two electron temperature model. The values for the parameters used in this calculation are shown on the figure.



increases since it is difficult to find a calibrated source for this region. The quartz-iodine or tungsten lamp normally used is not accurate in this region because the lamp intensity is very weak. A calibrated mercury source might help (Childs, 1962), but the error is still quite large in this region (greater than 30%) as compared with the region of above 2800 Å.

The experimental results for the relative population density of the  $np\ ^3P^o$  series of helium are shown in Fig. 3.2. The light was observed at position #1 in the afterglow (see Fig. 2.1) at a pressure of 1 torr and an electrode current of 500 ma. The solid line shown on the figure represents the value of the calculated populations based on the two electron temperature model. The significance of the parameters will be discussed in section 3.4 along with the dependences of the parameters on electrode current, pressure, and spatial changes.

### 3.3 Development of the Two Electron Temperature Model

As seen in Fig. 3.2, the experimental points for  $n > 6$  can be described by an electron temperature of 1400 K (0.12eV), while the points for  $n < 5$  can be described by a temperature of 11,500 K (1.0eV). Knowledge of the population of the  $2s\ ^3S - 2p\ ^3P^o$  transition helped verify this last fact. Thus, it is this empirical description of the population versus binding energy graph that provides the motivation for the two electron temperature model.

Before considering the problem of the bimodal electron distribution, it will be helpful to discuss the entire problem using a single electron distribution in which the electrons are in thermal equilibrium. Consider a perfectly insulated box containing helium atoms, helium ions and electrons at temperature  $T$ . The particles inside the box are uniformly distributed in configuration space, the total charge is zero and the electron density  $N_e$  is equal to the ion density  $N_i$ . In addition, we assume that the electrons can be described by a Maxwell-Boltzmann distribution function at a temperature  $T$ . In order for this assumption to be realized, the average de Broglie wavelength of the electrons must be less than the average particle separation:

$$h/\sqrt{2mkT} (N/V)^{1/3} \ll 1$$

Thus, as long as this inequality is satisfied, the Fermi distribution function for electrons goes to its classical limit, the Maxwell-Boltzmann function.

We require that the electron density be of the order of  $10^{12} \text{ cm}^{-3}$  so that the major mechanisms occurring in the box are three-body recombination and its inverse process (Bates and Dalgarno, 1962) (see equation 3.1). All other energy exchange mechanisms are assumed to be relatively unimportant. Thus, the only processes with which the particles interact are ionization and recombination by electrons. For this situation, the population of atoms in state  $n$ ,

$N_n$ , may be written in terms of the electron density  $N_e$ , the ion density  $N_i$ , and the electron temperature  $T$ :

$$N_n = g_n \frac{N_e}{g_e} \frac{N_i}{g_i} (h^2 \beta / 2\pi m)^{3/2} \exp(\beta X_n) \quad 3.3$$

where  $\beta = (kT)^{-1}$  and  $k$  is Boltzmann constant,  $m$  is the electron mass, and  $g_n$ ,  $g_i$ ,  $g_e$  are the statistical weights of the atoms, ions (2 for HeII) and the free electron.  $X_n$  is the binding energy of the electron in state  $n$ , and for helium it is given by

$$X_n = 24.586 - E_n,$$

where 24.586 is the first ionization potential for helium in electron volts and  $E_n$  is the energy of level  $n$  above the ground state.

Equation 3.3 was first developed by Saha who applied it to the study of ionization in stellar atmospheres (Fermi, 1966). Fermi derived the Saha equation by writing the Helmholtz free energy for the system discussed above and applying the condition for thermodynamic equilibrium which requires that the free energy be a minimum.

It will be useful to know the three-body recombination coefficient as a function of the electron density and temperature. The steady state rate equation for the processes described by equation 3.1 is

$$\frac{dN_n}{dt} = R_n - N_n C_n = 0$$

where  $R_n$  is the recombination rate in units of  $(\text{sec} - \text{cm}^3)^{-1}$  and  $C_n$  is the probability of ionizing an atom in state  $n$ . (See page 36 for justification of this rate equation.) The recombination coefficient for state  $n$ ,  $\alpha_n$ , is defined by the expression

$$R_n = N_i N_e \alpha_n$$

and has units of  $\text{cm}^3/\text{sec}$ . Thus, from the above rate equation and the Saha equation

$$\alpha_n = \frac{\epsilon_n}{\epsilon_e \epsilon_i} (h^3 \beta / 2\pi m)^{3/2} \exp(\beta X_n) C_n \quad 3.4$$

By assuming the major processes occurring in the box are the processes described by equation 3.1, we have calculated the three-body recombination coefficient. Actually, the steady state requirement is not necessary to derive  $\alpha_n$ ; it can be derived by using a less restrictive method, the principle of detailed balancing.

The probability of ionizing an atom in state  $n$  can be calculated using classical transport theory (Huang, 1963). Considering binary collisions between the free electrons and atoms of level  $n$ , the number of collisions,  $Z_n$ , per second per unit volume is (Huang equation 5.1):

$$Z_n = \iint d^3v_a d^3v_e \sigma_n v_e f_a f_e$$

where  $f_a$  and  $f_e$  are the distribution functions of the atoms and electrons.  $v_a$  and  $v_e$  are the velocities of the electrons and atoms. After integrating over the velocity space of the atoms, and using a Boltzmann electron distribution function in terms of energy,

$$Z_n = \sqrt{8/m\pi} N_n N_e \beta^{3/2} \int_0^{\infty} \sigma_n(E) E \exp(-\beta E) dE \quad 3.5$$

$\sigma_n(E)$  is the cross section for ionizing an atom in state  $n$ , and is taken as being proportional to the square of the impact parameter  $d_n$  of an electron with energy  $E$  passing a bound electron with binding energy  $X_n$  (Hinnov and Hirschberg, 1962).  $d_n$  is given by the classical Thomson formula (Thomson, 1924):

$$d_n^2 = e^4/E (1/X_n - 1/E)$$

The cross section may be written as

$$\sigma_n(E) = \pi d_n^2$$

$$\sigma_n(E) = \pi e^4/E (1/X_n - 1/E) \quad 3.6$$

where  $e$  is the charge of the electron. The functional form, not the absolute magnitude of this cross section is of importance. Hence for this discussion the choice of the proportionality constant is arbitrary. Since a free electron with energy less than the binding energy has zero probability of ionizing an atom in classical theory,

the lower limit of the integral in equation 3.5 can be replaced by  $X_n$ .  $Z_n$  can be written as

$$Z_n = N_n C_n$$

where  $C_n$  in units of  $\text{sec}^{-1}$  is:

$$C_n = \pi e^4 \sqrt{8/\pi m} \beta^{3/2} N_e \int_{X_n}^{\infty} (1/X_n - 1/E) \exp(-\beta E) dE$$

By rewriting the integral in a more convenient form (substituting  $z = \beta(E - X_n)$ ),  $C_n$  becomes

$$C_n = 4\pi e^4 (\beta/2\pi m)^{1/2} N_e \exp(-\beta X_n) F_n(\beta)/X_n \quad 3.7$$

where

$$F_n(\beta) = \int_0^{\infty} \frac{z \exp(-z)}{z + \beta X_n} dz \quad 3.8$$

The integral  $F_n(\beta)$  cannot be integrated directly. It has the following limits:

$$\lim_{\beta \rightarrow 0} F_n(\beta) = \int_0^{\infty} \exp(-z) dz = 1$$

$$\begin{aligned} \beta &\rightarrow 0 \\ T &\rightarrow \infty \end{aligned}$$

Figure 3.3

Values of the integral  $F_n(\theta)$  as a function of the electron binding energy at different electron temperatures.

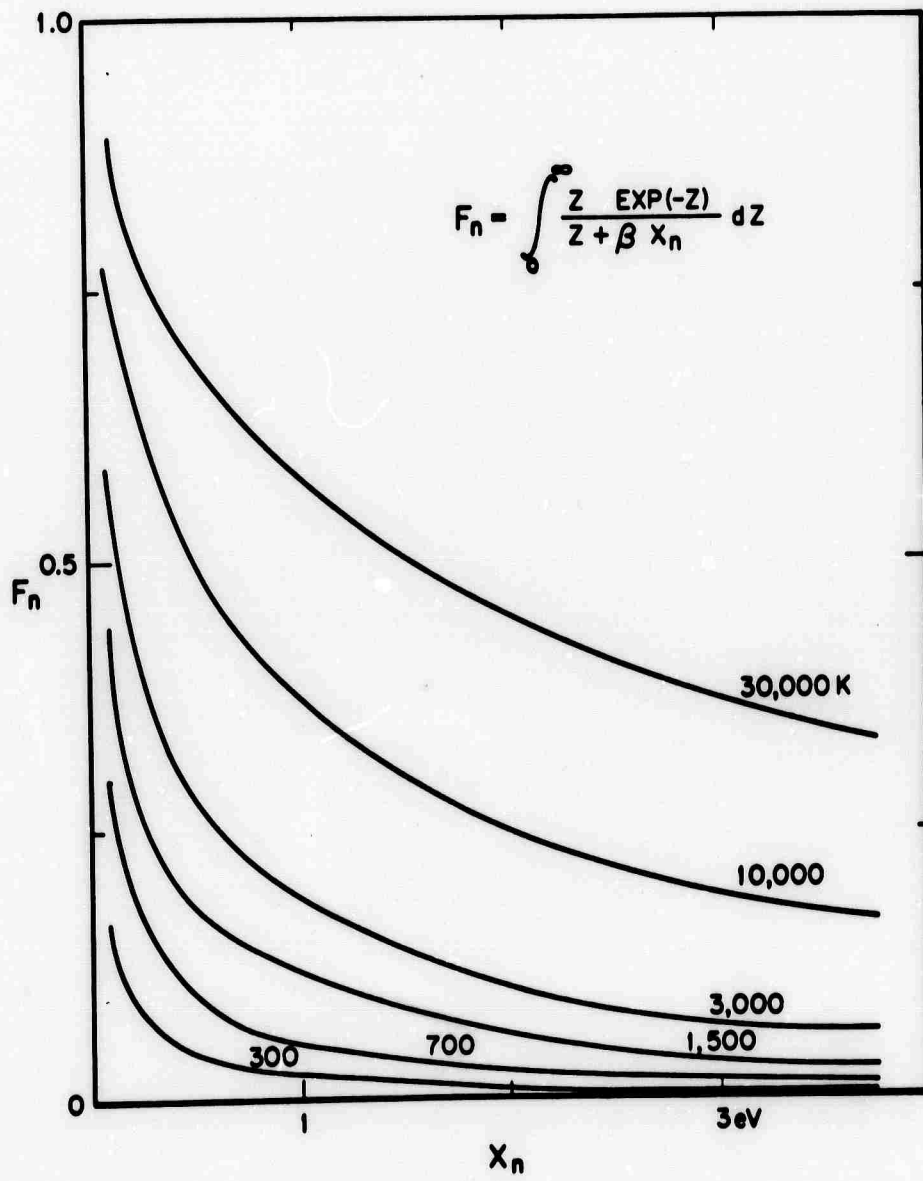


TABLE 3.2

Results of numerically integrating  $F_n(\beta)$        $F_n(\beta) = \int_0^{\infty} \frac{z \exp(-z)}{z + \beta X_n} dz$

n	$X_n$	T	300 K	700	1500	3000	10000	30000	$F_n$	$F_n$	$F_n$	$F_n$	$F_n$
		$\beta$	38.684 (eV) <sup>-1</sup>	16.579	7.737	3.868	1.161	0.387					
2	3.62 eV		0.00704	0.0161	0.0334	0.0629	0.168	0.340					
3	1.58		0.0158	0.0355	0.0709	0.126	0.292	0.500					
4	0.88		0.0278	0.0607	0.116	0.196	0.400	0.611					
5	0.56		0.0424	0.0898	0.165	0.264	0.488	0.668					
6	0.39		0.0589	0.121	0.213	0.326	0.558	0.744					
7	0.28		0.0787	0.156	0.264	0.388	0.619	0.789					
8	0.22		0.0966	0.187	0.305	0.435	0.661	0.817					
9	0.17		0.119	0.223	0.352	0.485	0.703	0.845					
10	0.14		0.139	0.253	0.388	0.523	0.733	0.863					
11	0.11		0.167	0.293	0.435	0.569	0.767	0.883					

$$\lim_{\substack{\beta \rightarrow \infty \\ T \rightarrow 0}} F_n(\beta) = 1/(\beta X_n) \int_0^{\infty} z \exp(-z) dz = 0$$

$$\begin{aligned} \beta &\rightarrow \infty \\ T &\rightarrow 0 \end{aligned}$$

Therefore, the temperature dependence of  $F_n(\beta)$  cannot be ignored. The results of numerically integrating  $F_n(\beta)$  are shown on Fig. 3.3 and in table 3.2.

The three-body recombination coefficient can now be written as:

$$\alpha_n = \frac{g_n}{g_e g_1} \frac{e^4 h^3}{\pi m^2} a^3 N_e F_n(\beta) / X_n \quad 3.9$$

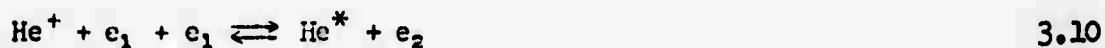
This is the desired result;  $\alpha_n$  is now given as a function of the temperature and density of the electrons. Note that the rate for three-body recombination,  $R_n$ , is proportional to the square of the electron density, since  $\alpha_n$  is proportional to  $N_e$ . This is what one would expect, since every time there is a recombination event it involves two electrons.

This concludes the discussion of the single mode electron distribution. The three-body recombination coefficient and the probability of ionizing an atom in state  $n$  have been derived as functions of the electron temperature and density. As stated in section 3.1, the single mode distribution is useful to explain the experimental data only when the principle quantum number is greater than six.

Now assume that the box contains helium atoms, helium ions, and

a non-Maxwellian distribution of electrons. As a first order approximation, we assume that this distribution can be expressed in terms of two non-interacting thermal electron distributions with different temperatures and densities. Also we assume that the most probable interactions among all the particles in the box are ionization from an excited state, and three-body recombination of electrons.

Futhermore, the electron group with the highest temperature will be the most likely one to participate in ionization, while the lower temperature group will be more likely to participate in recombination. Thus, the most probable energy exchange processes occurring in the box are



where  $e_1$  is a member of the low energy group, and  $e_2$  is a member of the high energy group of electrons. Equation 3.10 means that low energy electrons will recombine with ions and produce a high energy electron while leaving the atom in one of its energy states. This high energy electron can then ionize an atom in any one of its energy states and produce two low energy electrons. It may be possible that these two processes can maintain ionization in plasmas for some time. Factors working against these processes which are not built into the model are electron-electron relaxation, 'linked' diffusion of electrons and radiation. These processes and their experimental effects will be discussed in section 3.7 and 3.8.

The steady state rate equation can be written as:

$$\frac{dN_n}{dt} = N_i N_{e1} {}^1\alpha_n - N_n {}^1C_n + N_i N_{e2} {}^2\alpha_n - N_n {}^2C_n = 0 \quad 3.11$$

where the 1, 2 denote quantities which pertain to the low, and high energy group of electrons respectively. Terms which are concerned with the transfer of bound electrons during collisions between excited helium atoms and electrons are neglected in this rate equation. These terms are assumed to be negligible because the ionizing cross sections (from excited states) are large compared with the cross sections for the transfer of a bound electron. (It was difficult to justify this assumption because no theoretical or experimental information on ionization from excited states could be located.) Cascading terms are neglected because of the general shape of the population curve (Fig. 3.2) and because of the frequency to the fourth term present in the expression for the transition probabilities. Radiation terms are neglected because the ionizing collision time is less than the radiation time (see page 51).

Solving for  $N_n$ , we have

$$N_n = N_i N_{e1} \frac{({}^1\alpha_n + \rho {}^2\alpha_n)}{{}^1C_n + {}^2C_n} \quad 3.12$$

where  $\rho = N_{e2}/N_{e1}$ . Using equations 3.4 and 3.7, the population density becomes:

$$N_n = \text{Saha}_{N_n}(\beta_1, N_{e1}) \left( \frac{1 + {}^2F_n/{}^1F_n (\rho\beta_2/\beta_1)^2}{1 + r_n} \right)$$

where

$$r_n = {}^2C_n/{}^1C_n = \rho(\beta_2/\beta_1)^{1/2} ({}^2F_n/{}^1F_n) \exp(\beta_1 - \beta_2)X_n \quad 3.13$$

$\text{Saha}_{N_n}(\beta_1, N_{e1})$  is the Saha population for the low energy group of electrons given by equation 3.3. It is useful to rewrite equation 3.12 as

$$N_n = b_n \text{Saha}_{N_n}(\beta_1, N_{e1}) \quad 3.14$$

where

$$b_n = \frac{1 + {}^2F_n/{}^1F_n (\rho\beta_2/\beta_1)^2}{1 + r_n}$$

and

$$N_n = \left( \text{Saha}_{N_n}(\beta_1, N_{e1}) + r_n \text{Saha}_{N_n}(\beta_2, N_{e2}) \right) 1/(1 + r_n) \quad 3.15$$

Table 3.3 lists the values of the pertinent quantities discussed above for  $T_1 = 1400$  K,  $T_2 = 11,500$  K and  $\rho = 0.07$ . The results for  $N_n$  are shown by the curve in Fig. 3.2. The population density can be calculated as a function of the principle quantum number given the

TABLE 3.3

$n$	$T_1 = 1400 \text{ K}$ (0.12 eV)	$T_2 = 11,500$ (1.0 eV)	$\rho = 0.07$			
$n$	$\chi_n$	$r_n$	$b_n$	${}^2F_n$	${}^1F_n$	${}^3F_n/\chi_n$
2	3.62 eV	$1.12 \times 10^{10}$	$8.96 \times 10^{-11}$	0.186	0.033	5.7
3	1.58	$6.21 \times 10^9$	$1.61 \times 10^{-4}$	0.317	0.069	4.6
4	0.88	$3.97 \times 10$	$2.46 \times 10^{-2}$	0.427	0.114	3.8
5	0.56	3.63	$2.16 \times 10^{-1}$	0.516	0.162	3.2
6	0.39	$9.60 \times 10^{-1}$	$5.10 \times 10^{-1}$	0.586	0.210	2.8
7	0.28	$4.17 \times 10^{-1}$	$7.06 \times 10^{-1}$	0.642	0.258	2.5
8	0.22	$2.38 \times 10^{-1}$	$8.08 \times 10^{-1}$	0.688	0.304	2.3
9	0.17	$1.61 \times 10^{-1}$	$8.61 \times 10^{-1}$	0.725	0.347	2.1
10	0.14	$1.20 \times 10^{-1}$	$8.93 \times 10^{-1}$	0.756	0.387	2.0
11	0.11	$9.57 \times 10^{-2}$	$9.13 \times 10^{-1}$	0.782	0.424	1.8

three parameters, the temperatures of the two distributions and the relative density between them.

From equation 3.15 and the values of  $r_n$  from table 3.3, the asymptotic limits of  $N_n$  are:

$$\lim_{n < 5} N_n = \text{Saha}_{N_n}(e_2, N_{e2}) \quad \text{since } r_n > 1,$$

$$\lim_{n > 6} N_n = \text{Saha}_{N_n}(e_1, N_{e1}) \quad \text{since } r_n < 1.$$

The above asymptotic behavior means that the logarithm of the population density should approach a linear dependence as a function of the electron binding energy for both large and small  $n$ . This can be seen in Fig. 3.2.

It is necessary to consider the following when studying the asymptotic behavior for  $n > 6$ . For the present situation, the Saha equation provides a valid description of the level population for a value of the principle quantum number of less than thirteen. The population of the levels for  $n > 13$  is less than one would expect from the Saha equation because the electron binding energies for  $n > 13$  fall within the range of the energy spectrum of the room temperature ambient gas of the plasma. In other words, a significant fraction of ambient gas atoms have sufficient energy to ionize helium atoms which are populated in these states. In addition, an

estimate of the time between collisions indicates that it is less than the radiative lifetime ( $10^{-5}$  sec) of excited helium atoms for  $n > 13$ . Thus, for these states, collisions with the room temperature helium atoms should be taken into account.

### 3.4 Data Interpretation

The two electron temperature model for the population density (equation 3.15) was fit to the experimental data by using a computer program which finds a least-squares estimation of nonlinear parameters (Marquardt, 1963). The program adjusts the parameters to minimize the sum of the squares of the difference between the theoretical model and the experimental data. The best fit of the data was obtained when the data points were weighted by the square of the reciprocal of the error per data point. This was important in the present experiment since the error per data point varied considerably (see section 3.2). The results of this fit are shown on Fig. 3.2. Table 3.4 indicates the results of parameterizing the experimental data which was taken at different electrode currents and two positions in the afterglow. The estimated accuracy of the temperatures indicated in the table is  $\pm 15\%$ . All data was taken at a pressure of one torr and a helium flow rate of approximately  $6 \times 10^{21}$  atoms per sec (275 atm-cc/sec).

The values for  $T_1$  are in good agreement with other workers. Collins and Robertson (1964a) reported a value of 1700 K (0.15eV) for the temperature of the low energy group of electrons in a

TABLE 3.4

	#1 ←	Position in Afterglow	→	#2
			Current	
			100 ma	
$T_1$	1400 K			940 K
$T_2$	11400			10000
$\rho$	0.11			0.12
$T_1$	1400 K		250	1100 K
$T_2$	11400			9700
$\rho$	0.08			0.11
$T_1$	1400 K		500	1700 K
$T_2$	11500			10100
$\rho$	0.07			0.2

flowing helium afterglow at a pressure of 20 torr. This is a typical value for the parameter  $T_1$  (see section 3.9). The temperature of the low energy group of electrons remained fairly constant through spatial and electrode current changes, as can be seen from table 3.4. The main source of the low energy electrons is ionization, as can be seen from equation 3.10. In addition, a few low energy electrons will result from elastic collisions with high energy electrons (see section 3.7).

As seen from table 3.4, the temperature of the high energy group increased slightly when measured closer to the discharge, but did not change when the electrode current was varied. The value of  $T_2$  is about  $10^4$  K (1eV), just about one order of magnitude greater than  $T_1$ . The only results which are available for comparison are those of Thornton (1968). He measured the temperature of the high energy electrons in a solenoidal-coil type rf discharge tube to be  $10 \pm 5$ eV by using a double Langmuir probe. A comparison between this result and the result of the present experiment may not be meaningful since the latter applied to the afterglow region rather than to the discharge. The method of measurement is also different; Langmuir probe measurements tend to be higher than the actual electron temperature (Powers, 1966), while spectroscopic measurements based on the Saha equation are more accurate since the plasma is not perturbed by the presence of a probe.

To a large degree, the value of  $T_2$  depends on the energy level

structure of the helium atoms. This is illustrated by considering the source of the high energy electrons. As discussed in section 3.1, the higher energy electrons are produced during three-body recombination. The energy which is released during the capturing of a low energy electron is transferred to a second electron (the third body). The magnitude of this released energy depends on which energy state the helium atom is left in after the recombination event. Thus, the energy spectrum of the electrons depends on the value of these various energy states in the helium atom. Furthermore, repeated ionization by a high energy electron may explain why the distribution for the high energy electrons appears to be thermal. For example, a 20eV electron may ionize many atoms which are populated only a few electron volts from the ionization limit prior to losing its energy.

Before discussing the significance of the changes in  $\rho$ , the density ratio of high energy electrons to low energy electrons, it is necessary to point out that the intensity of the light emitted from position #1 was about nine times the intensity of the light emitted from position #2. Using equations 3.2 and 3.3 and from the fact that the density of atomic helium ions is about equal to the electron density  $N_{e1}$  (Collins and Robertson, 1964a), the density of low energy electrons and the ion density were each about a factor of three larger at position #1 than at position #2. This will be useful in discussing the spatial changes of  $\rho$ .

As observed from table 3.4,  $\rho$  is slightly larger at position #2 in the afterglow. This means that the number of high energy electrons increases relative to the low energy ones as the distance from the discharge into the afterglow increased. Why should this be? One possible explanation is that this is just a matter of "name calling" since the temperature of the high energy electrons at position #1 is larger than the temperature at position #2. The energy contained in the high energy electron distribution at both positions in the afterglow may be about equal; there are either less electrons with more energy per electron, or there are more electrons with less energy per electron. However, there will be a point in the afterglow where  $\rho$  would begin to decrease with increasing distance from the discharge due to 'linked' diffusion and relaxation of the high energy electrons (see section 3.7 and 3.8). It would be helpful to study the spatial dependence of  $\rho$  in more detail.

Pressure studies of the intensity of the light emitted from the plasma were not made. All data was taken at a pressure of one torr. A pressure dependence may be predicted by using the ideal gas approximation that the ion density is directly proportional to the pressure. Using equation 3.2, 3.3 and 3.14 and the fact that the ion density is about equal to the low energy electron density, the pressure (P) dependence of the light intensity (I) may be written as:

$$I \propto P^a \quad \text{where } 1 < a < 2$$

This assumes that no other energy exchange processes will occur as the pressure varies. For example, in the present source, a strong emission from a neon impurity is observed when the pressure is in the neighborhood of 10 torr. The energy exchange mechanism becomes more complicated and the assumption used to arrive at the above relationship may no longer be valid. In addition, as the pressure increases in the plasma, the intensity of light from molecular helium increases, indicating that the concentration of the helium molecular ion has increased (see section 3.9). Since the total charge of the plasma is zero, the assumption that densities of electrons and atomic ions are equal becomes less realistic.

More experimental studies are needed to help substantiate the above discussion. Variable ambient temperature and pressure measurements should be made. Absolute intensity measurements should be made in order to measure the density of the low energy electrons. Also spatial measurements of  $N_{e1}$  would be useful.

### 3.5 Application to Stellar Atmospheres

Saha first developed his equation to explain ionization in stellar atmospheres. Since in these atmospheres the electron density is about  $10^{12}$   $\text{cm}^{-3}$ , one probable mechanism for radiation of light is three-body recombination. Thus, the energy exchange mechanisms may be similar to those in the helium plasma, and the two electron temperature model may be useful in interpreting the

relative intensity of spectra from these atmospheres.

Aller (1968) writes the Saha equation in the following form:

$$N_n = b_n \text{Saha}_{N_n}(\beta_1, N_{e1})$$

where  $b_n$  is a factor which measures the degree of departure from thermodynamic equilibrium at the electron temperature  $T$ . This is the exact form of equation 3.14 where

$$b_n = \frac{1 + {}^2F_n/{}^1F_n (\rho\beta_2/\beta_1)^2}{1 + r_n}$$

It would be worthwhile to know if the data from stellar atmospheres could be interpreted with the three parameters used to describe the emission of atomic light from the helium plasma.

### 3.6 The Three-Body Recombination Coefficient

It is of interest to calculate the total recombination coefficient for electrons in the helium plasma as a function of the three parameters used to describe the two electron temperature model. From equation 3.12 an effective recombination coefficient can be written:

$$\alpha_n(\beta_1, \beta_2) = {}^1\alpha_n + \rho {}^2\alpha_n = (N_n/(N_1 N_{e1}))({}^1C_n + {}^2C_n)$$

where  $\Pi_n$  is given by equation 3.14. Using equations 3.7 and 3.9,  $\alpha_n(\bar{\epsilon}_1, \bar{\epsilon}_2)$  can be expressed as:

$$\alpha_n(\bar{\epsilon}_1, \bar{\epsilon}_2) = {}^1\alpha_n \left( 1 + \frac{{}^2F_n}{{}^1F_n} \left( \frac{\bar{\epsilon}_2}{\bar{\epsilon}_1} \right)^2 \right)$$

From table 3.3, it can be seen that the product of terms involving the ratio of the electron temperatures is much less than one. Thus  $\alpha_n(\bar{\epsilon}_1, \bar{\epsilon}_2)$  is essentially given by the recombination coefficient for the low energy electrons,  ${}^1\alpha_n$ . Substituting the value of the constants in equation 3.1, the total recombination coefficient  $\alpha$  may be written as:

$$\alpha = \sum_n \alpha_n(\bar{\epsilon}_1, \bar{\epsilon}_2)$$

$$\alpha(\text{cm}^3/\text{sec}) =$$

$$(1.0 \times 10^{-27}) \left( \frac{N_1 \bar{\epsilon}_1^2}{S_1 S_0} \right) \sum_{n=1}^{n_c} \left( {}^1F_n + \frac{{}^2F_n}{{}^1F_n} \left( \frac{\bar{\epsilon}_2}{\bar{\epsilon}_1} \right)^2 \right) C_n / X_n$$

where  $\bar{\epsilon}$  is in units of  $(\text{eV})^{-1}$  and  $X_n$  is in units of eV.

The cutoff value of the principle quantum number  $n_c$  is determined from the validity of the rate equation 3.11 from which the above expression was derived. This rate equation allows for ionization and recombination of electrons. Other mechanisms such as collisions with ambient gas atoms and molecules and transfer of bound electrons become important at larger values of the principle quantum number.

According to the discussion on page 37 and 40,  $n_0$  is about thirteen. In order to calculate the contribution to the recombination coefficient for terms with  $n > 13$ , the rate equation 3.11 must be modified to take into account other energy exchange mechanisms.

The recombination coefficient is most sensitive to the temperature of the low energy electrons since the probability is greater that the low energy electrons will recombine with helium ions rather than the high energy electrons. The contributions of the high energy electrons to the recombination coefficient is very small for the range of parameters used in the present experiment.

There are two features in the above expression which differ from existing theories. First is the inclusion of the bimodal electron distribution function approximated by the sum of two distribution functions at different densities and temperatures. Second, the presently accepted theory has assumed a constant value of  $2/5$  for the integral  $F_n$  defined by equation 3.5 (Hinnov and Hirschberg, 1962). As mentioned in section 3.3, this integral has a very definite temperature dependence which should be considered. More important, however, is the dependence of the integral on the principle quantum number. From table 3.3, it is seen that for a temperature of 1400 K, the value of this integral changes by a factor

factor of fifteen from  $n = 2$  to  $n = 11$ .

It is significant to note that the expression for the recombination coefficient was derived from evidence based on spectroscopic data. The temperature dependence of  $\alpha$  should be confirmed directly from experiment.

### 3.7 Electron-Electron Relaxation

An order of magnitude estimate of the relaxation time between two Boltzmann distributions of electrons is necessary to learn if the high energy group of electrons can last long enough in the plasma to lose their energy by ionizing helium atoms rather than by losing it through elastic collisions with the low energy group of electrons. The problem of electron-electron relaxation can be discussed using the formalism of Spitzer (1962, 1940). He considers the rate at which equipartition of energy is established between two groups of charged particles. Both groups are assumed to be described by a Boltzmann distribution function. Spitzer's results apply to fully ionized gases. It is assumed that these results apply to the present case (to within an order of magnitude) even though there is a large neutral density in the plasma. It is not the purpose here to give a detailed description of Spitzer's work, but only to present the results in order that they may be applied to the present problem.

The time constant for approach to equilibrium is taken as the

relaxation time  $t_r$ . By requiring conservation of energy, the following expression for  $t_r$  can be written (Spitzer equation 5-31):

$$t_r \approx \left( T_2^{3/2} / N_{e1} \right) \times 10^{-3} \text{ sec} \quad 3.16$$

where  $T_2$  is the temperature of the high energy electrons and  $N_{e1}$  is density of the low energy group. This expression takes into consideration the center of mass motion of the electrons, but is only valid when the temperature of the low energy group is much less than  $T_2$ . There is no problem in applying equation 3.16 to the present situation since

$$T_2/T_1 \approx 10$$

The estimated accuracy of  $t_r$  calculated by equation 3.16 is about one order of magnitude.

Knowledge of the electron density  $N_{e1}$  is the most important factor in determining the relaxation time since  $N_{e1}$  can vary as much as three orders of magnitude in various helium plasmas, while the temperature of the high energy electrons can vary only about a factor of two or three. The electron density can be measured by performing an absolute calibration of the light emitted from the plasma and by using equation 3.14. This measurement was not done for the present set of experiments because the value  $N_{e1}$  was not needed elsewhere in the discussion of the theory, and because of the inherent difficulty in this type of measurement. The density

of the low energy electrons was estimated to be on the order of  $10^{11}$   $\text{cm}^{-3}$  (Ferguson, et al. 1969). With this estimate of electron density and with a value for  $T_2$  of  $10^4$  K, the approximate value for the relaxation time is  $10^{-7}$  sec.

An estimate of the reciprocal of the collision frequency between the high energy electrons and the helium atoms in the plasma would give a meaningful comparison with the electron relaxation time. For a pressure of one torr and gas temperature of 300 K, the density of helium atoms is about  $10^{16}$   $\text{cm}^{-3}$ . Since we are assuming the primary mechanism in which electrons lose their energy is by ionizing helium atoms from an excited state, it is necessary to estimate the density of excited state atoms in the plasma. Assuming that one helium atom in ten thousand is in any state other than the ground state, the excited state density is about  $10^{12}$   $\text{cm}^{-3}$ . The collision frequency  $\nu$  for electrons colliding with excited helium atoms of density  $N$  can be written as:

$$\nu = \sigma N V \approx 10^7 \text{ sec}^{-1}$$

where  $\sigma$  is the ionization cross section determined from equation 3.6 to be about  $10^{-13}$   $\text{cm}^2$ , and  $V$  is the velocity of a 1eV electron,  $5.9 \times 10^7$  cm/sec. Thus, an order of magnitude estimate of the time between "ionizing" collision is about  $10^{-7}$  sec. It is important to note that the lifetime for excited states in helium ranges from  $10^{-7}$  sec for small values of the principle quantum number to  $10^{-5}$  sec for large values of  $n$ . Thus, the excited helium atoms will last

long enough to be ionized by this high energy electron.

The electron-electron relaxation time is about the same or slightly longer than the "ionizing" collision time. In summary then, the high energy electron lose their energy both by ionizing helium atoms and by elastic scattering with the low energy electrons.

### 3.8 'Linked' Diffusion of Electrons

It has been established that there are two electron temperatures in the helium plasma. Up to this point, it has not been necessary to discuss the ambient temperature of the plasma. This is because the electrons lose very little energy by elastic collisions with heavy particles. The average fractional energy loss per collision for electrons colliding with helium atoms is

$$2m/M \approx 0.0003$$

where  $M$  is the mass of the helium atom. The electrons must have many elastic collisions with the helium species in order to lose an appreciable amount of their energy. Thus, three temperatures can be used to describe the plasma: the ambient gas temperature (300 K) and two electron temperatures ( $10^3$  and  $10^4$  K).

The effect of the temperature difference between the electron and the ambient temperatures can be described by 'linked' diffusion of electrons (Hasted, 1964). If the plasma is contained in a bottle whose dimensions are greater than the Debye length for

electrons, the 'linked' diffusion is called ambipolar. For the present situation, the Debye length is about  $10^{-6}$  cm, while the container dimensions are on the order of centimeters. Thus, the electron diffusion is controlled by ambipolar diffusion. This means that the electrons move outward towards the walls where they remain or move along the surface until they finally recombine with positive ions. Eventually, the ions migrate to the walls because they find themselves surrounded by a new positive charge created by the absence of electrons, and they feel an attraction towards the walls from the excess amount of electrons present there. Hasted writes the temperature dependence of the ambipolar diffusion coefficient as:

$$D_a \propto T_{\text{gas}}^{1/2} (1 + T_e/T_{\text{gas}}) \quad 3.17$$

where  $T_e$  is the electron temperature, and  $T_{\text{gas}}$  is the ambient gas temperature.

Equation 3.17 means the higher the electron temperature is with respect to the gas temperature, the greater the diffusion of electrons. In addition, when two electron distributions are present, the higher energy group will diffuse more than the low energy group. The ratio of the diffusion coefficient for the two electron groups discussed in the present experiment is:

$${}^2D_a/{}^1D_a \approx 8$$

High temperature electrons diffuse to the walls about eight times faster than their low energy partners. It is this fact along with the electron-electron relaxation which explains why the ratio of the densities of the high energy group to the low energy group ( $n$ ) is less than one.

An apparatus similar to that shown in Fig. 2.1 was used to learn what the experimental results would be if the vessel containing the helium plasma were kept at liquid nitrogen temperature (77 K). The entire flow apparatus was surrounded with liquid nitrogen which was contained in a glass dewar. At the start, the plasma showed its characteristic pink color, but when the liquid nitrogen was added to the dewar, the afterglow was quenched. Pink light from the discharge region could still be seen, indicating that the electrons were absorbing energy from the electric field present in the discharge region. The quenching of the afterglow was due to the effects of ambipolar diffusion. When the gas temperature approached 77 K, the diffusion of the high energy electrons was increased by about a factor of two (see equation 3.17). Since it is these high energy electrons which maintain ionization in the afterglow, the increased diffusion brought on by reducing the gas temperature was sufficient to reduce the level of ionization to the point where equation 3.11 was no longer valid, and the atomic emission of radiation stopped. The rate of diffusion of the low energy electrons also increased, but since they are more numerous

than the high energy electrons, and their main function is to participate in recombination, their increased loss was not as important in maintaining the afterglow as was the reduction of their higher energy partners.

### 3.9 General Discussion of the Model

From the evidence presented, the bimodal electron distribution is a convenient method for describing the actual electron distribution function in the helium plasma. The high energy electrons do exist long enough to ionize atoms before relaxing to their low energy partners. Thus, the high energy electrons must be considered as another energetic species present in the helium plasma. This is verified in the following chapter where one of the mechanisms for producing excited atomic nitrogen involves collisions between these electrons and ground state nitrogen atoms.

The high energy limit for these electrons is the first ionization limit for helium (24.59eV). An electron with this energy is produced when a low energy electron is captured by a helium ion, and the resulting atom is left in the ground state. The excess energy is 24.59eV and is carried off by the high energy electron. Another possible mechanism for production of high energy electrons in the plasma involves superelastic collisions between electrons and the metastable helium species:



When a metastable atom collides with an electron, the metastable atom will de-excite to the ground state, imparting the excitation energy to the electron.

The energy distribution function for electrons described by the two electron temperature model can be written as:

$$\frac{dN_E}{dE} \propto E^{1/2} \left( B_1^{3/2} \exp(-E_1/E) + \alpha B_2^{3/2} \exp(-E_2/E) \right)$$

where  $E$  is the electron energy. A graph of the energy distribution function is shown in Fig. 3.4. From this figure one can understand why conductivity, microwave phase shift, and ordinary Langmuir probe measurements have failed to detect the small high energy tail indicated on the figure. These measurements are mainly sensitive to the more numerous low energy group of electrons.

Figure 3.4

The dotted curve is the Maxwell-Boltzmann energy distribution function for electrons at a temperature of 1400 K. The solid curve is the first order approximation to the actual energy distribution function for electrons in a helium plasma. It was calculated from the following parameters:  $T_1 = 1400$  K,  $T_2 = 11500$  K,  $\rho = 0.07$ .

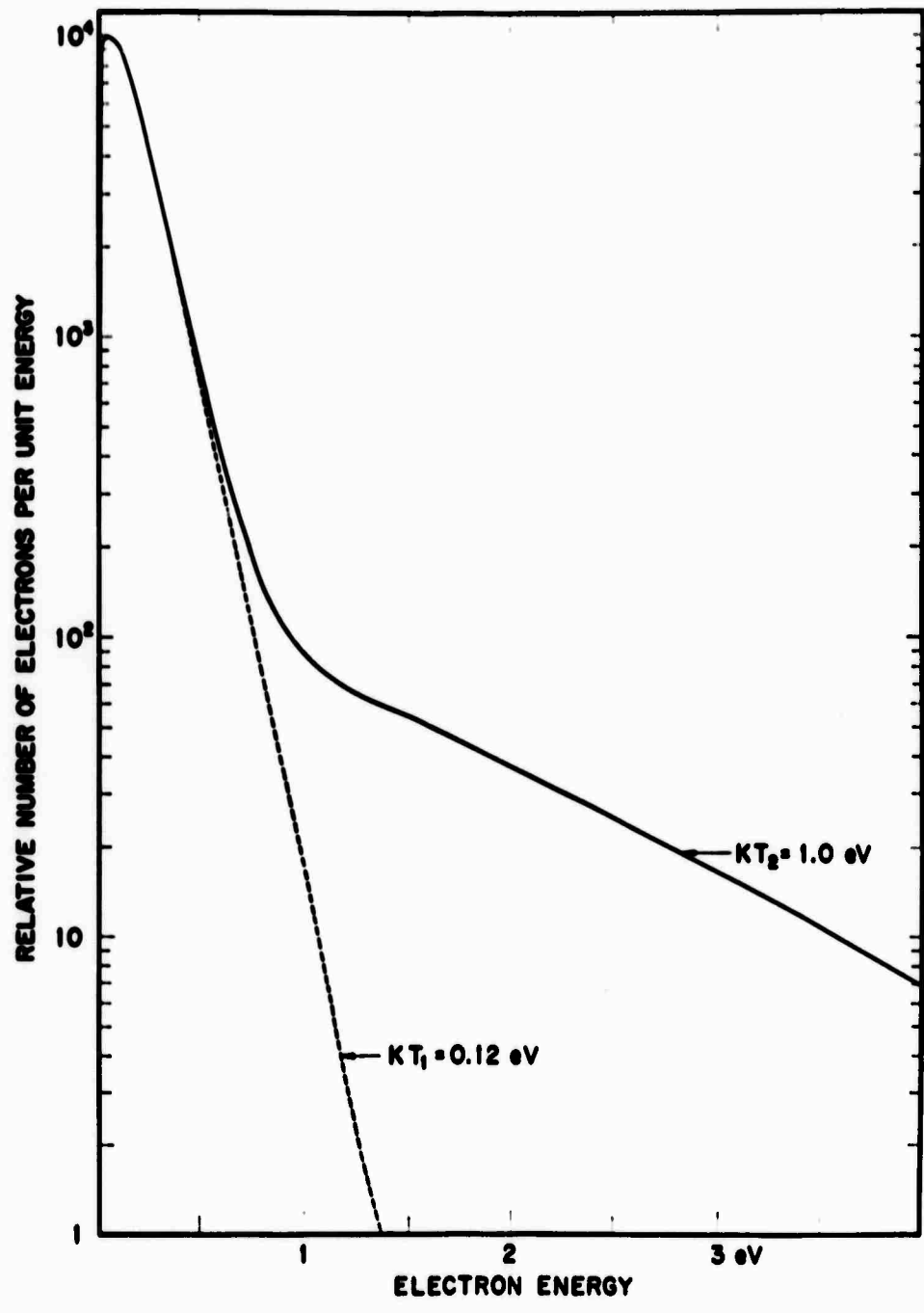
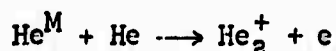


Fig. 3.5 shows the experimental data of Thornton fit by the two electron temperature model. He observed light from the  $nd\ ^3D$  series in a solenoidal-coil type rf discharge tube at a pressure of 0.037 torr. Thornton reported a value for  $kT_1$  of 0.1eV which is in agreement with the present analysis. His value for  $\rho$  was 0.03 as compared with the value of 0.05 from the present calculation.

Fig. 3.6 indicates the results of Hinnoy and Hirschberg's experiment in which light from the  $nd\ ^3D$  series in helium was observed from the magnetically confined quiescent afterglow of the B-1 stellarator. The time-resolved intensities of the light emitted from this series was observed during the peak of the afterglow, one half and one millisecond later at a pressure near  $10^{-3}$  torr. The curves shown on the figure represent the value of the calculated populations based on the two electron temperature model. The parameters used in the calculation are indicated on the figure. Hinnoy and Hirschberg reported similar values for  $kT_1$ . The value of the temperature for the high energy group of electrons may not be too meaningful since the range of the electron binding energy is limited for the  $nd\ ^3D$  series. It is important to note that the general relative position of the experimental points shown on this figure and figures 3.2 and 3.5 is the same whether the plasma was maintained by a rf or dc field, whether the light from the helium was observed in the discharge or afterglow, or whether a magnetic field was present.

It is pertinent to discuss the formation and destruction of the atomic metastable species in the plasma. These metastables are populated by the same method in which all other excited states are populated with the addition of cascading from the upper levels. The two main processes in which the metastable are de-populated are by superelastic collisions with electrons and by molecule formation. The latter is verified by the detection of  $\text{He}_2$  emission in the afterglow (see Fig. 2.3). Excited  $\text{He}_2$  is formed in the following reactions:



Collisions between metastable and ground state atoms forms  $\text{He}_2^+$  in the ground state. Light from molecular helium is produced by collisional-radiative recombination of  $\text{He}_2^+$  (Collins and Robertson, 1964b). Thus the presence of excited molecular helium can be traced to the basic mechanisms occurring in the plasma: ionization and recombination of electrons.

As stated previously, the helium plasma can be described by three temperatures: the ambient gas temperature, and two electron temperatures. The major factor in determining the

temperature of the high energy distribution is the internal energy level structure of helium. These electrons appear to be thermal because they are initially formed in a thermal distribution.

The main source of the high energy electrons is three-body recombination of electrons. Another source of these electrons may be superelastic collisions between metastable helium atoms and electrons. The energy of these high temperature electrons is dissipated in the plasma by ionization, by elastic scattering with low temperature electrons and by collisions with walls. The density of these electrons is less than the low energy group because of electron-electron relaxation and the increased rate of diffusion to the walls. The effect of this diffusion to the walls was increased by cooling the plasma until all emission from the afterglow stopped. A similar quenching result was observed when a rf field was directed towards the afterglow (see Fig. 4.5). As stated in section 2.3, the result of applying the rf field to the afterglow was to heat the low energy electrons. Both the cooling of the plasma, and the application of the rf field produced the same result because the ambipolar diffusion coefficient depends on the ratio of the electron to ambient gas temperatures. In the former situation, the diffusion coefficient for high energy electrons was increased by lowering the gas temperature, while in the latter, the diffusion coefficient for low energy became larger

by increasing the temperature of the low energy electrons. Thus, cooling the plasma reduced the amount of ionization to a level where the plasma could no longer sustain itself, and the application of the rf field inhibited recombination to the point where the plasma could no longer be maintained.

Spectroscopic evidence indicates that the distribution function used to describe the electrons in a helium plasma is bimodal consisting of a group of electrons described by a temperature which is approximately one order of magnitude greater than the temperature of a more numerous group of electrons. The density of the high temperature group is about one to two orders of magnitude less than the low temperature electrons, and it is this high temperature group which is responsible for maintaining ionization in the plasma. By assuming that the major energy exchange processes occurring in the plasma are ionization and recombination of electrons, it was possible to fit the experimental data for the population of energy levels with a simple closed expression as a function of the principle quantum number. The most significant experimental observation reported here is that the population of atomic helium energy levels for small values of the principle quantum number can be described by the Saha equation.

Figure 3.5

The relative population density (arbitrary units) observed in a solenoidal-coil type rf discharge tube at a pressure of 0.037 torr as a function of the electron binding energies of the nd <sup>3</sup>D states (Thornton, 1968). The curve represents the value of the calculated populations based on the two electron temperature model. The values of the parameters used in these calculations are shown on the figure.

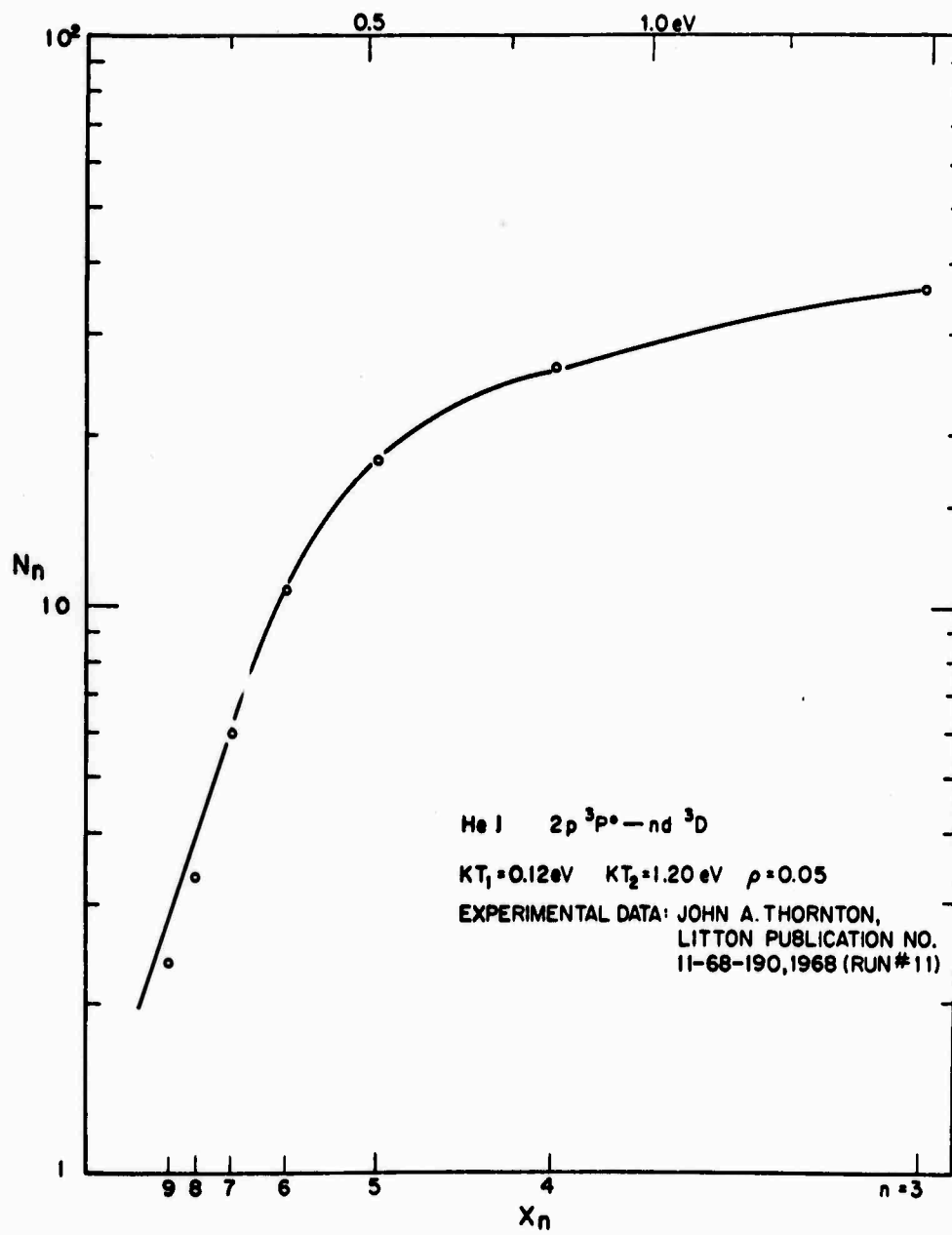
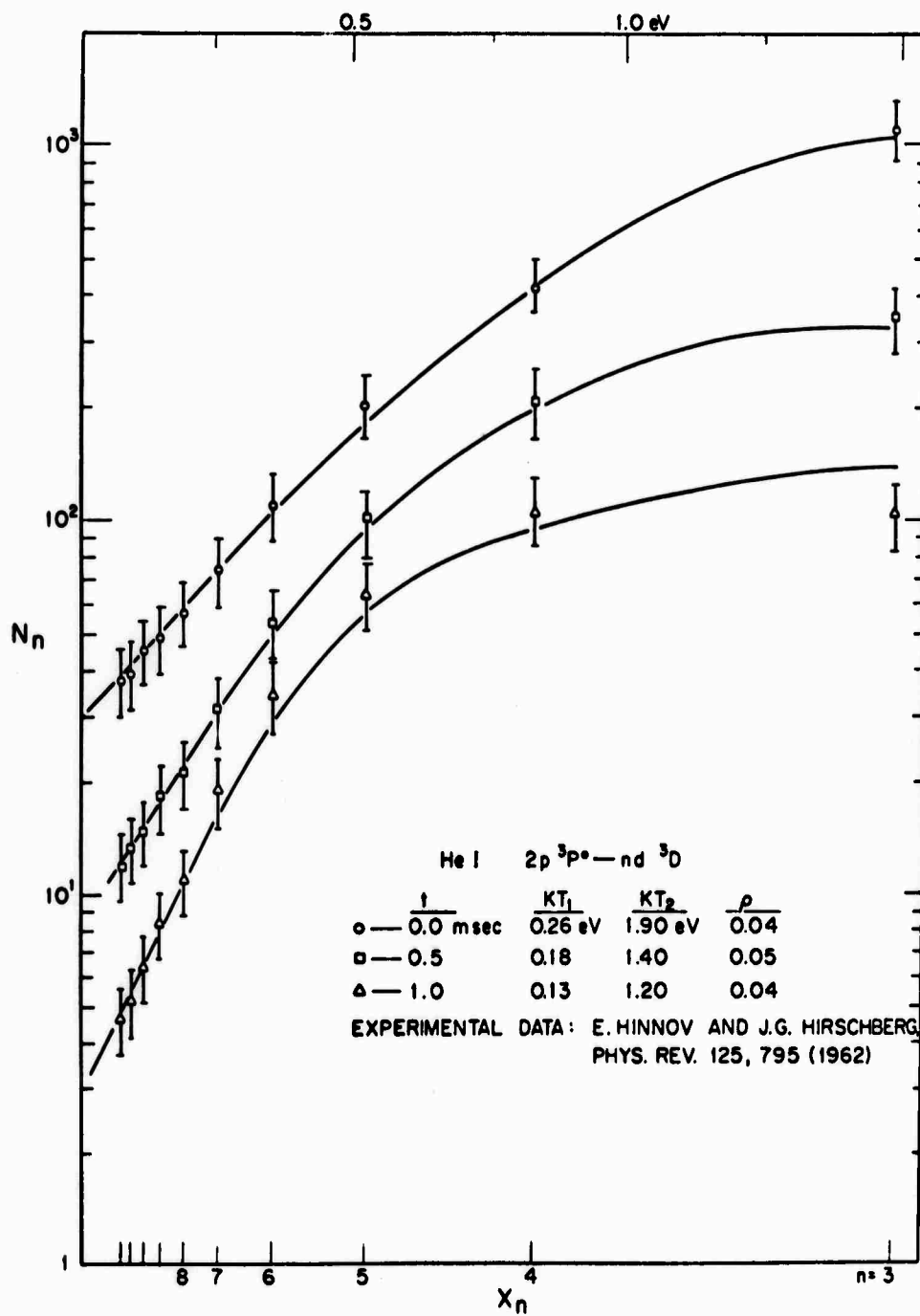


Figure 3.6

The relative population density (arbitrary units) observed in the quiescent afterglow of the B-1 stellarator at a pressure near  $10^{-3}$  torr as a function of the electron binding energies of the nd  $^3D$  states (Hinnov and Hirschberg, 1962). The three sets of data represent  $N_n$  at the peak of the afterglow (denoted 0.0 m sec on the figure), and 0.5, 1.0 milliseconds later. The curves represent the value of the calculated populations based on the two electron temperature model. The values of the parameters used in these calculations are shown on the figure.



#### IV ATOMIC NITROGEN

##### 4.1 Spectra and Data

Figure 4.1 is a spectrum of atomic nitrogen from 3800 to 8800 Å under the green glow condition. It was taken when molecular nitrogen was injected into the helium afterglow at gas inlet #2 with an approximate flow rate of 15 atm-cc/sec. The ambient pressure was 1.0 torr, the electrode current was 500 ma, and the ratio of helium to molecular nitrogen was about 20. In order to achieve the cleanest and brightest condition for atomic nitrogen emission, the gas inlet #2 was rotated 180° from the position shown in Fig. 2.1. The atomic nitrogen glow appeared green to the eye and had a long tail (similar to a comet tail) about 6 to 12 inches in length. The intensity of individual NI lines in the spectral region between 5000 to 6000 Å was two or three orders of magnitude less intense than atomic emission from the helium afterglow in the same region (see Fig. 2.3).

The intensity of NI was extremely sensitive to the application of a rf field. A very small amount of rf power would quench the atomic emission completely, indicating that electrons and ions must be important in populating the atomic nitrogen states. It is known

from similar experiments (Collins and Robertson, 1961c) that the energy of the atomic helium ion is dissipated by the reaction:



Thus a probable mechanism for populating nitrogen atoms is:



Recombination with two electrons, or three body recombination, was eliminated as a possible mechanism because the electron density in the region of the NI glow was too low. This can be shown by appealing to charge conservation, using the Saha equation (3.3) and the fact that the intensity from the atomic helium in the region of the NI glow was reduced about 3 orders of magnitude (see Fig. 2.3). In addition, single electron recombination is a slow reaction compared to three body recombination and thus this mechanism seems to fit with the appearance of the NI plasma described above.

Photoelectric survey spectra were taken of the green NI glow under the conditions described above from 3500 to 10,500 Å using an Ebert scanning monochromator with various gratings and optical filters. Resolution of the spectra varied from 1.0 to 0.1 Å, depending on the spectral region. In addition to the NI emission, the spectra consisted of light from HeI, NeI, N<sub>2</sub>, N<sub>2</sub><sup>+</sup> and intense lines of CrI and FeI. Light from the atomic nitrogen comprised at least 90% of the total radiation emitted in the visible and near infrared. The source of chromium and iron was electrode sputtering. This NI

source is unique in that no radiation was detected from excited states of the nitrogen ion, yet radiation from energy levels near the ionization limit of the neutral atom were observed. These facts also fit with the electron recombination mechanism discussed above.

The results of the survey spectra are listed in Appendix I. Two wavelength "finding lists" were used to help in identifying the spectra (Moore, 1950; Striganov and Sventitskii, 1968). The data listed in Appendix I is composed of the NI lines and the lines of HeI, CrI, FeI and NeI which were used to calibrate the wavelength scale. Other lines from these latter elements and bands from  $N_2^+$  and  $N_2$  were omitted from the tabulation. Wavelengths of calibrating lines are put in brackets. Inspection of Appendix I reveals that there are many lines which could not be identified from the wavelength finding lists. Most of these lines are believed to be unclassified lines which originate from transitions whose upper levels are near the ionization limit of the nitrogen atom. The reason for this can be seen from Fig. 4.8 where the population of the classified lines which originate from these levels is inverted. (This fact is also compatible with the single electron recombination mechanism.)

Striganov and Sventitskii have completed the latest and what appears to be an accurate finding list of the elements. Their references on NI included the latest and most pertinent papers on the subject. For these reasons their NI list was selected as the standard for the current list in Appendix I. (K. B. S. Eriksson of

the University of Sweden Lund, Sweden is currently preparing such a list for the visible but unfortunately it is not available at this writing).

The work of Kamiyama et al. (1942, 1940, 1939), which was not referred to in the Striganov reference, should be mentioned. They reported some NI lines which are not mentioned in Appendix I because it has been reported that a systematic error of 1.0 Å exists in their results (Eriksson, 1958).

The data listed in Appendix I is an "over all view" of the spectra shown in Fig. 4.1.

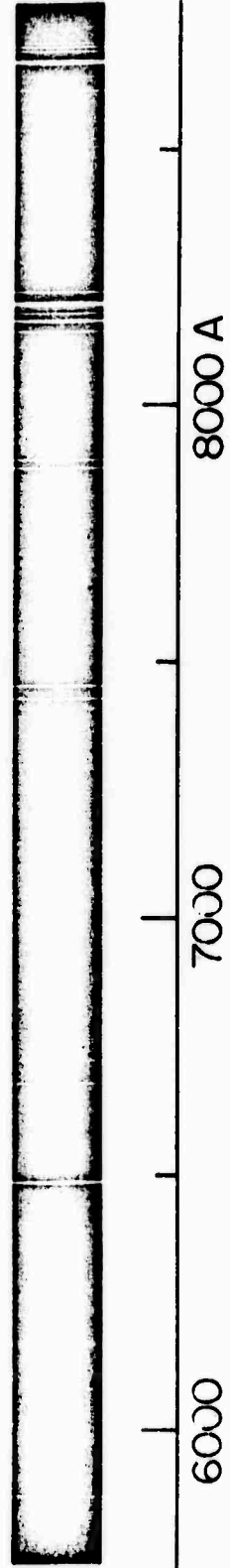
#### 4.2 Complete Energy Level Diagrams for NI

Figures 4.3 and 4.2 list the observed energy levels for atomic nitrogen. Figure 4.4 shows the spectral regions where the series limits may be found. From this figure, it can be seen that the short wavelength limit for NI lines occurs around 3300 Å. The data in the latter part of Appendix I list lines which may be new atomic nitrogen lines in the spectral region between 3400 - 3800 Å. This data should be analyzed in order to classify some of these lines. Because they are located in this spectral region, they probably originate from levels very close to the ionization limit.

The purpose in designing Fig. 4.4 was to make an energy level diagram which listed all states independent of their particular coupling schemes, and to facilitate the recognition of electric

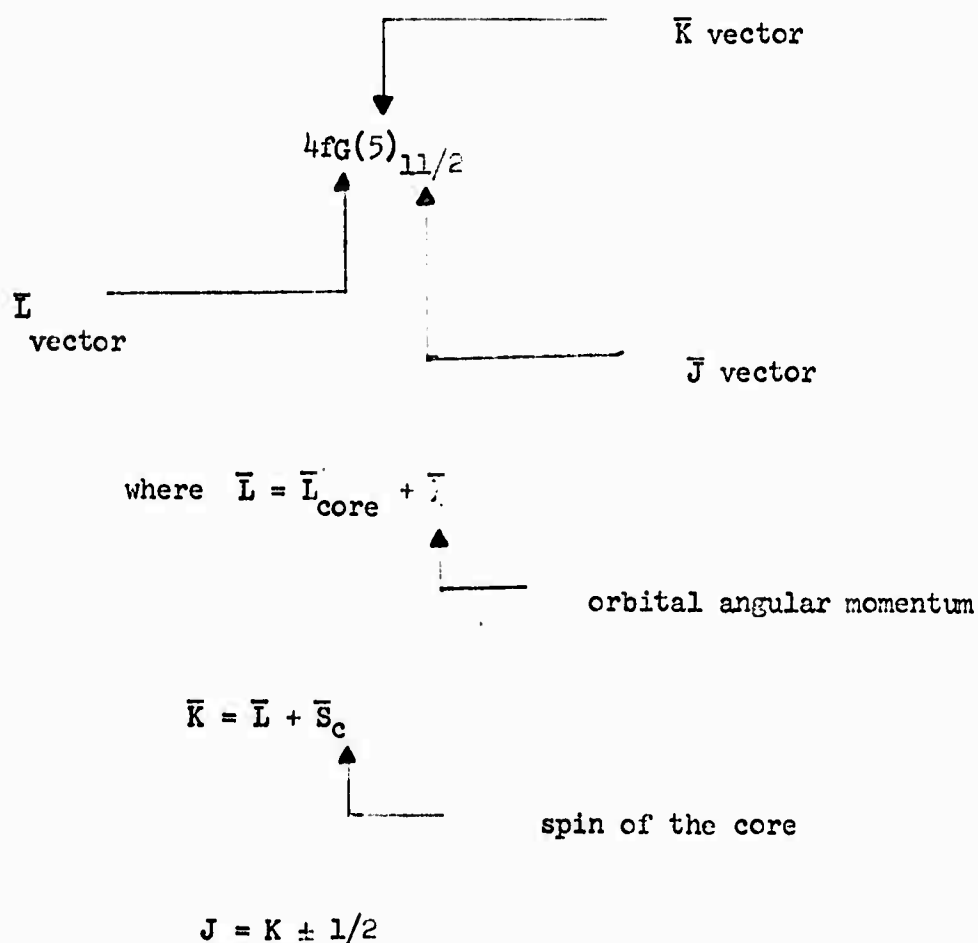
Figure 4.1

All spectra were taken with a Bass-Kessler f/5.6 grating spectrograph. The upper spectrum of pure helium was taken on an Eastman-Kodak 103 a-f plate with an exposure of 10 sec. The middle spectrum was taken under the identical experimental conditions as the above with the exception that a trace of molecular nitrogen was added through gas inlet #2. It consists mainly of atomic nitrogen except for a weak emission from the (0,0) band of the  $B^2\Sigma - X^2\Sigma$  first negative system of  $N_2^+$ . The spectrum was exposed for 6 minutes on an Eastman-Kodak 103 a-f plate. The lower spectrum of atomic nitrogen was taken with the addition of a short wavelength cutoff filter (Corning 3-69) to the spectrograph and was exposed on an Eastman-Kodak I-N photographic plate for 20 minutes. It consists of NI emission with very faint emission from the molecular nitrogen first positive system between 7500 and 8000 A.



dipole transitions. Racah (1960) states that there should be more of an effort to include these states along with Russel-Saunders states. This is difficult because the spectroscopic notation is different for different coupling schemes. But as one can see for nitrogen, the states are not all Russel-Saunders coupling and any complete discussion of the problem must include these other coupling schemes.

For nitrogen, intermediate coupling (IK) is used when the excited electron assumes large values of orbital angular momentum. In this case the spin coupling of this electron has lost most of its significance. The notation for these states is best explained with an example. Consider the following state of 4f electron in nitrogen:



Radiation from these states was not detected from either of the NI sources (see section 4.8).

The notation used in the energy level diagram (Fig. 4.3, 4.4) is as follows: The numbers in the "matrix array" located in the upper center of Fig. 4.3 are the values of the K vector. The capital letters represent the L vectors as described above. The lower left subscripts of this capital letter indicate the type of coupling used (for this case LK). The superscript on the upper right of the letter represents the parity of the state: "o" means odd parity; "blank" means even parity (just as in the Russel-Saunders case).

Figure 4.2

This diagram shows the energy of the various "terms" of neutral atomic nitrogen. The ionization limit at 14.53eV is indicated by the horizontal dashed line. The "terms" in the upper center of the figure are groups of levels described by intermediate coupling (LK) (Eriksson, 1961). The sextet terms located in the upper left of the diagram were identified by Eriksson (1969). The energy region between the arrows is expanded on the following figure.

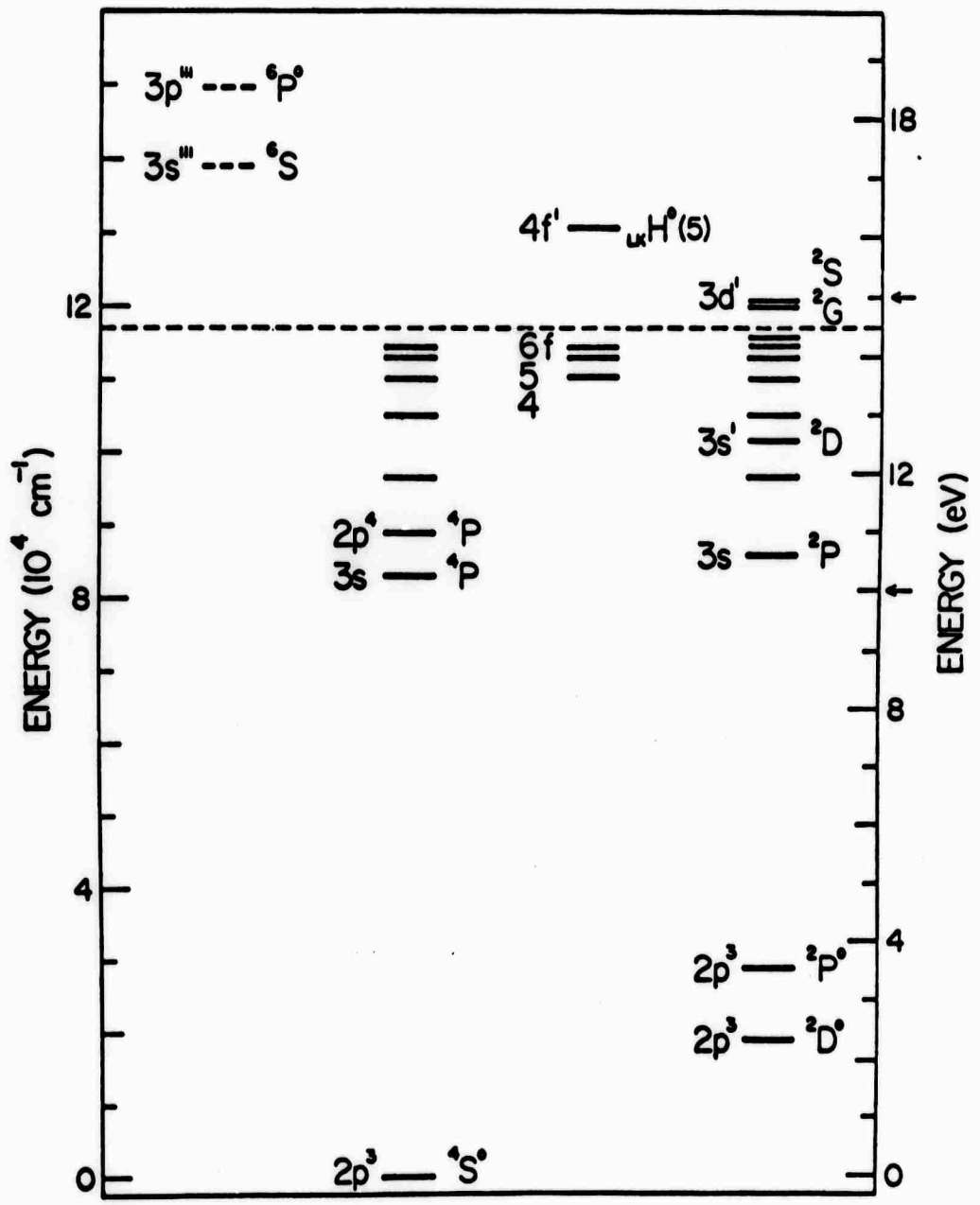


Figure 4.3

A partial energy level diagram for atomic nitrogen (ground state not shown). Russel-Saunders states are located on the extreme left (quartet system) and right (doublet system) of the diagram. Each member of a major vertical group share the same parity quantum number. The diagram was designed to incorporate more than Russel-Saunders states and to facilitate recognition of electric dipole transitions. Note the symmetry in energy between the terms of the quartet and doublet system. The short dashed lines are terms which are predicted on the basis of this symmetry. (See text for notation of LK coupling states).

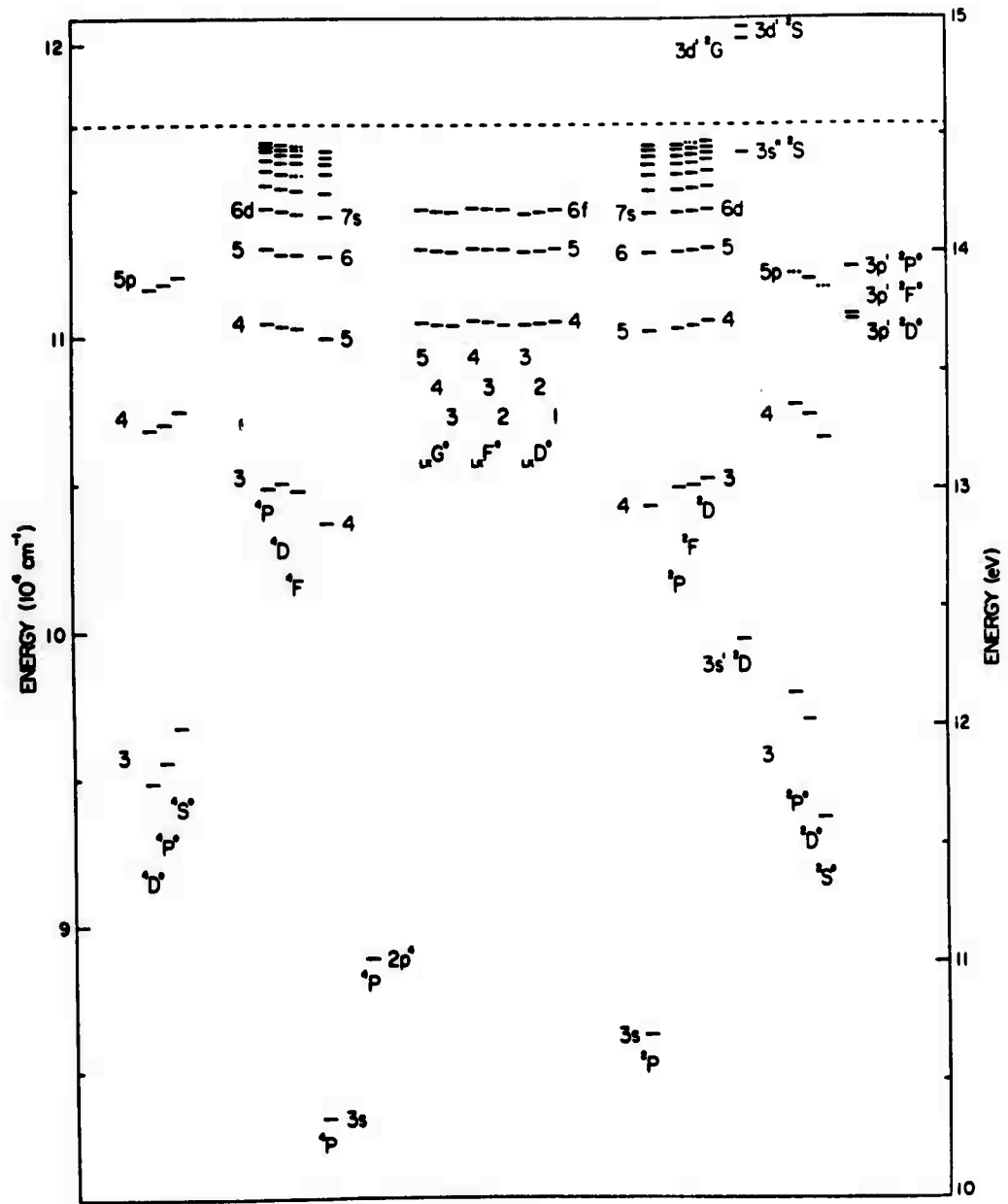
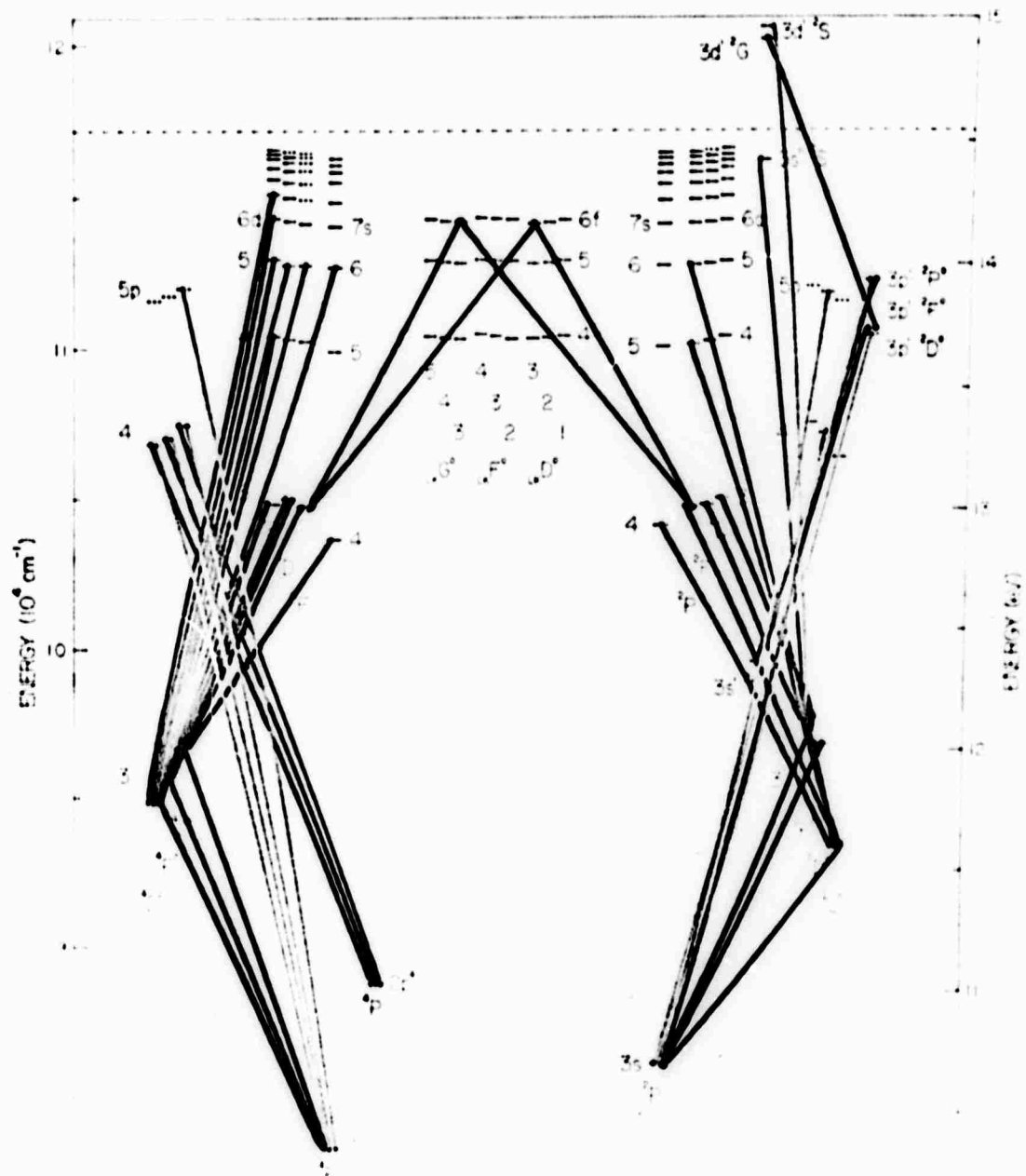


Figure 4.4

A partial energy level diagram for atomic nitrogen (ground state not shown). The diagram was designed to aid in identifying the spectroscopic data. The colored lines represent the observed electric dipole transitions. The red indicates transitions whose wavelengths are longer than 6000 Å, the green, transitions between 6000 and 4500 Å and the blue, transition with wavelengths shorter than 4500 Å. As seen in the figure, the intermediate coupling states help to connect the quartet and doublet systems.



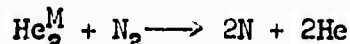
#### 4.3 Two Mechanisms for Production of NI

When molecular nitrogen is injected into the helium afterglow a strong blue glow appears which is due predominately to the first negative system of  $N_2^+$ . Spectra of this glow from 2500 to 9000 Å are shown by Dunn (1966). Figures 4.6 (upper) and 4.7 (upper) show parts of the spectral region associated with the blue glow. There also is radiation from atomic nitrogen in this glow, but with a different population distribution than in the green NI glow (see Fig. 4.8). This blue glow always precedes the green in the afterglow. The NI lines from the blue were not sensitive to the application of a rf field, while the lines from the green glow were extremely sensitive to the field (see Fig. 4.5). This information suggests two mechanisms for producing the NI. The blue glow population distribution of NI was determined by using a rf field to quench contributions from the recombination mechanism. The result was a linear distribution corresponding to a temperature of  $10^4$  K (Fig. 4.8).

The mechanism for the excitation of atomic nitrogen in the blue region was determined from energetics and qualitative observation discussed in section 2.3. It takes about 10eV to dissociate the nitrogen molecule, and since NI states from energy levels of 14eV were observed in the blue region, a minimum of 23 or 24eV is required. Since there is no helium species remaining which has that much energy,

a two step process must be involved. The qualitative experiments with argon (see section 2.3) demonstrated that the metastable helium atom had nothing to do with exciting the atomic nitrogen.

Thus, the only species left with sufficient energy were the metastable helium molecules and the high energy electrons. Since it is known that the temperature of atomic levels reflects the electronic temperature, the nitrogen molecule was most likely dissociated by  $\text{He}_2^M$  and the NI levels excited by collisions with the high energy electron (see chapter III). The two step process in which the NI lines were excited in the blue region is referred to as the collisional mechanism and is written as:



The fact that the metastable helium molecule dissociates the nitrogen molecule instead of the metastable helium atom was not expected according to the literature (Duffendack and Wolfe, 1929). Figure 4.5 is an example of the actual photoelectric data which formed the basis for postulating these two independent mechanisms for exciting atomic nitrogen lines.

No experimental evidence was found to connect either of the two mechanisms of NI with  $\text{N}_2^+$ . The energy of  $\text{N}_2^+$  is most likely dissipated on the walls (Ghosh and Jain, 1966).

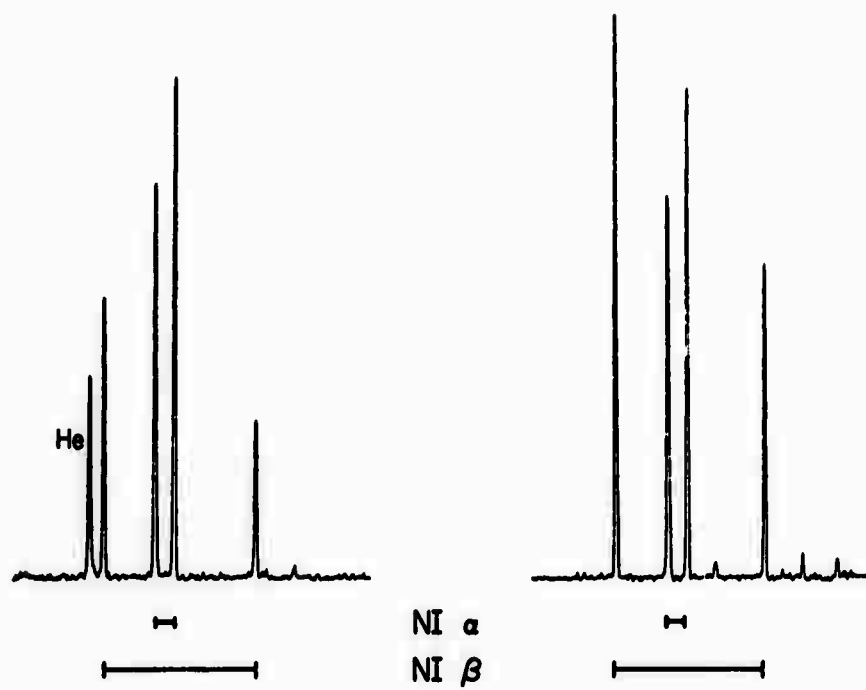
Figure 4.5

These figures are actual photoelectric data which form the bases for postulating two independent mechanisms for producing excited NI. The top left spectrum shows NI lines excited in the  $N_2$  blue flame (collisional), while the right spectrum shows the same lines excited in the green flame (recombination). Notice that the relative intensity of the nitrogen multiplets has changed. Also observed in the top left figure is a HeI line. The lower spectra were taken under identical experimental conditions except that a rf field was directed towards the plasma. Notice the HeI and NI lines which were produced by electron recombination have vanished, while the NI lines produced by the collisional mechanism still remain (lower left spectrum). The weak NI emission seen in the lower right spectrum is due to the collisional mechanism.

NI  $\alpha$  refers to  $2p\ 3s\ ^2D - 2p^2\ (^1D)\ 3p\ ^2F^o$

NI  $\beta$  refers to  $2p^2\ 3p\ ^2S^o - 2p^2\ (^3P)\ 3d\ ^2P$

(a) no RF field



(b) RF field

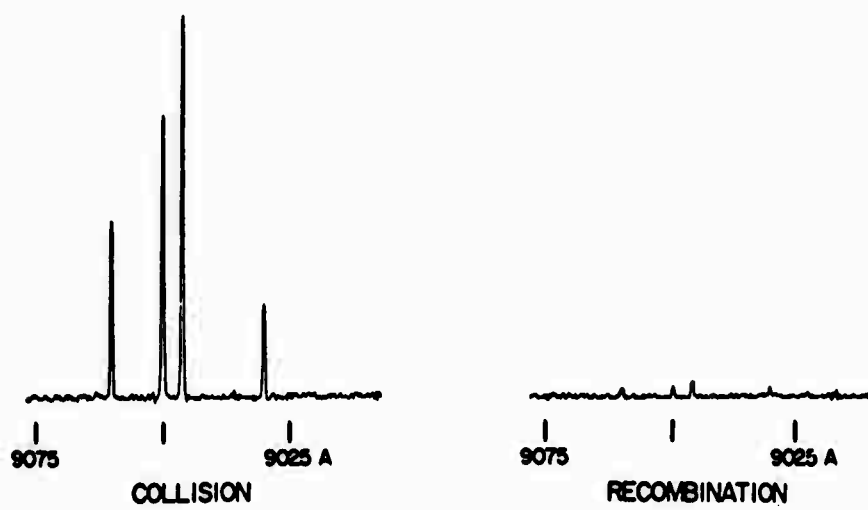


Figure 4.6

This figure demonstrates the experimental control one can use to identify spectroscopic lines. The spectra are actual photoelectric data taken during three different experimental conditions: 1) blue molecular nitrogen flame, 2) green atomic nitrogen flame, 3) helium only. All three spectra were taken at a pressure of one torr and electrode current of 450 ma. The top spectrum was taken of the blue  $N_2$  flame. As shown on the figure there is strong emission from the  $N_2^+$  first negative system and weak emission from NI (collisional plus recombination mechanism). The middle spectrum was taken of the green NI flame (recombination mechanism). The lines labeled with lower case letters were assigned to the NI ( $3s^4P - 4p^4D^0$ ) multiplet. The bottom spectrum was taken of helium only. It shows the chromium and iron lines which were used for wavelength calibration (there are no helium lines in this spectral region). The chromium and iron came from electrode sputtering.

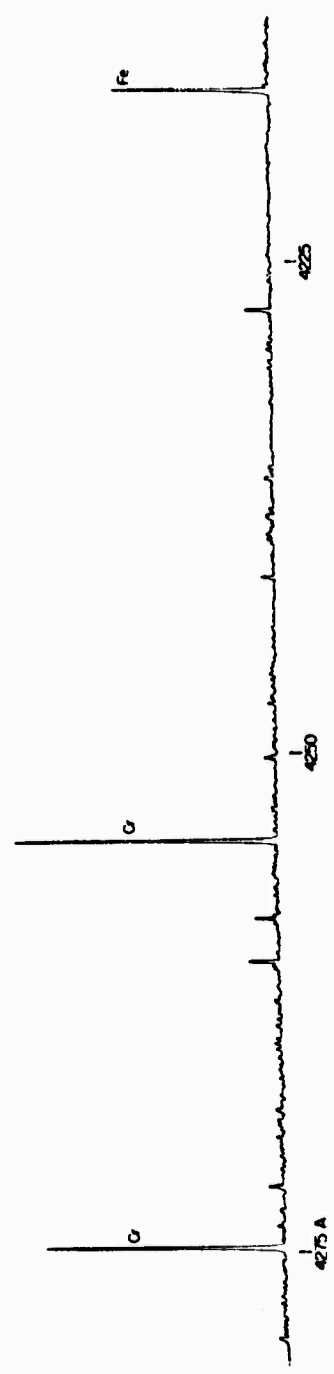
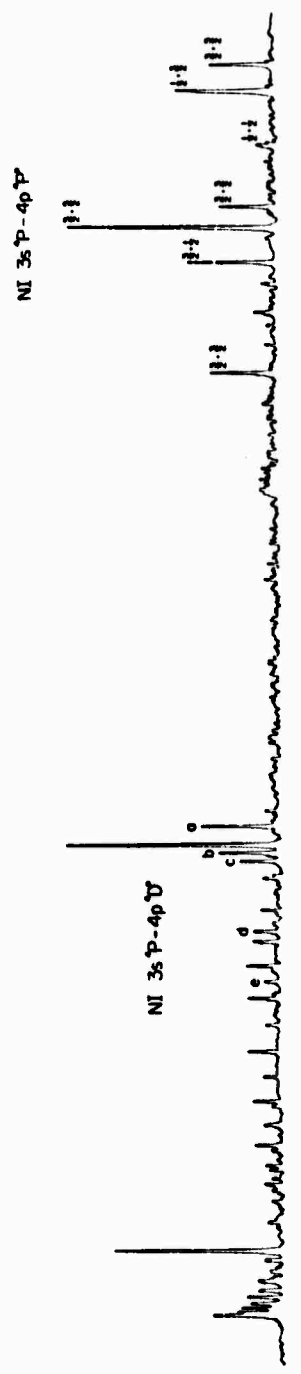
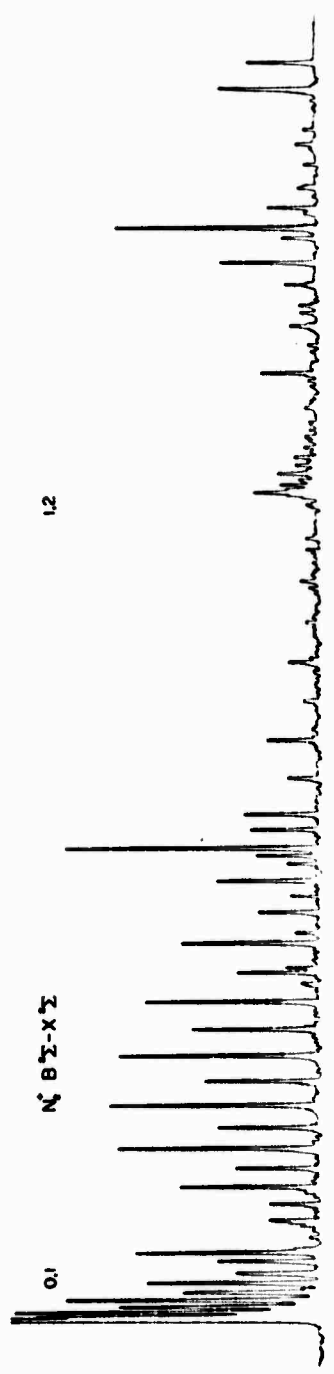
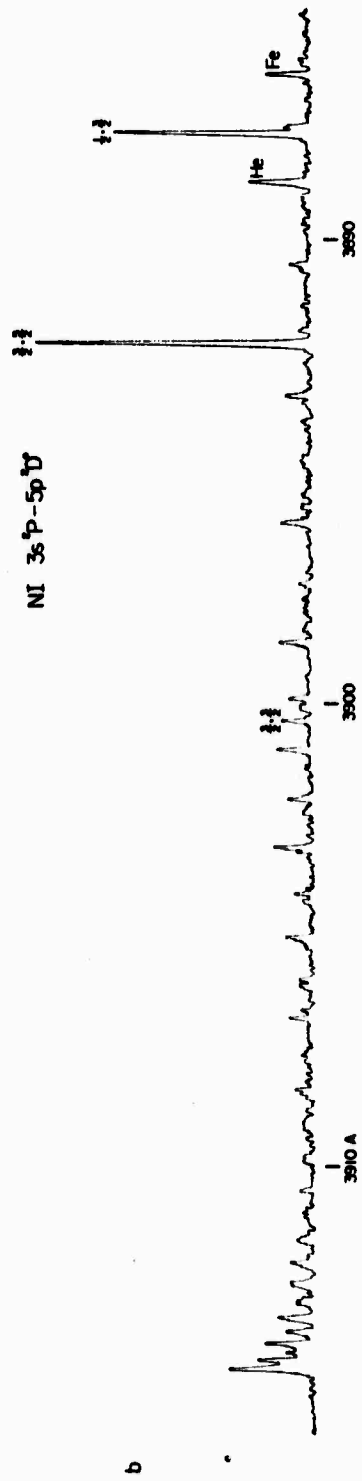
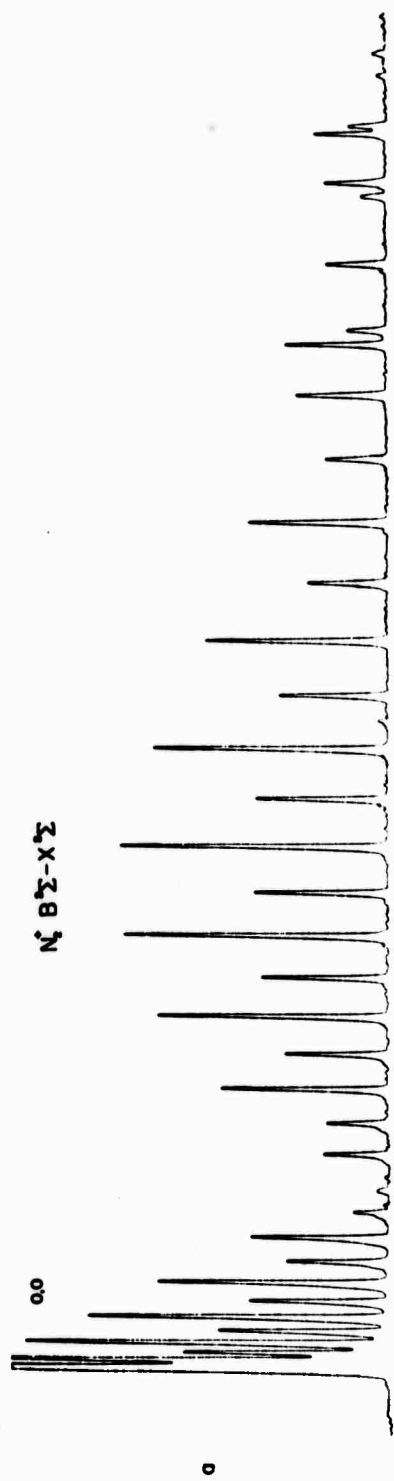


Figure 4.7

The upper trace is of the photoelectric spectrum of the  $N_2$  blue flame near 3920 Å region. It was taken with a double-pass Ebert scanning monochromator using a 2160 line/mm grating in first order. The spectral resolution of the system was 0.1 Å. The spectrum consists of strong emission from the (0,0) band of  $N_2^+$  first negative system and weak emission from atomic nitrogen (collisional plus recombination mechanisms). The lower trace is the spectrum of the atomic nitrogen green flame (recombination mechanism) under the same experimental condition as the above spectrum. Shown on the figure is the first observation of the NI ( $3s^2P - 5p^2D^0$ ) multiplet.



#### 4.4 The Problem of Identification of Lines

Figures 4.6 and 4.7 illustrate the control which the experimenter can use to identify lines for the present sources of NI. The problem of identifying lines from the blue region is very difficult because there are many molecular bands which occur throughout the entire spectral region. Since the green NI glow was predominately atomic nitrogen, it was helpful to use this source to find a particular NI line in the blue region. The line was observed under the green condition and then a small adjustment of the molecular nitrogen flow rate would allow the line to be observed under the blue condition. Adjustment of the flow rate would move different regions of the nitrogen plasma in front of the spectrometer slits.

#### 4.5 Interpretation of Results

The population of levels excited by the two mechanisms is shown on Fig. 4.8. The population was calculated using measured intensities and calculated transition probabilities (Griem, 1964 and Wiese, Smith and Glennon, 1966) and equation 3.2. It is seen from Fig. 4.8 that as the levels approach the ionization limit for nitrogen (14.53eV), the population due to the recombination mechanism is about one order of magnitude greater than the population due to the collisional mechanism. The two distributions were normalized around 12eV as can be seen from

Fig. 4.8. The structure in the recombination distribution around 13.2eV is probably due to cascading. From Fig. 4.4 it can be seen that cascading is important when the upper levels are inverted in nitrogen.

Compare the energy level distribution for the NI (green) shown by the dashed line on Fig. 4.8 to the level distribution for helium shown on Fig. 3.2. The important difference between these two distributions is that as the binding energy of the excited electron approaches zero, the population of the NI levels rapidly increases, while the population of the HeI levels rapidly decreases. This decrease of the HeI levels is explained by ionization from an excited state by electrons. The source of these ionizing electrons is three body recombination (see equation 3.10). Perhaps the reason why the NI levels increase in population as this energy region is approached is because there are no electrons to depopulate these states by ionization. This indicates that two body recombination, or single electron recombination is probably the mechanism for populating the NI levels. (A third body other than an electron is possible, but this would require additional investigation.) The NI levels should continue to increase in population until the excited electron binding energy approaches about  $5(KT_{room})$  or 0.1eV where the room temperature ambient gas particles would have sufficient energy to depopulate the NI states before radiating (see the last paragraph of section 3.3).

More work needs to be done to learn how the NI levels are

populated by the recombination mechanism. In other words, how does the probability for recombination depend on the quantum numbers of the states such as parity, multiplicity, and orbital angular momentum? For example, high orbital angular momentum states ( $f$ ) do not seem to be populated as much as reported in other sources (McConkey, Burns and Kernahan, 1967). The levels need to be sorted according to their quantum numbers and the population of these levels studied as a function of their quantum numbers. Also, additional experimental information would be useful. If the continuum from the captured electron could be observed, it would be possible to confirm the single electron recombination mechanism and to measure the matrix elements of the electron going from a free to a bound state. From the energetics, the continuum should peak around 2 microns.

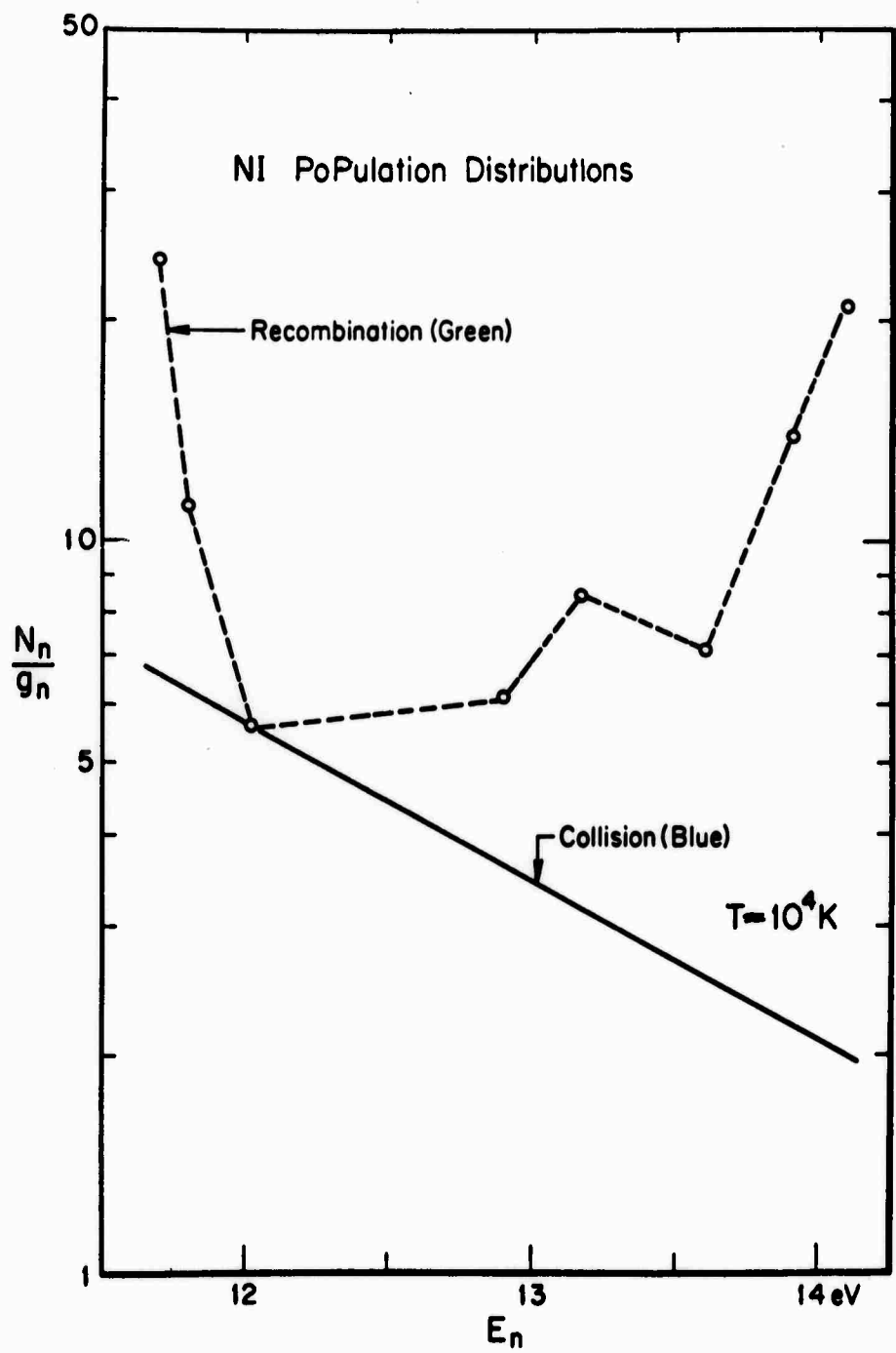
Two separate mechanisms were found to excite atomic nitrogen.  $\text{He}^+$  was the precursor of the green atomic nitrogen spectrum and  $\text{He}_2^M$  was the precursor for III lines in the blue glow. The green glow was found to be the cleanest and brightest source of atomic nitrogen thus reported. It would be an excellent source for accurate wavelength measurements which in turn would allow precise determination of many new energy levels near the ionization limit. Since the manner in which these levels are populated is not understood qualitatively, intensity measurements could not be used to determine transition probabilities. However, the collisional mechanism for producing excited III resulted in a level distribution which was in

equilibrium, and thus could be used to measure transition probabilities. The problem with this source is that the atomic emission is obscured by stronger molecular emission and the intensity of the transitions near the ionization limit is very weak (see Fig. 4.8). Thus with this source one would not have the experimental control he would have with the recombination source. A solution would be to combine the best features of both sources in order to measure the transition probabilities. The NI lines could be isolated using the recombination source and with a turn of a dial, the intensity from the equilibrium situation could be recorded. This procedure would be a good method for determining transition probabilities of levels very near the ionization limit of the atom.

One of the most important features of Fig. 4.8 is the population inversion of the nitrogen levels. Calculations of densities and other important quantities necessary for laser action should be completed in order to test the possibility for constructing a NI laser from this source.

Figure 4.8

The relative population per unit statistical weight (arbitrary units) as a function of the electron excitation energy in atomic nitrogen. The dashed line represents an averaged population function for the recombination mechanism. The states below 13eV were mainly populated by cascading from levels near the ionization limit for nitrogen. When the recombination mechanism is quenched, the collisional mechanism predominates (solid line). This solid line represents an averaged population distribution for the collisional mechanism. The NI levels populated by this mechanism appear to be in equilibrium at a temperature near 10,000 K.



## V MOLECULAR NITROGEN

When molecular nitrogen is added to the flowing helium afterglow many different reactions occur simultaneously in time and space (Wright and Winkler, 1968). Dunn (1966) has studied systems of  $N_2^+$  which radiate under these conditions. Reported here are three new vibrational distributions of the first positive system of neutral molecular nitrogen,  $B^3\Pi_g - A^3\Sigma_u^+$ . No complete analysis in regard to the mechanism of these reactions was made; only the experimental data is reported.

The spectra shown in Fig. 5.1a was taken of a glow which appeared red to the eye, and was unusual in that the tenth vibrational level was more populated than neighboring levels. Figure 5.2 shows the population distribution of the vibrational levels excited in the glow. Populations of the levels were calculated from relative intensities, Franck-Condon factors and r-centroids (Zare, Albrighton, and Schemltekopf, 1968). Approximately 1% of the nitrogen molecules in the  $B^3\Pi_g$  state were in the "tenth level distribution," while the population distribution of the remaining molecules could be described by a temperature of 4050 K ( $\pm 3\%$ ).

A possible explanation for the large population of the tenth level may be that the level is being populated from some other state in the molecule. Figure 5.3 illustrates a collision induced level crossing with the  $B' \ ^3\Sigma$  state. The explanation is based on a Franck-Condon overlap. In addition, there are many metastable  $N_p$  states that somehow may be involved (Oldenberg, 1967). The 4050 K temperature may come about by collision with the 1.0eV electrons and nitrogen molecules.

Another experimental fact available is that the  $N_2$  flow rate (200 atm-cc/sec) is large. This may imply that collisions between  $N_2$  and metastable nitrogen molecules may be involved or that nitrogen atom recombination may be important.

The spectra in Fig. 5.1b occur when  $N_2$  is injected into the afterglow at a flow rate of about 1.0 atm-cc/sec and a helium gas pressure of 0.1 torr and flow rate of about 10 atm-cc/sec. This source of the first positive system is very constant and uses very little gas, thus making it a good source for very long time exposures at high resolution. At such low flow rates, the source could operate without interruption for days. The population distribution for this source is shown in Fig. 5.4. Experiments with an rf field indicate that the mechanism for the distribution involves reactions with metastable species.

The spectra in Fig. 5.1c occur when hydrogen is added in inlet #1 at a flow rate of about 0.2 atm-cc/sec. The spectra was taken at

inlet #2 where  $N_2$  was added with a flow rate of about 4.0 atm-cc/sec. The total pressure was 0.6 torr. The population distribution is shown in Fig. 5.4. It can be seen from the figure that a small amount of the tenth level distribution is mixed with this distribution.

The spectra in Fig. 5d was taken of the nitrogen afterglow with helium added. The experimental apparatus is described by Oldman and Broida (1969). The purpose of the experiment was to learn if there were any similarity between the level distribution of the top three spectra shown in Fig. 5.1 and this spectra. From Fig. 5.4, it can be seen that an important similarity of the level distributions is that all have a group of vibrational levels which can be described by a temperature of 4050 K. This may be a clue about the exciting mechanism.

Table 5.1 summarizes the results of adding molecular nitrogen to a flowing helium afterglow. Only neutral nitrogen radiating species were investigated. A "rf" in the column labeled "Remarks" means that light from the particular reaction was quenched when a rf field was directed towards the plasma. The figure numbers of the populating distributions for the various radiating species are also indicated in the column. The radiation from the  $N_2(E^3\Sigma)$  state (2100-2600 Å) should be confirmed.

TABLE 5.1

Radiating Species	Color	Electrode Current ma	Pressure torr	Flow Rate		Position in Afterglow		Spectra (Figure)	Remarks
				He	N <sub>2</sub>	N <sub>2</sub> Injected	Spectra Observed		
HeI	Pink	500	1	275			#2	2.3	rf Fig. 3.2
NI	Green	500	1	275	15	#2*	#2	2.3, 4.1 4.5, 4.6 4.7	rf Fig. 4.8
NI	Blue	500	1	275	15	#2*	#1	4.5	Fig. 4.8
N <sub>2</sub> (B <sup>3</sup> Π)	Red	200	1	275	200	#1	#2	5.1	v' <sup>+</sup> =10 Fig. 5.2
N <sub>2</sub> (B <sup>3</sup> Π)	Pink	50	0.1	10	1	#1*	#1	5.1b	Metastable Precursor Fig. 5.4
N <sub>2</sub> (B <sup>3</sup> Π)	Dark Red	200	0.6	160	4	#2*	#2	5.1	H <sub>2</sub> added at #1 (0.2 atm- cc/sec) Fig. 5.4
N <sub>2</sub> (B' <sup>3</sup> Σ)	Red	200	1	275	200	#1	#2		Occurs with N <sub>2</sub> (B <sup>3</sup> Π) v' <sup>+</sup> =10
N <sub>2</sub> (E <sup>3</sup> Σ)	Turquoise Blue	200	1	275	500	#1	#2		Needs confirma- tion
N <sub>2</sub> (C <sup>3</sup> Π)	Blue	500	1	275	15	#2*	#1		

\*Gas inlet was rotated 180° from position shown in Fig. 2.1.

Figure 5.1

Photoelectric spectra of the various vibrational distributions of the first positive system excited in a helium plasma. The spectra were taken with a double-pass Ebert scanning monochromator using a 1200 line/mm grating in first order blazed at 6000 Å under the following experimental condition:

- a) Pressure = 1.0 torr;  $[\text{He}]/[\text{N}_2] \approx 1$ .
- b) Pressure = 0.1 torr;  $[\text{He}]/[\text{N}_2] \approx 10$ .
- c) Pressure = 0.6 torr;  $[\text{He}]:[\text{N}_2]:[\text{H}_2] \approx 800:20:1$ .
- d)  $\text{N}_2$  afterglow pressure = 1.0 torr;  $[\text{He}]/[\text{N}_2] \approx 1$

(Oldman and Broida, 1969).

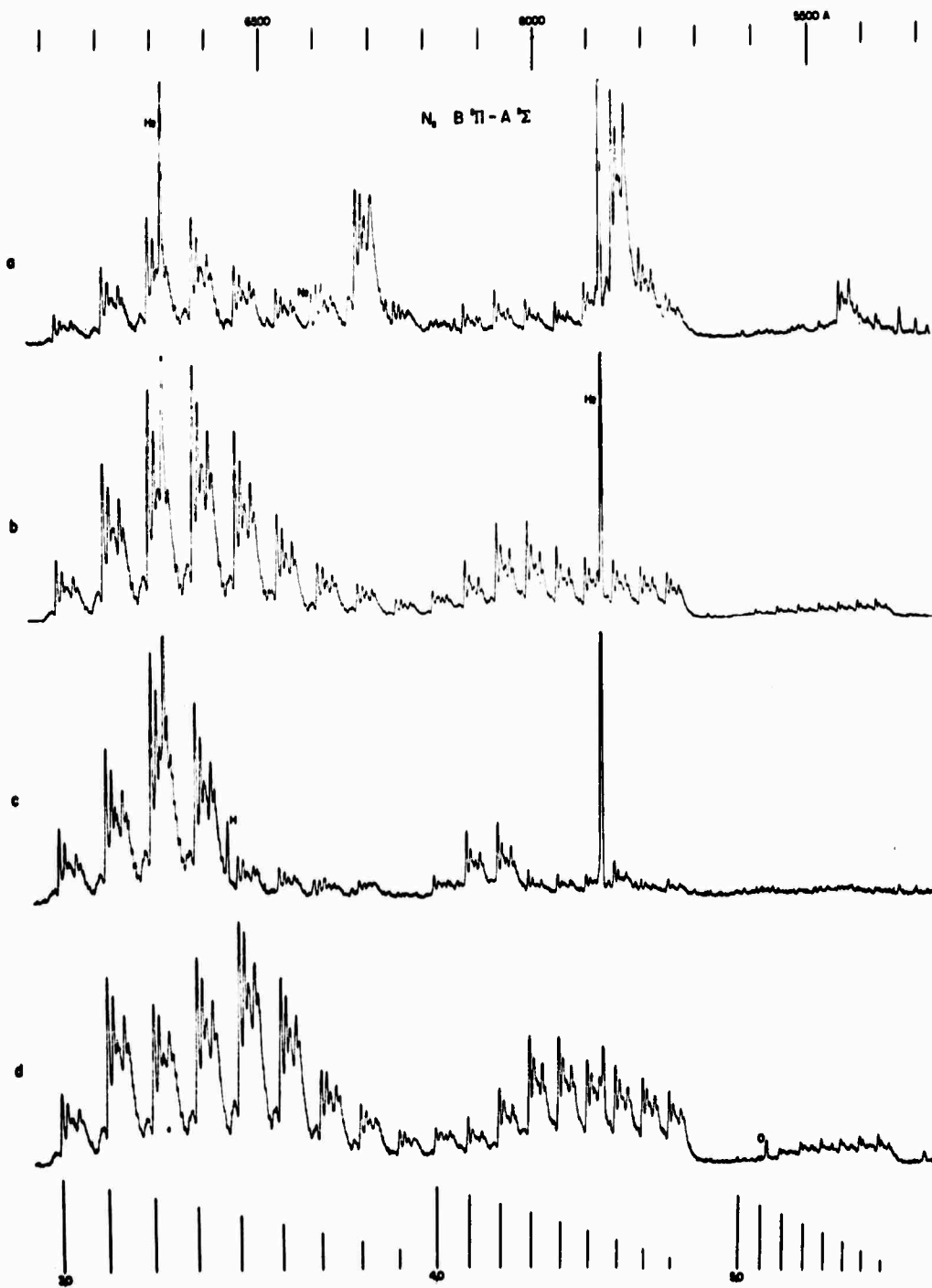


Figure 5.2

Relative populations (arbitrary units) of the  $N_2$  B  $^3\Pi$  state as a function of the electron excitation energy. Data for this graph was obtained from the spectra shown in Fig. 1a. The symbols represent the following vibrational progressions:

$\Delta v$	
0	●
1	▲
2	*
3	○
4	△
5	†

As seen from the figure, the vibrational levels between  $v' = 0$  to 8 can be described by a temperature of 4050 K ( $\pm 3\%$ ). Levels  $v' > 8$  are populated also by another mechanism. The tenth vibrational level is clearly inverted with respect to  $v'=7, 8$  and 9.

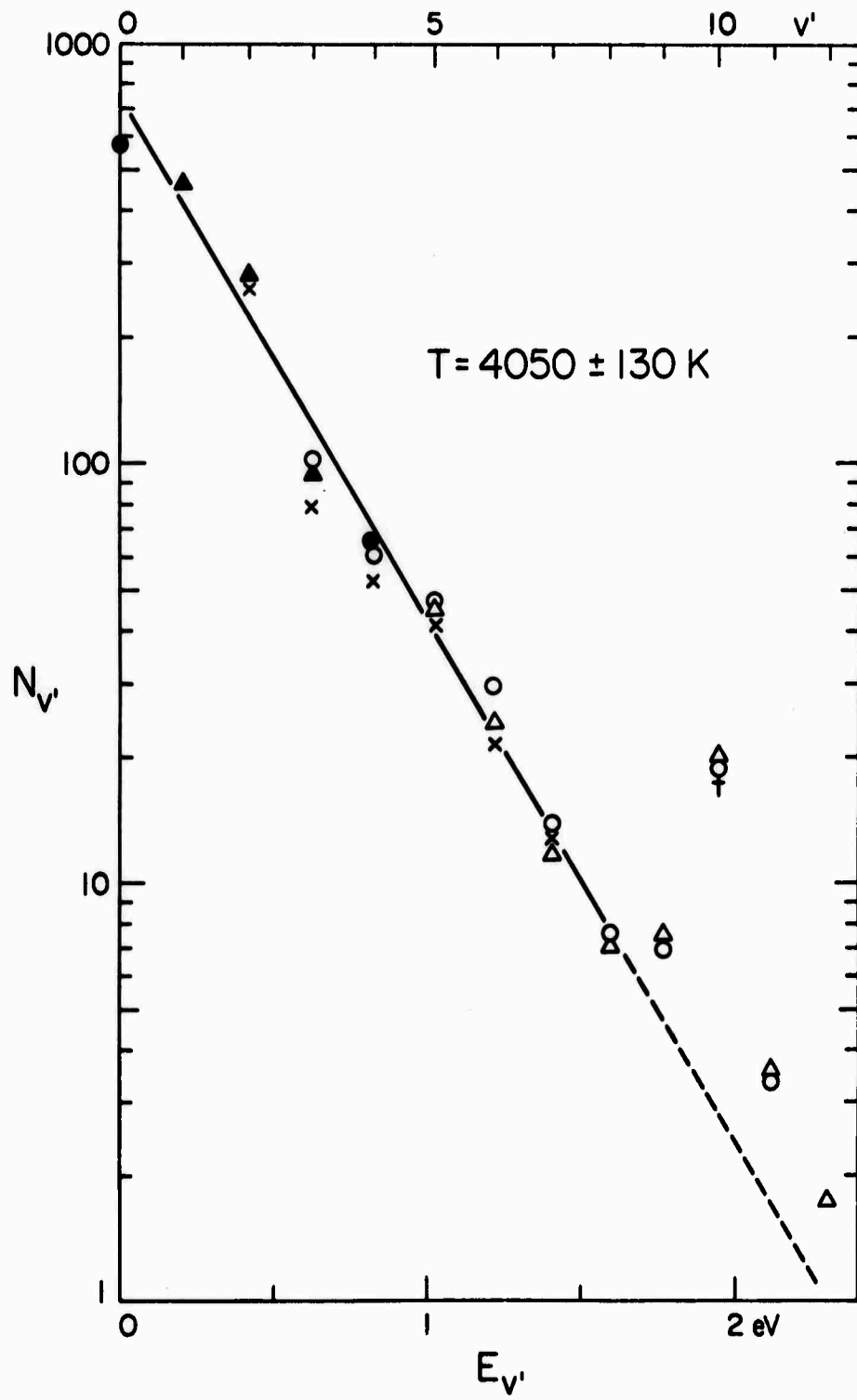


Figure 5.3

A partial energy level diagram of  $N_2$  which shows the level crossing of the B and B' curves at  $v'_p=10$ . The probability of crossing may be proportional to the overlap of the classical turning points of the two curves. This could result in an asymmetrical shape for the probability function as seen in the figure.

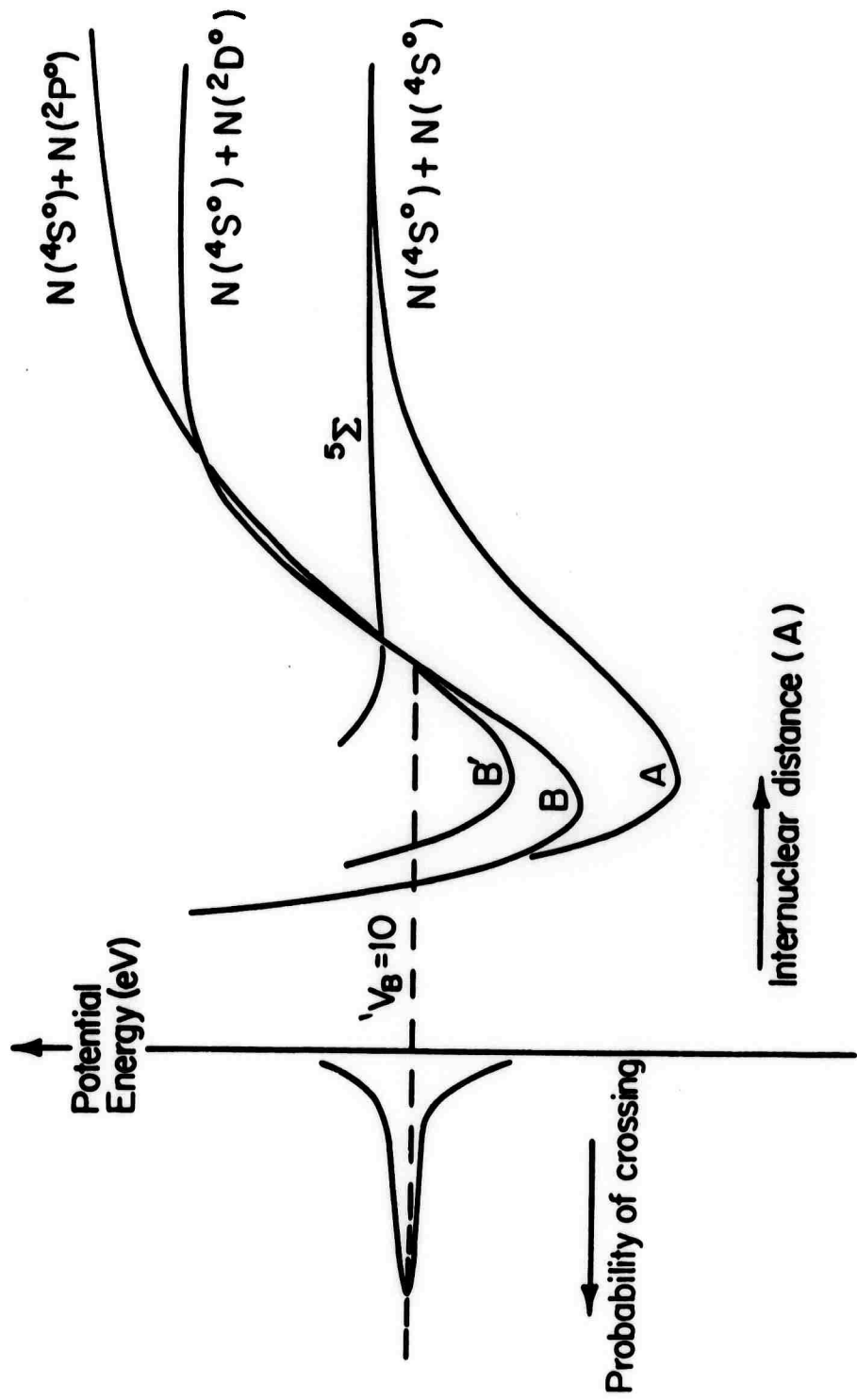
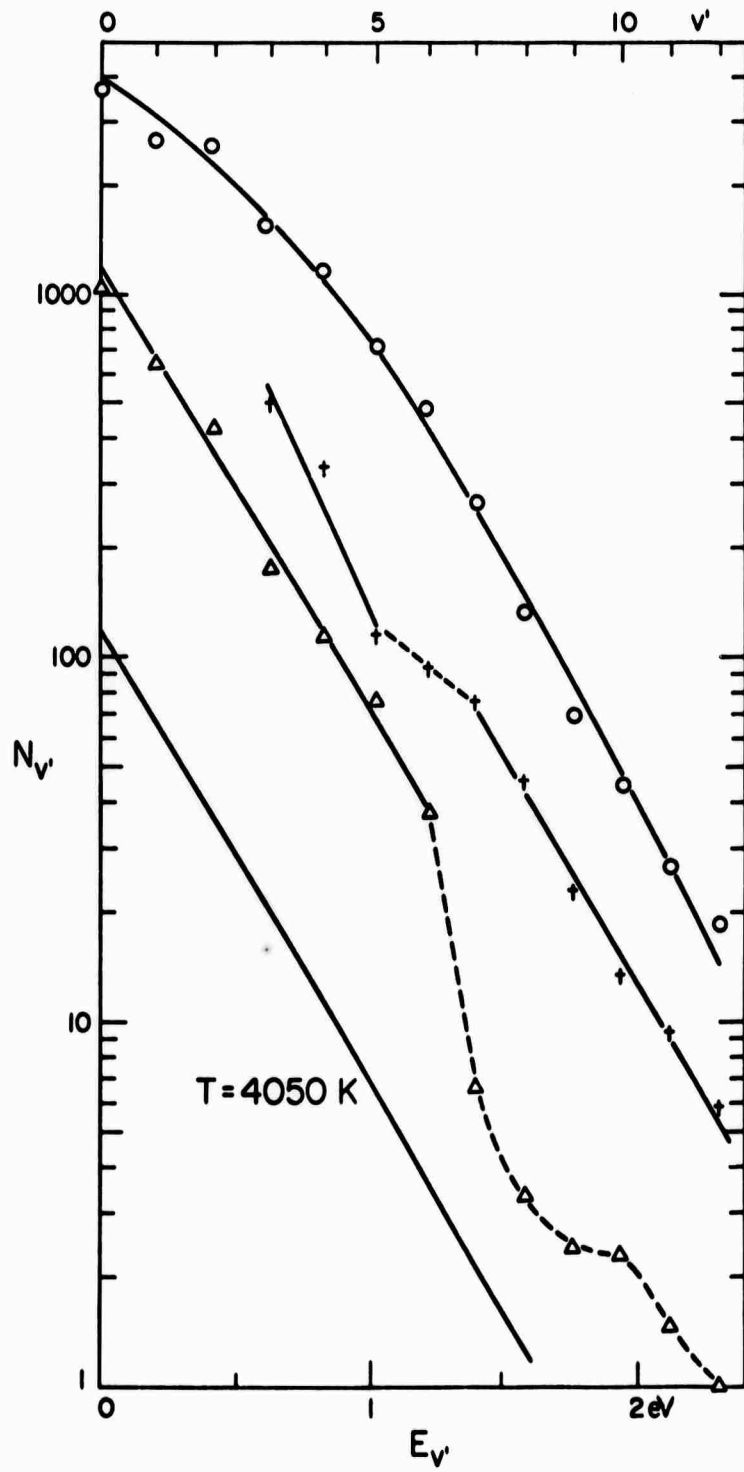


Figure 5.4

Relative populations (arbitrary units) of the  $N_2$  B  $^3\Pi$  state as a function of the electronic excitation energy. The symbol "O" refers to the data under conditions of Fig. 5.1b; the symbol "A", Fig. 5.1c (hydrogen added); and "†", Fig. 5.1d ( $N_2$  afterglow). A line whose slope corresponds to a temperature of 4050 K is drawn for comparison. As seen in the figure all the distributions have a group of vibrational levels which can be described by that temperature.



## VI CONCLUSION

It has been demonstrated that the population distribution of atomic helium levels excited in a cool, high dense plasma can be understood in terms of a bimodal electron distribution. From a fit of the Saha equation to the experimental data, it was shown that both of these electron distributions appear to be Boltzmann. In addition, evidence has been presented to show that the major energy exchange mechanisms occurring in the plasma are three body electron-ion recombination and its inverse process, ionization from an excited state. The role of ionization from an excited state of an atom may be very important in understanding cool plasmas in general. Both theoretical and experimental investigations on the cross sections for this process need to be made.

More experimental work needs to be done to verify many of the conclusions reached in this work. For example, a simple experiment can be done to verify that the ambient temperature dependence of the emission of atomic light from the plasma is given by the temperature dependence of the ambipolar diffusion coefficient. Also accurate pressure and spatial measurements of the emission of atomic light

would be useful. In addition, absolute light measurements would allow accurate spatial dependence of the electron densities to be made and using calculated transition probabilities useful information regarding the cross sections for ionization from excited states would be obtained.

Finally, the procedure discussed here for a helium plasma may be applicable to plasmas composed of other atoms as well. Schlüter (1963) has used a two electron distribution and Saha equation to describe the behavior of a hydrogen plasma. His approach did not go into as much detail as was presented in the present discussion. It may prove useful to apply the present procedure to hydrogen and other plasmas.

Two separate mechanisms were found to excite atomic nitrogen. One mechanism consisted of a two step collisional process where  $N_2$  was dissociated by metastable molecular helium and the excited neutral atomic nitrogen was produced by collisions with electrons. The temperature of the NI levels was about  $10^4$  K. The other mechanism was single electron recombination of nitrogen atomic ions. The ions were formed in the dissociative charge transfer reaction of ionized helium with molecular nitrogen. This source of atomic nitrogen was very clean and approximately 400 new NI lines were observed with an inverted population distribution. Together, these two sources could be used to measure transition probabilities very near the ionization limit of the atom. The possibility of using the population inversion

shown on Fig. 4.8 to make a laser should be investigated. If a super-radiant situation could be made, it may be possible to produce an ultraviolet or X-ray laser.

More experimenting needs to be done to determine the mechanism for the various vibrational distributions of the  $N_2$  first positive spectrum. Perhaps with further investigation of this source, new information about the complicated energy level structure of the nitrogen molecule may be learned.

## REFERENCES

- Aller, L. H. and Litter, William, in Nebulae and Interstellar Matter, edited by Middlehurst, B. M. and Aller, Lawrence H. (The University of Chicago Press, Chicago, 1968) Chap. 9.
- Applebaum, T. and Manalis, M., private communication (1970).
- Bates, D. R. and Dalgarno, A., in Atomic and Molecular Processes, edited by D. R. Bates (Academic Press, Inc., N.Y., 1962) Chap. 7.
- Childs, C. B., Appl. Opt. 1, 711 (1962).
- Collins, C. B. and Robertson, W. W., J. Chem. Phys. 40, 2202 (1964a).
- Collins, C. B. and Robertson, W. W., J. Chem. Phys. 40, 2208 (1964b).
- Collins, C. B. and Robertson, W. W., J. Chem. Phys. 40, 701 (1964c).
- Condon, E. U., Shortley, G. H., The Theory of Atomic Spectra (Cambridge University Press, London, 1963).
- Coleman, Charles De Witt, Bozman, William R. and Meggers, William F., Table of Wavenumbers (Vol. I and II), Nat. Bur. Stand. Mono. 3 (1960).
- Duffendack, O. S. and Wolfe, R. A., Phys. Rev. 34, 409 (1929).
- Dunn, J. L., Ph.D. Thesis, University of California at Santa Barbara, Spectral Analysis of Mechanisms and Kinetics of Thermal Energy Reactions of Long-Lived Energetic Helium Species with Simple Molecules, (1966).
- Eriksson, K. B. S., private communication (1969).
- Eriksson, K. B. S., Phys. Rev. 102, 102 (1966).
- Eriksson, K. B. S., Arkiv Fysik 19, 229 (1961).
- Eriksson, K. B. S., Arkiv Fysik 19, 235 (1961).

- Eriksson, K. B. S., Arkiv Fysik 13, 429 (1958).
- Ferguson, E. E., Fehsenfeld, F. C. and Schmeltekopf, A. L., in Advances in Atomic and Molecular Physics (Academic Press, Inc., N.Y., 1969).
- Fermi, Enrico, Molecules, Crystals, and Quantum Statistics (W. A. Benjamin, Inc., N.Y., 1966) Chap. 8.
- Ghosh, S. N. and Jain, S. K., Brit. J. Appl. Phys. 17, 765
- Goldberg, L., Astrophys. J. 90, 414 (1939).
- Griem, H. R., Plasma Spectroscopy, (McGraw-Hill, Inc., N.Y., 1964).
- Hasted, J. B., Physics of Atomic Collisions (Butterworth and Co., London, 1964).
- Hinnov, E. and Hirschberg, J. G., Phys. Rev. 125, 795 (1962).
- Huang, Kerson, Statistical Mechanics (John Wiley & Sons, Inc., N.Y., 1963) Chap. 5.
- Inokuti, Mitio, and Kim, Yong-Ki, Phys. Rev. 186, 100 (1969).
- Kamiyama, M. and Noguchi, H., Sci. Papers Inst. Phys. Chem. Research (Tokyo) 39, No. 1100, 475 (1942).
- Kamiyama, M. and Sugiura, T., Sci. Papers Inst. Phys. Chem. Research (Tokyo) 37, Nos. 982 and 983, 479 (1940).
- Kamiyama, M., Sci. Papers Inst. Phys. Chem. Research (Tokyo) 36, No. 933, 375 (1939).
- Liu, Chelcie Bosland, Ph.D. Thesis, University of California at Santa Barbara, Optical Spectra Observed During Ion-Molecule Collisions with Low-Energy  $H_2^+$  and  $Ar^+$  Beams (1969).
- Marquardt, Donald W., J. Soc. Indust. Appl. Math. 11, No. 2, 431 (1963).

- Martin, W. C., J. Res. Natl. Bur. Standards 64A, 19 (1960).
- McConkey, J. W., Burns, D. J. and Kernahan, J. Quant. Spectrosc. Radiat. Transfer, 3, 323 (1963).
- Moore, C. E., A Multiplet Table of Astrophysical Interest, Parts I, II, N.B.S., Washington, 1945; An Ultraviolet Multiplet Table, Circular 488, Section I, N.B.S., Washington, 1950.
- Oldenberg, O., A Theory of the Auroral Afterglow of Nitrogen (Air Force Cambridge Research Laboratories, L.G. Hanscom Field, Bedford, Massachusetts, 1967), (AFORL-67-0252).
- Oldman, R. J. and Broida, H. P., J. Chem. Phys. 51, 2254 (1969).
- Powers, Robert S., Jr., J. Appl. Phys. 31, 511 (1966).
- Recah, Giulio, Transactions of the Joint Commission for Spectroscopy, 50, 408 (1960).
- Schluter, Von H., Z. Naturforschg, 18a, 439 (1963).
- Spitzger, Lyman, Jr., Physics of Fully Ionized Gases (John Wiley & Sons, Inc., N.Y., 1962) Chap. 5.
- Spitzer, L., Monthly Notices, Roy. Astron. Soc. (London) 100, 396 (1940).
- Striganov, A. R. and Sventitskii, N. S., Tables of Spectral Lines of Neutral and Ionized Atoms (IFI/Plenum, N.Y., Washington, 1968).
- Thomson, J. J., Phil. Mag. 47, 337 (1924).
- Thornton, John A., An Investigation of the Energy Exchange Processes for Nonequilibrium Plasmas (Litten Publication No. 11-68-190, 1968).

Wiese, W. L., Smith, M. W. and Glennon, B. M., Atomic Transition Probabilities, National Bureau of Standards, NSRDS-NBS 4, Vol. One, U.S. Dept. Commerce (1966).

Wright, A. H. and Winkler, C. A., Active Nitrogen (Academic Press, N.Y., 1968).

Zare, R. N., Albrighton, D. A. and Schmeltkopf, A., Private communication (1968). These calculations include values for the r-centroid but otherwise are similar to those of W. Benesch, J. T. Vanderslice, S. G. Tilford, and P. G. Wilkinson, Astrophys. J. 144, 408 (1966).

## APPENDIX I

## Wavelengths for NI spectrum (recombination - green)

## Table Code \*

Id Means identification. A NI in the column means that the line has been identified as an atomic nitrogen line. If the column is blank, this means that the line is most likely a new atomic nitrogen line and has not been detected before because it was obscured by other emission or it was not populated in other sources. Any other element in this column means there is a confusion between lines of this element and a new atomic nitrogen line.

 $\lambda$  Wavelength (Å) (measured in air)

The wavelength scale was set by those wavelengths enclosed in brackets.

## Wavelength Error Code

"blank" =  $\pm 0.1$  Å

(a) =  $\pm 0.2$  Å

(b) =  $\pm 0.5$  Å

(c) =  $\pm 0.7$  Å

(d) =  $\pm 1.0$  Å

 $\nu$  Wavenumber ( $\text{cm}^{-1}$ ) (vacuum)

Tables of Wavenumbers (Coleman, et al. 1960)

I Intensity in arbitrary units (relative precision). The intensity was measured from linear photoelectric spectra (the height of the line was assumed to be proportional to the intensity). "?" means that the reproducibility was in doubt.

\* Note: Read page 145 for additional information regarding the lines whose wavelength is less than 3800 Å.

Id	$\lambda$ A	$\nu$ $\text{cm}^{-1}$	I
NI	[10549.64]	9476.436	326.2
NI	[10539.55]	9485.517	677.6
NI	10520.4 (d)	9502.739	285.7
NI	10505.1 (d)	9516.579	240
	10479.7 (d)	9539.644	175 ?
	10406.1 (d)	9607.116	175 ?
	10397.6 (d)	9614.969	175 ?
NI	10164.6 (d)	9835.273	131.8
Fe ?	10157.8 (d)	9841.954	76.92
NI	[10147.27]	9852.138	131.8
NI	[10128.29]	9870.620	432.3
NI	[10114.64]	9883.989	1343.8
NI	[10112.48]	9886.042	835.6
NI	[10108.90]	9889.562	743.9
NI	[10105.15]	9893.186	435.5
	10024.6 (d)	9972.727	31.4
NI	10002.8 (d)	9994.461	21 ?
	9983.3 (d)	10013.98	28.5
	9940.8 (d)	10056.80	20.8
	9899.3 (d)	10098.96	47.9

Id	$\lambda$	$\nu$ cm <sup>-1</sup>	I
	9890.9 (d)	10107.53	31.5
	9875.5 (d)	10123.29	14 ?
NI	9872.5 (d)	10126.370	38.9
NI	[ 9863.33 ]	10135.785	181.0
	9851.33 (d)	10148.131	23.2
NI	9834.7 (d)	10165.291	48.8
	9828.0 (d)	10172.22	42.6
NI	9822.7 (b)	10177.658	83.0
NI	9810.2 (b)	10190.678	21.9
NI	9798.9 (b)	10202.430	22.3
	9797.7 (b)	10203.68	36.1
NI	9788.5 (b)	10213.269	9.7
NI	9787.0 (b)	10214.835	17.4
	9780.1 (b)	10222.04	28.5
NI	9776.8 (b)	10225.492	11.8
	9772.1 (b)	10230.51	42.9
	9767.6 (d)	10235.12	7 ?
	9751.6 (b)	10251.92	13.4
	9706.6 (b)	10299.44	32.7
	9691.7 (b)	10315.28	55.6
	9688.6 (b)	10318.58	28.6
N <sub>2</sub> ?	9679.1 (b)	10328.71	12.2

Id	$\lambda$ A	$\nu$ cm <sup>-1</sup>	I
	9663.1 (b)	10345.81	81.3
	9660.1 (b)	10349.02	21.2
	9645.6 (b)	10364.58	21.2
	9643.1 (b)	10367.27	15.6
	9617.6 (d)	10394.75	22 ?
	9613.5 (b)	10399.19	16.1
	9600.7 (b)	10413.05	13.2
	9594.5 (d)	10419.78	7 ?
	9562.1 (b)	10455.09	10.7
	9559.1 (b)	10458.37	8.1
	9523.5 (b)	10497.462	14.6
	9521.1 (b)	10500.11	11.6
	9501.9 (d)	10521.44	11 ?
	9485.1 (b)	10539.96	8.6
NI & He	9464.9 (a)	10562.455	7 ?
NI	[ 9460.676 ]	10567.166	42.6
	9402.6 (b)	10632.44	20 ?
NI	[ 9392.789 ]	10643.544	355.0
NI	[ 9386.805 ]	10650.325	221.3
	9344.8 (a)	10698.20	5.7
	9316.5 (a)	10730.70	7.0

Id	$\lambda$ A	$\nu$ cm <sup>-1</sup>	I
	9301.9 (a)	10747.54	4.3
	9301.8 (b)	10747.66	3.4
Cr	9293.9 (a)	10756.69	10.7
	9289.9 (a)	10761.43	1.8
	9234.8 (a)	10825.63	5.8
Ne	9221.9	10840.78	14.0
	9218.8 (a)	10844.42	4.0
NI	[ 9208.001]	10857.142	84.6
	9194.9 (a)	10872.61	25.9
	9193.5 (c)	10847.27	4.9
NI	[ 9187.449]	10881.427	106.8
	9177.8 (c)	10892.87	4.1
	9138.6 (b)	10939.59	2.6
	9102.8 (b)	10982.62	0.5
	9094.5 (c)	10992.64	2.2
NI	[ 9060.472]	11033.927	102.2
NI	9050.0 (a)	11046.692	90.3
NI	[ 9045.878]	11051.723	95.5
	9039.8 (a)	11059.16	0.5
NI	[ 9028.918]	11072.483	65.7

Id	$\lambda$ A		$\nu$ cm <sup>-1</sup>	I
	9020.8	(a)	11082.45	4.4
	9013.0	(a)	11092.04	4.9
	8992.9	(b)	11116.83	6.0
	8980.6	(a)	11132.06	5.3
	8976.0	(a)	11137.76	5.0
	8942.1	(b)	11179.99	6.8
	8937.3	(b)	11185.99	3.6
	8899.2	(a)	11233.88	13.4
	8886.7	(a)	11249.68	14.6
	8871.6	(a)	11268.83	15.1
	8822.3	(a)	11331.80	14.7
NI	8747.5	(a)	11428.699	25.0
NI	8728.9	(b)	11453.052	59.4
	8722.3	(a)	11461.72	7.3
NI	[ 8718.841 ]		11466.833	307.3
NI	[ 8711.708 ]		11475.651	397.3
NI	[ 8703.255 ]		11486.806	412.2
Fe	8698.4	(a)	11493.21	
	8691.5	(a)	11502.34	8.4
NI	[ 8686.161 ]		11509.406	408.3

Id	$\lambda$ Å	$\nu$ cm <sup>-1</sup>	I
NI	[ 8683.40]	11513.064	806.9
NI	[ 8680.27]	11517.216	1000.2
Fe	8667.1 (a)	11534.72	49.0
NI	8655.9 (a)	11549.642	142.1
NI	[ 8629.238]	11585.324	175.4
	8602.1 (a)	11621.88	8.6
NI	8594.2 (a)	11632.559	73.6
Ne	8591.6 (a)	11636.08	4.2
NI	8567.9 (a)	11668.266	31.8
	8420.0 (c)	11873.22	2.9
NI	[ 8242.374]	12129.099	264.4
NI	[ 8223.121]	12157.492	257.7
NI	[ 8216.312]	12167.569	636.0
NI	8210.8 (a)	12175.734	100.5
NI	8201.9 (a)	12188.946	86.4
NI	8200.5 (a)	12191.027	43.1
NI	[ 8188.005]	12209.623	236.8
NI	[ 8184.852]	12214.337	233.4
NI	8166.3 (a)	12242.082	120.1
	8152.3 (c)	12263.11	2.2

Id	$\lambda$ A	$\nu$ cm <sup>-1</sup>	I
	8112.6 (a)	12323.12	5.3
NI	[ 7915.419]	12630.094	132.7
NI	7899.4 (a)	12655.708	211.0
N <sub>2</sub>	7753.85 (a)	12893.27	9.4
	7744.5 (a)	12908.84	4.6
	7735.7 (a)	12923.52	6.1
	7730.6 (a)	12932.05	10.6
	7725.0 (a)	12941.42	4.6
	7713.9 (a)	12960.05	4.8
	7711.5 (c)	12964.08	4.8
N <sub>2</sub>	7626.7 (a)	13108.22	6.2
	7604.7 (a)	13146.14	7.4
	7551.6 (a)	13238.58	14.4
	7547.0 (a)	13246.65	6.8
	7536.4 (a)	13265.28	5.2
NI	[ 7468.309]	13386.224	205.6
NI	[ 7442.299]	13433.00	115.4
NI	[ 7423.639]	13466.772	48.8
	7406.3 (a)	13498.30	26.0
	7386.2 (c)	13535.03	6.1

Id	$\lambda$ Å		$\nu$ cm <sup>-1</sup>	I
	7270.6	(a)	13750.23	2.1
	7177.3	(a)	13928.98	1.8
	7159.3	(a)	13964.0	32.9
	7135.8	(a)	14009.98	34.3
NI	6982.0	(a)	14318.595	6.5
NI	6979.3	(a)	14324.134	5.7
	6973.1	(a)	14336.87	2.9
NI	[ 6951.50]		14381.418	6.1
NI	[ 6945.22]		14394.422	13.7
NI	6926.8	(a)	14434.221	5.5
	6795.3	(a)	14711.99	3.5
NI	6793.8	(a)	14715.242	3.3
N <sub>2</sub>	6788.3	(a)	14727.16	6.3
	6758.2	(a)	14792.76	9.9
	6751.9	(a)	14806.56	9.2
NI	6741.0	(a)	14830.501	5.3
NI	[ 6733.48]		14847.063	14.2
	6726.0	(a)	14683.58	7.1
NI	[ 6723.12]		14869.942	30.4
	6722.5	(a)	14871.31	59.2

Id	$\lambda$ A		$\nu$ $\text{cm}^{-1}$	I
	6720.9	(a)	14874.85	12.6
	6717.0	(a)	14883.49	4.9
	6715.9	(a)	14885.93	2.6
NI	6713.2	(a)	14891.915	8.3
NI	6708.8	(a)	14901.682	16.5
NI	6706.1	(a)	14907.681	15.0
NI	6667.06	(a)	14995.110	10.0
	6666.1	(a)	14997.13	11.2
NI	6656.7	(a)	15018.312	7.3
NI	6653.4	(a)	15025.761	15.7
	6648.9	(a)	15035.70	9.7
NI	6646.6	(a)	15041.133	6.9
NI	[ 6644.963 ]		15044.777	24.7
NI	6636.9	(a)	15063.116	6.8
NI	6623.0	(b)	15094.729	13.7
NI	6622.5	(a)	15095.869	
Cr	6612.5	(a)	15118.698	6.8
	6596.5	(a)	15155.36	5.8
N <sub>2</sub>	6545.0	(a)	15274.62	8.6
	6533.0	(a)	15302.68	6.5

Id	$\lambda$ A		$\nu$ $\text{cm}^{-1}$	I
NI	6506.5	(a)	15365.001	20.5
NI	6499.6	(a)	15381.313	12.1
NI	6491.3	(a)	15400.979	11.6
NI	[ 6484.88]		15416.226	104.5
NI	[ 6483.75]		15418.913	83.1
NI	[ 6482.74]		15421.315	153.2
NI	[ 6481.73]		15423.718	49.8
NI	6471.1	(a)	15449.055	3.7
NI	6468.5	(a)	15455.264	15.0
NI	6458.1	(a)	15480.129	1.6
NI	6441.8	(a)	15519.323	20
NI	6441.0	(a)	15521.250	4.5
	6437.8	(a)	15528.97	6.9
NI	6436.8	(a)	15531.378	3.7
NI ?	6423.2	(a)	15564.26	8.5
NI	6420.7	(a)	15570.322	11.3
NI	6417.2	(a)	15578.815	4.2
N <sub>2</sub>	6394.4	(a)	15634.36	4.9
	6384.5	(b)	15658.61	3.3
	6378.5	(a)	15673.34	6.4

Id	$\lambda$ A		$\nu$ cm <sup>-1</sup>	I
	6369.2	(a)	15696.22	4.8
NI ?	6304.0	(a)	15858.56	5.9
	6298.4	(a)	15872.66	6.6
	6289.4	(a)	15895.37	7.2
NI ?	6286.1	(a)	15903.72	13.8
NI ?	6275.7	(a)	15930.07	5.0
NI ?	6273.1	(a)	15936.67	17.6
	6259.3	(a)	15971.81	1.6
N <sub>2</sub>	6253.1	(a)	15987.65	1.5
	6243.2	(a)	16013.00	3.5
	6237.8	(a)	16026.86	5.6
	6234.2	(a)	16036.2	4.6
	6230.3	(a)	16046.15	2.4
	6217.7	(a)	16078.67	1.6
	6194.1	(b)	16139.93	1.8
	6188.8	(b)	16153.75	1.2
	6182.1	(b)	16171.26	0.9
	6175.3	(b)	16189.07	0.8
	6117.1	(b)	16343.09	2.4

Id	$\lambda$ A		$\nu$ cm <sup>-1</sup>	I
	6096.1	(a)	16399.39	6.1
	6095.7	(a)	16400.47	4.4
	6080.7	(a)	16440.92	0.9
NI	6075.9	(a)	16453.912	1.5
N <sub>2</sub>	6069.9	(a)	16470.18	3.9
NI	6017.7	(a)	16613.016	14.8
N <sub>2</sub>	6013.3	(a)	16625.20	4.1
NI	[ 6008.48]		16638.536	43.4
NI	[ 5999.47]		16663.496	23.3
	5989.9	(a)	16690.15	2.4
	5962.3	(a)	16767.41	1.7
NI & Fe ?	5856.0	(a)	17071.771	6.9
NI & Cr ?	5854.4	(a)	17076.437	15.0
NI	5840.9	(a)	17115.905	4.3
NI	5834.6	(a)	17134.386	7.8
	5832.0	(b)	17142.03	4.1
	5831.0	(b)	17144.96	3.2
NI	[ 5829.53]		17149.288	16.8
NI	5816.6	(a)	17187.409	8.2
	5790.0	(a)	17265.18	4.1

Id	$\lambda$ Å	$\nu$ cm <sup>-1</sup>	I
	5772.1 (a)	17320.21	4.2
	5768.7 (a)	17330.12	4.4
	5768.1 (a)	17331.93	2.6
	5764.9 (a)	17341.55	17.1
	5758.1 (a)	17362.03	8.8
NI	[ 5752.64 ]	17378.503	29.3
NI	5747.3 (a)	17394.650	12.9
	5744.5 (a)	17403.13	1.7
NI	5740.8 (a)	17414.345	6.7
	5740.3 (a)	17415.86	8.2
NI	5625.5 (a)	17771.265	9.1
NI	5623.3 (a)	17778.218	20.8
NI/Fe	5618.4 (a)	17793.722	8.4
NI	[ 5616.54 ]	17799.583	29.3
NI/Fe	5611.5 (a)	17815.601	9.4
NI	5604.4 (a)	17838.171	1.5
NI	[ 5600.54 ]	17850.466	5.6
	5591.5 (b)	17879.33	0.7
	5571.5 (a)	17943.51	2.3
	5564.54	17965.948	8.1

Id	$\lambda$ A	$\nu$ $\text{cm}^{-1}$	I
NI	[ 5564.37]	17966.497	95.8
NI	[ 5560.37]	17979.422	74.2
	5559.74	17981.459	9
NI	5557.40	17989.031	16.0
	5556.07	17993.337	1.7
	5551.13	18009.349	7.0
	5548.23	18018.762	4.9
	5545.26	18028.445	4
NI	5545.11	18028.901	11
	5544.66	18030.364	1.2
	5542.84	18036.284	1.1
	5540.50	18043.901	4.9
	5535.57	18059.971	4.9
	5533.6 (a)	18066.40	0.9
	5530.11	18077.802	4.5
	5529.65	18079.31	6.0
	5523.6 (a)	18199.11	2.0
	5519.7 (a)	18111.90	1.5
	5503.9 (a)	18163.89	0.8
	5500.42	18175.381	6.0

Id	$\lambda$ Å	$\nu$ $\text{cm}^{-1}$	I
	5497.15	18186.192	10.6
	5496.75	18187.52	2.7
	5485.8 (b)	18223.82	0.8
	5478.1 (a)	18249.43	1.1
	5472.40	18268.44	4.5
Fe	5394.4 (a)	18532.59	6.3
	5381.4 (a)	18577.360	2.0
NI	5378.44	18587.583	8.7
	5376.26	18595.121	6.1
	5374.89	18599.86	2.8
NI	[ 5372.66 ]	18607.580	9.1
	5370.91	18613.643	18.6
NI	[ 5367.27 ]	18626.266	8.4
	5363.67	18638.768	10.1
	5361.96	18644.712	4.2
	5361.06 (a)	18648.05	1.1
	5359.77	18652.33	4.5
NI	5356.77	18662.776	21.2
	5355.2 (a)	18668.25	
Fe	5353.1 (a)	18675.57	0.9

Id	$\lambda$ A	$\nu$ cm <sup>-1</sup>	I
	5350.1 (a)	18686.04	1.2
	5346.96	18697.016	2.3
	5346.1 (a)	18700.02	1.1
NI	5344.22	18706.602	4.8
	5343.73	18708.32	2.1
	5343.47	18709.23	1.0
	5341.32	18716.758	2.3
	5339.50	18723.138	3.7
	5337.76	18729.241	4.8
	5336.72	18732.891	4.0
NI	5334.38	18741.108	8.0
Ne	5330.85	18753.518	2.7
NI	[ 5328.7 ]	18761.085	33.6
	5328.43	18762.035	7.4
	5326.34	18769.397	2.7
	5324.00	18777.647	4.3
	5314.95	18809.62	1.3
	5310.69	18824.708	1.2 ?
	5310.60	18824.991	2.1 ?
	5305.12	18844.472	2.6

Id	$\lambda$ Å	$\nu$ cm <sup>-1</sup>	I
	5298.11	18869.406	1.7
	5297.46	18871.751	2.7
	5293.50	18885.838	4.2
NI	[ 5292.75]	18883.514	11.3
NI/Fe	[ 5281.18]	18929.895	16.1
	5275.9	18948.839	3.7
	5234.8 (a)	19097.61	1.4
	5232.6 (a)	19105.64	1.8
	5218.98	19155.499	4.9
	5208.72	19193.231	1.1
	5203.97	19210.750	2.0
NI	[ 5201.71]	19219.059	85.4
	5199.87	19225.896	33.7
Fe	5197.86	19233.331	22.8
	5193.09	19254.705	18.8
	5191.78	19255.855	27.9
	5189.43	19264.574	97.1
	5186.64	19275.829	5.4
	5185.91	19277.651	25.1
	5182.88	19288.290	13.9

Id	$\lambda$ A	$\nu$ $\text{cm}^{-1}$	I
	5181.34	19294.653	10.8
	5179.78	19300.464	4.0
	5179.53	19301.396	7.2
	5179.38	19301.955	8.8
	5169.58	19338.55	14
	5168.81	19341.426	3.5
	5167.82	19345.131	82.0
	5167.41	19346.666	3.8
	5165.90	19352.321	8.0
	5165.77	19352.808	8.5
	5165.66	19353.183	4.7
	5163.77	19360.303	1.6
	5162.91	19363.528	32.5
NI	5162.78	19364.016	1.4
	5162.61	19364.654	1.6
	5160.7 (a)	19371.82	2.3 ?
	5158.49	19380.12	5.2
	5156.72	19386.771	4.3
	5155.87	19389.968	3.9
	5155.37	19391.848	2.6

Id	$\lambda$ Å	$\nu$ $\text{cm}^{-1}$	I
	5155.26	19392.262	5.3
	5154.5 (a)	19395.121	2.1 ?
	5153.76	19397.906	1.3
	5153.05	19400.579	2.6
	5151.33	19407.056	4.3
	5149.62	19413.501	1.6
	5146.6 (a)	19424.89	1.3 ?
Fe	5146.0 (a)	19427.16	2.3 ?
	5141.93	19438.754	5.4
	5141.16	19445.446	2.0
	5136.31	19463.807	4.1
	5135.79	19465.778	3.1
	5134.39	19471.086	6.1
	5132.5 (a)	19478.26	1.4
	5120.3 (a)	19524.665	1.6
	5117.88	19533.897	1.6
	5116.6 (a)	19538.555	1.4 ?
	5115.44	19543.215	2.3
	5110.52	19562.030	4.5
	5100.69	19599.729	4.4

Id	$\lambda$ A	$\nu$ $\text{cm}^{-1}$	I
	5100.45	19600.651	8.8
	5080.47	19677.734	9.4
Ne	5037.68	19844.874	8.4
	5031.5 (a)	19869.25	2.0
	5009.2 (b)	19957.7	1.4
	5009.4 (a)	19956.9	1.5
	5007.6 (a)	19964.08	1.4
	4997.1 (a)	20006.03	1.6
	4993.3 (a)	20021.25	1.4
	4987.47	20044.654	3.9
Fe	4987.3 (a)	20045.34	1.6
	4982.0 (a)	20066.66	2.2
	4976.31	20089.606	0.7
	4974.82	20095.623	2.7
	4973.37	20101.482	4.6
	4971.51	20109.043	10.5
	4968.31	20121.95	3.3
	4966.41	20129.652	2.0
	4965.54	20133.179	1.0
	4963.98	20139.506	20.6

Id	$\lambda$ A	$\nu$ $\text{cm}^{-1}$	I
	4952.29	20146.771	4.6
	4957.42	20166.156	3.9
	4955.74	20172.992	10.3
	4953.42	20182.440	4.8
	4951.48	20190.347	6.7
	4950.23	20195.446	14.0
	4949.13	20199.934	1.0
	4947.74	20205.609	2.4
	4946.53	20210.552	2.9
	4945.90	20213.126	2.0
	4945.79	20213.576	3.1
	4943.61	20222.489	2.0
	4942.89	20225.435	2.1
	4937.5 (b)	20247.51	0.8
NI	4935.03	20257.647	37
	4933.55	20263.724	2.5
	4918.85	20324.281	1.1
	4916.08	20335.733	1.5
NI	[ 4914.9 ]	20340.615	16.2
	4914.0 (a)	20344.34	0.6

Id	$\lambda$ A	$\nu$ cm <sup>-1</sup>	I
	4913.0 (a)	20348.48	0.6
	4895.03	20423.182	1.9
	4890.0 (a)	20444.19	1.5
	4886.6 (a)	20458.41	3.0
NI & Fe	4881.8 (a)	20478.529	2.4
	4879.3 (a)	20489.02	1.8
	4878.7 (a)	20491.54	2.1
	4869.10	20531.942	3.4
	4866.90	20541.223	3.2
	4865.68	20546.373	2.3
N <sub>2</sub> ?	4864.6 (a)	20550.94	2.8
	4863.19	20556.89	3.3
	4858.80	20575.466	4.5
	4855.56	20589.196	1.3
	4852.55	20601.967	4.9
NI	[ 4847.38]	20623.939	14.9
	4845.0 (a)	20612.80	2.0
	4839.85	20656.026	2.4
	4836.42	20662.131	4.4
NI	[ 4837.93]	20664.224	3.7

Id	$\lambda$ Å	$\nu$ cm <sup>-1</sup>	I
	4834.60	20678.457	2.0
NI	4831.21	20692.967	15.9
	4830.69	20695.194	4.6
	4829.89	20698.622	2.3 ?
	4829.85	20698.793	2.4 ?
	4829.10	20702.008	4.0
	4828.06	20706.467	5.2
	4827.86	20707.375	1.4
	4825.64	20716.851	2.7
	4823.80	20724.753	0.7
	4822.22	20731.543	5.3
	4820.69	20738.123	0.8
	4819.38	20743.760	3.9
	4819.10	20744.966	2.6
	4809.03	20788.405	0.9
	4754.01	21028.993	2.6
	4753.54	21031.073	1.3
NI	4753.30	21032.134	3.8
	4751.21	21041.386	2.5
	4747.4 (a)	21058.27	0.9

Id	$\lambda$ Å	$\nu$ $\text{cm}^{-1}$	I
	4744.73	21070.122	5.7
	4742.0 (a)	21087.25	1.5
	4738.73	21096.8	1.6
	4732.6 (a)	21124.13	1.1
	4718.36	21187.877	1.9
	4709.33	21228.504	2.5
	4686.4 (a)	21332.37	0.6 ?
NI	4685.8 (a)	21335.102	0.7 ?
	4684.31	21341.889	1.5 ?
	4683.91	21343.711	1.2
	4679.51	21363.78	1.6
NI	4678.52	21368.301	5.6
	4677.82	21371.498	2.3 ?
	4675.44	21382.38	2.2
	4669.894	21407.789	21.0
	4660.46	21451.105	12.4
	4656.48	21469.439	5.0
	4652.31	21488.682	0.9
NI	4651.76	21491.223	3.8
	4650.2 (a)	21498.43	0.8 ?

Id	$\lambda$ Å	$\nu$ cm <sup>-1</sup>	I
	4647.00	21513.237	1.6 ?
	4646.60	21515.089	0.5
	4558.5 (a)	21930.894	1.2
NI	4554.3 (a)	21951.118	1.7
NI	4553.1 (a)	21956.904	0.5 ?
	4552.2 (a)	21961.244	0.9
	4499.1 (a)	22220.435	0.9
	4494.81	22241.642	4.9
	4492.51	22253.029	4.4
	4485.81	22286.266	1.1
	4485.29	22288.849	2.8
	4477.38	22328.225	1.4
	4477.12	22329.522	1.0
	4476.36	22333.313	0.8
NI	4358.3 (a)	22938.280	0.6
	4351.24	22975.497	1.2
	4343.60	23015.908	2.1
	4340.8 (a)	23030.754	1.5
	4323.90	23120.769	2.5
	4321.32	23134.572	1.4

Id	$\lambda$ Å	$\nu$ cm <sup>-1</sup>	I
	4317.79	23153.485	9.4
NI	4313.13	23178.500	4.6
	4313.4 (a)	23177.050	4.3
NI	4305.46	23219.791	7.8
NI	4284.96	23330.877	1.3
NI	4281.37	23350.440	2.1
	4278.11	23368.233	11.2
	4269.59	23414.863	1.2 ?
	4267.41	23426.824	1.2
Cr	4263.21	23449.904	1.4
	4258.76	23474.406	3.5
	4255.18	23494.155	6.5
NI	4254.74	23496.585	10.8
NI	4253.31	23504.484	11.5
NI	4230.52	23631.102	8.7
NI	4224.81	23663.040	11.8
NI	[ 4223.05 ]	23672.901	27.2
NI	4222.09	23678.28	7.9
NI	4218.93	23696.02	3.0
NI	4216.01	23711.08	6.2

Id	$\lambda$ Å	$\nu$ cm <sup>-1</sup>	I
NI	4214.85	23718.96	10.1
	4211.7 (a)	23736.7	1.2
NI	4205.8 (a)	23769.993	1.6
N <sub>2</sub> <sup>+</sup>	4167.0 (a)	23991.318	3.4 ?
NI	[ 4151.46 ]	24081.122	30.8
NI	4143.44	24127.731	18.3
NI	4137.58	24161.903	8.8
NI	[ 4113.972 ]	24300.565	6.4
NI	[ 4109.959 ]	24324.274	57.6
NI	[ 4099.951 ]	24383.660	34.1
Fe	4045.89	24709.46	12.2
	4044.31	24719.114	4.5
	4037.48	24760.929	7.0
	4035.51	24773.016	1.2
	4035.06	24775.779	3.1
	4030.02	24806.763	3.4
	4024.57	24840.355	13.2
	4021.72	24864.140	2.4
	4011.53	24921.100	10.7 ?
	4010.87	24925.201	1.3

Id	$\lambda$ Å	$\nu$ cm <sup>-1</sup>	I
	4004.4 (a)	24965.472	1.3
	4002.516	24978.45	4.6
NI	3999.98	24993.059	10.6
	3989.00	25061.853	4.2
	3986.405	25065.56	1.3
	3987.0 (a)	25074.42	1.6
	3982.71	25101.43	2.4
	3974.03	25156.257	4.2
	3960.45	25242.514	2.6
NI	3957.20	25263.245	4.9
NI	3952.21	25295.141	4.5
	3906.04	25594.127	0.8 ?
	3904.16	25606.451	0.9
	3900.16	25632.712	7.0
	3899.93	25634.224	1.0
	3892.14	25685.53	53.2
	3887.15	25718.501	37.5
	3886.16	25724.92	8.0
	3835.53	26064.622	4.7
NI	3834.27	26073.187	14.6

Id	$\lambda$ A	$\nu$ cm <sup>-1</sup>	I
NI	[ 3830.39]	26099.598	57.3
	3829.93	26102.732	30 ?
	3823.65	26145.603	2.3 ?
	3822.82	26151.279	2.8
NI	3822.00	26156.889	24.7
NI	3818.28	26182.373	8.2

The following data is preliminary, and should be confirmed. It is presented here because there are not many NI classified lines in this wavelength region (3800 - 3400 Å) and it is the region where many of the series limits may be found. More careful analysis of the data needs to be done in that some confusion exists with molecular lines. More careful experimenting needs to be done. The wavelength accuracy is between 0.1 and 0.2 Å.

Id	$\lambda$ Å	$\nu$ cm <sup>-1</sup>	I
	3791.96	26364.10	5
	3781.32	26438.282	6
	3758.33	26600.003	8
	3749.81	26660.44	5
	3749.40	26663.356	2
Fe	3748.35	26670.824	5
	3734.96	26766.438	1
	3713.88	26918.361	4
	3713.43	26921.623	5
	3700.28	27017.294	11

Id	$\lambda$ Å	$\nu$ cm <sup>-1</sup>	I
	3652.37	27371.684	15
	3651.29	27379.780	14
	3641.61	27452.558	6
	3639.65	27467.342	5
	3624.62	27581.235	6
	3610.52	27688.944	6
	3581.10	27916.413	24
	3563.86	28051.453	9
	3554.81	28122.866	12
	3534.11	28287.582	23
NI	3532.61	28299.673	12
	3524.47	28364.952	21
Fe	3523.39	28373.646	14
	3522.09	28384.118	7
	3520.26	28498.873	10
	3515.25	28439.346	7
	3514.92	28442.017	14
	3472.31	28791.029	10
	3461.46	28881.271	20
	3456.79	28920.289	6

Id	$\lambda$ Å	$\nu$ cm <sup>-1</sup>	I
	3440.43	29057.806	9
	3433.29	29118.234	6
	3414.60	29277.609	23

## DOCUMENT CONTROL DATA - R&amp;D

(Security classification of title, body of abstract and indexing annotation must be entered when the overall report is classified)

1. ORIGINATING ACTIVITY (Corporate author)		28. REPORT SECURITY CLASSIFICATION	
Regents of the University of California Santa Barbara, California		Unclassified	
		29. GROUP	
3. REPORT TITLE			
An Optical Spectroscopic Investigation of Helium and Nitrogen Plasmas			
4. DESCRIPTIVE NOTES (Type of report and inclusive dates)			
Technical Report			
5. AUTHOR(S) (Last name, first name, initial)			
Manalis, M. S. (H. P. Broida, thesis advisor & Principal Investigator)			
6. REPORT DATE		7a. TOTAL NO. OF PAGES	7b. NO. OF REFS
August 18, 1970		156	46
8a. CONTRACT OR GRANT NO.		8b. ORIGINATOR'S REPORT NUMBER(S)	
N00014-69-A-0200-8004		Technical Report # 31	
a. PROJECT NO. NR 014-113			
c. ARPA Order No. 125 and 1479		8c. OTHER REPORT NO(S) (Any other numbers that may be assigned to this report)	
d.			
10. AVAILABILITY/LIMITATION NOTICES			
Distribution of this document is unlimited			
11. SUPPLEMENTARY NOTES		12. SPONSORING MILITARY ACTIVITY	
		Office of Naval Research Washington, D.C.	
13. ABSTRACT			
<p>Energetic species and their respective energy exchange processes in a cool, high density helium plasma has been reviewed. Light from a flowing helium afterglow was observed from 2500 to 10,500 Å using an Ebert double-pass scanning monochromator coupled to standard dc detecting equipment. Experimental data in the form of relative populations of atomic helium states provided motivation for a theory which may explain the manner in which ionization is maintained in the afterglow region of the helium plasma. A bimodal electron distribution was found to exist in this plasma; the electron temperatures were measured spectroscopically to be in the neighborhood of <math>10^3</math> and <math>10^4</math> K.</p> <p>Molecular nitrogen was used as a probe to detect various energetic species present in the helium afterglow. In addition to the usual systems observed when <math>N_2</math> is injected into the helium afterglow, light from many levels of atomic nitrogen and three new vibrational population distributions of the first positive system of molecular nitrogen were observed. Two independent mechanisms for exciting the atomic nitrogen were isolated. One mechanism consisted of a two step collisional process where <math>N_2</math> was dissociated by metastable molecular helium <math>He_2^*</math>, and the excited N was produced by collisions with electrons. The temperature associated with the N level population was about <math>10^4</math> K, confirming the existence of the high energy electrons found in the helium afterglow. The second mechanism for populating N was single electron recombination of nitrogen atomic ions formed in the dissociative charge transfer reaction of ionized helium, <math>He^+</math>, with molecular</p>			

14 KEY WORDS	LINK A		LINK B		LINK C	
	ROLE	WT	ROLE	WT	ROLE	WT
Optical Spectroscopy Atoms Diatomic molecules Free radical reactions; recombinations Nitrogen Helium						

**INSTRUCTIONS**

**1. ORIGINATING ACTIVITY:** Enter the name and address of the contractor, subcontractor, grantee, Department of Defense activity or other organization (*corporate author*) issuing the report.

**2a. REPORT SECURITY CLASSIFICATION:** Enter the overall security classification of the report. Indicate whether "Restricted Data" is included. Marking is to be in accordance with appropriate security regulations.

**2b. GROUP:** Automatic downgrading is specified in DoD Directive 5200.10 and Armed Forces Industrial Manual. Enter the group number. Also, when applicable, show that optional markings have been used for Group 3 and Group 4 as authorized.

**3. REPORT TITLE:** Enter the complete report title in all capital letters. Titles in all cases should be unclassified. If a meaningful title cannot be selected without classification, show title classification in all capitals in parenthesis immediately following the title.

**4. DESCRIPTIVE NOTES:** If appropriate, enter the type of report, e.g., interim, progress, summary, annual, or final. Give the inclusive dates when a specific reporting period is covered.

**5. AUTHOR(S):** Enter the name(s) of author(s) as shown on or in the report. Enter last name, first name, middle initial. If military, show rank and branch of service. The name of the principal author is an absolute minimum requirement.

**6. REPORT DATE:** Enter the date of the report as day, month, year, or month, year. If more than one date appears on the report, use date of publication.

**7a. TOTAL NUMBER OF PAGES:** The total page count should follow normal pagination procedures. I.e., enter the number of pages containing information.

**7b. NUMBER OF REFERENCES:** Enter the total number of references cited in the report.

**8a. CONTRACT OR GRANT NUMBER:** If appropriate, enter the applicable number of the contract or grant under which the report was written.

**8b, 8c, & 8d. PROJECT NUMBER:** Enter the appropriate military department identification, such as project number, subproject number, system numbers, task number, etc.

**9a. ORIGINATOR'S REPORT NUMBER(S):** Enter the official report number by which the document will be identified and controlled by the originating activity. This number must be unique to this report.

**9b. OTHER REPORT NUMBER(S):** If the report has been assigned any other report numbers (*either by the originator or by the sponsor*), also enter this number(s).

**10. AVAILABILITY/LIMITATION NOTICES:** Enter any limitations on further dissemination of the report, other than those

imposed by security classification, using standard statements such as:

- (1) "Qualified requesters may obtain copies of this report from DDC."
- (2) "Foreign announcement and dissemination of this report by DDC is not authorized."
- (3) "U. S. Government agencies may obtain copies of this report directly from DDC. Other qualified DDC users shall request through \_\_\_\_\_."
- (4) "U. S. military agencies may obtain copies of this report directly from DDC. Other qualified users shall request through \_\_\_\_\_."
- (5) "All distribution of this report is controlled. Qualified DDC users shall request through \_\_\_\_\_."

If the report has been furnished to the Office of Technical Services, Department of Commerce, for sale to the public, indicate this fact and enter the price, if known.

**11. SUPPLEMENTARY NOTES:** Use for additional explanatory notes.

**12. SPONSORING MILITARY ACTIVITY:** Enter the name of the departmental project office or laboratory sponsoring (paying for) the research and development. Include address.

**13. ABSTRACT:** Enter an abstract giving a brief and factual summary of the document indicative of the report, even though it may also appear elsewhere in the body of the technical report. If additional space is required, a continuation sheet shall be attached.

It is highly desirable that the abstract of classified reports be unclassified. Each paragraph of the abstract shall end with an indication of the military security classification of the information in the paragraph, represented as (TS), (S), (C), or (U).

There is no limitation on the length of the abstract. However, the suggested length is from 150 to 225 words.

**14. KEY WORDS:** Key words are technically meaningful terms or short phrases that characterize a report and may be used as index entries for cataloging the report. Key words must be selected so that no security classification is required. Identifiers, such as equipment model designation, trade name, military project code name, geographic location, may be used as key words but will be followed by an indication of technical context. The assignment of links, roles, and weights is optional.